Using quantum chemistry muscle to flex massive systems: How to respond to something perturbing

by

Colleen Bertoni

A dissertation submitted to the graduate faculty

in partial fulfillment of the requirements for the degree of

DOCTOR OF PHILOSOPHY

Major: Physical Chemistry

Program of Study Committee:
Mark S. Gordon, Major Professor
Theresa L. Windus
Xueyu Song
Gordon J. Miller
Monica H. Lamm

Iowa State University

Ames, Iowa

2016

TABLE OF CONTENTS

CHAPTER 1. GENERAL INTRODUCTION

General Overview

Computational chemistry uses the theoretical advances of quantum mechanics and the algorithmic and hardware advances of computer science to give insight into chemical problems. It is currently possible to do highly accurate quantum chemistry calculations, but the most accurate methods are very computationally expensive. Thus it is only feasible to do highly accurate calculations on small molecules, since typically more computationally efficient methods are also less accurate. The overall goal of my dissertation work has been to try to decrease the computational expense of calculations without decreasing the accuracy. In particular, my dissertation work focuses on fragmentation methods, intermolecular interactions methods, analytic gradients, and taking advantage of new hardware.

Fragmentation methods can decrease the computational cost of an *ab initio* method drastically and retain accuracy.[1] Fragmentation methods typically begin by splitting a large chemical system into many smaller parts (monomers). Using a many-body expansion approach, one can split the total energy for the system into the sum of the monomer energies, the sum of the dimer energies, the sum of the energies of each set of three monomers, and so on. Thus, the energy (or any other property) for the total system is computed by calculating energies (or properties) for monomers, dimers, etc., and recombining the results. A calculation on the total system is never required, so the computational cost is dramatically decreased. Additionally, fragmentation methods are naturally parallelizable, since each monomer/dimer/etc calculation can be done

separately. Two fragmentation methods are the Fragment Molecular Orbital (FMO) method and the Effective Fragment Molecular Orbital (EFMO) method[2 3 4].

Intermolecular interaction methods usually are much less computationally expensive than *ab initio* methods since molecules are typically expressed as potentials and not wavefunctions.[5] Intermolecular interaction methods can be used to provide interaction energies and are often also used to shed light onto non-covalent interactions and how molecules are interacting with each other. Despite the fact the non-covalent interactions are weak compared to covalent bonds, non-covalent interactions are responsible for hydrogen-bonding in water, the double helix in DNA, and are a potential explanation for how geckos cling to glass walls[6]. Intermolecular interaction methods range in functional form, accuracy, and computational cost. One intermolecular interaction method is the Effective Fragment Potential (EFP) method.[7]

Gradients are important and necessary for any energy method. Geometry optimizations, transition state searches, molecular dynamics simulations, response properties, and reaction path following all rely on the derivative of the energy with respect to the geometry. A numeric finite-difference method can be used to calculate a gradient. However, in a numeric finite-difference procedure, each gradient element involves doing at least two energy calculations. Thus, it is important to derive and implement analytic gradients for a method so that more information can be calculated from an energy method without using a computationally expensive numeric finite-difference procedure.

All of the above methods are limited by the computational resources available, and quantum chemistry would not be where it is today without computers. The ability to

solve a self-consistent field calculation was made possible by the efforts to build computers in the twentieth century. However, computers have finite resources, and the size of a feasible energy or property calculation is bounded by the resources and hardware available and by the ability of the software to use the resources efficiently. When there have been advances in computer hardware, there have been advances in quantum chemistry, but only because chemists have written software to take advantage of the available computing power. As an example, as computers moved from uniprocesser to multiprocessor, parallel chemistry programs were written to take advantage of the hardware, allowing larger calculations to be run. Currently, the scientific computing platform is typically a cluster of multiprocessors connected with a network. The number of cores and memory on the nodes varies extensively. However, additional hardware can be incorporated, such as Graphical Processing Units and Remote Area RAM, which can ideally be used to speed up a calculation. As one designs chemistry software, it is important to consider what the future of scientific computing will look like, and see how new hardware trends can be incorporated.

Together, all of the foregoing considerations support the goal of accurate and computationally inexpensive calculations.

Dissertation Organization

Chapter 1 of the thesis provides a general overview of the parts of quantum chemistry and the methods that are relevant to the rest of the chapters. Chapter 2 discusses the derivation and implementation of the gradient for the Effective Fragment Molecular Orbital (EFMO) method. Chapter 3 Chapter benchmark different sets of

multipole moments in the Effective Fragment Potential (EFP) method, and Chapter 4 discusses using the EFMO method to calculate the melting temperature of ice.

Theoretical Background and Methods

Before describing the work in this dissertation, some background on quantum chemistry is necessary. In particular, background is provided on the Schrodinger equation, Hartree-Fock method, many-body expansions and perturbation theory, and response and gradient theory.

In classical mechanics, the dynamics of a system—the manner in which particles in a system progress over time—is described by Newton's second law, $F = ma$. However, in the late 1800s and early 1900s, scientists discovered that classical mechanics and Maxwell's electromagnetism equations couldn't properly describe physical phenomena, such as how the intensity of radiation emitted from a blackbody varies with frequency, or how the kinetic energy of an electron emitted from a metal varies with the frequency of the incoming light that causes the electron emission. Thus, it was discovered that microscopic "particles" have both wave-like and particle-like properties, that there are theoretical limits on how well the position and velocity of a wave-particle can be simultaneously known, and that classical mechanics is not applicable to microscopic particles. A different type of mechanics, called quantum mechanics, was developed. In quantum mechanics, the motion of a particle is governed by the time-dependent Schrodinger equation[8 9], shown in Eq. (1):

$$\begin{aligned} \frac{\hbar}{i}\frac{\partial \Psi(x,t)}{\partial t} &= \hat{H}\Psi(x,t) \\ &= (\hat{T}+\hat{K})\Psi(x,t) \end{aligned} \tag{1}$$

$\Psi(x,t)$ is the wavefunction, or state function that contains all of the possible information about the particle. In classical mechanics, the "state" would specify the position and velocity of all particles in a system, and the forces acting on the particles. As mentioned above, in quantum mechanics one cannot know with infinite precision both the position and velocity of a particle. Thus, the wavefunction does not specify the classical "state". Instead, the Born density of the wavefunction gives the probability at time *t* of finding the particle between *x* and *x*+*dx*. $\hat{H}$ is the Hamiltonian operator, which is the sum of the kinetic and potential energy operators ($\hat{K}$ and $\hat{T}$, respectively). The kinetic energy operator is $-\frac{\hbar^2}{2m}\nabla^2$, where ∇^2 is the Laplacian operator, *m* is the mass of the particle, and $\hbar$ is Planck's constant divided by 2π. The form of the potential energy operator depends on the system.

If $\hat{T}$ is independent of time, then Eq. (1) can be separated into a time-dependent equation and a time-independent equation. Most of computational chemistry works with potential energy operators that are assumed not to change much with time. Thus, the time-independent form of the Schrodinger equation is what most computational chemists work with. The time-independent equation can be written as

$$\hat{H}\psi(x) = E\psi(x) \tag{2}$$

where $\psi(x)$ is the time-independent wavefunction, and *E* is the total energy of the system.

For a molecular system, with electrons and nuclei, the Hamiltonian (in atomic units) is

$$\hat{H} = -\sum_{i}^{electrons}\frac{1}{2}\nabla^2 - \sum_{A}^{nuclei}\frac{1}{2M_A}\nabla^2 - \sum_{i}^{electrons}\sum_{A}^{nuclei}\frac{Z_A}{r_{iA}} + \sum_{i}^{electrons}\sum_{j<i}^{electrons}\frac{1}{r_{ij}} + \sum_{A}^{nuclei}\sum_{B<A}^{nuclei}\frac{Z_A Z_B}{r_{AB}} \tag{3}$$

where M_A is the ratio of the mass of nucleus A to the mass of an electron, Z_A is the atomic number of nucleus A, r is a position vector, and $r_{xy} = |r_x - r_y|$ The first two terms in Eq. (3) are the kinetic energy operators for the electrons and nuclei, respectively, and the last three terms are the Coulomb potential energy operators between electrons and nuclei, electrons and electrons, and nuclei and nuclei, respectively.

Nuclei are much heavier than electrons, and their velocities are much smaller. Thus, a good approximation to Eq. (3) is to assume the nuclei are stationary (have no kinetic energy), and only solve for the electronic part of the wavefunction. This assumption is called the Born-Oppenheimer (BO) approximation.[10] Applying the Born-Oppenheimer approximation, the Hamiltonian becomes

$$\hat{H}_{elec} = -\sum_{i}^{electrons} \frac{1}{2}\nabla^2 - \sum_{i}^{electrons}\sum_{A}^{nuclei} \frac{Z_A}{r_{iA}} + \sum_{i}^{electrons}\sum_{j<i}^{electrons} \frac{1}{r_{ij}} \tag{4}$$

and the electronic wavefunction and energy can be solved as:

$$\hat{H}_{elec}\psi_{elec} = E_{elec}\psi_{elec} \tag{5}$$

The energy can also be computed as an expectation value of the wavefunction:

$$E_{elec} = \langle \psi_{elec} | \hat{H}_{elec} | \psi_{elec} \rangle \tag{6}$$

where the wavefunction is normalized. An important consequence of the BO approximation is that, since the nuclei are stationary, ψ_{elec} (referred to just as ψ from now on) depends explicitly on the electronic coordinates, and implicitly (parametrically) on the nuclear coordinates.

In the Born-Oppenheimer approximation, the total energy is:

$$E_{tot} = E_{elec} + \sum_{A}^{nuclei}\sum_{B<A}^{nuclei} \frac{Z_A Z_B}{r_{AB}} \tag{7}$$

The function E_{tot}, which depends explicitly on the nuclear coordinates in the second term on the right-hand side of Eq. (7), and parametrically on the nuclear coordinates in the first term on the right-hand side of Eq. (7), can be thought of as the potential energy surface that the nuclei move on. Unfortunately, Eq. (5) can only be solved exactly for systems with one electron, because the electron-electron repulsion term in the Born-Oppenheimer electronic Hamiltonian (Eq. (4)) is not separable. Thus, approximate methods are necessary to solve for the electronic wavefunction of molecules with multiple electrons.

One of the most common approximate methods is the Hartree-Fock method.[8] The Hartree-Fock method uses several key concepts: one-electron spin-orbitals, the antisymmetry principle, and the variational principle. In the Hartree-Fock method, the wavefunction is an antisymmetrized product of one-electron functions (spin-orbitals). A spin-orbital is a product of a molecular orbital and a spin function. The wavefunction must be antisymmetrized, since electrons are fermions (the antisymmetry principle). One way of ensuring that the wavefunction is antisymmetric is by writing it in terms of Slater determinants. A further approximation is made that the wavefunction is a single Slater determinant. Using Eq. (6) and Eq. (7), the energy of a Slater determinant is

$$E_{tot} = \sum_{i}^{N} \langle \phi_i | \hat{h}_i | \phi_i \rangle + \frac{1}{2} \sum_{ij}^{N} \left(\langle \phi_j | \hat{J}_i | \phi_j \rangle - \langle \phi_j | \hat{K}_i | \phi_j \rangle \right) + V_{nn} \tag{8}$$

where $\hat{h}_i$ is a one electron operator arising from the kinetic energy of the electrons and the Coulombic potential energy of the electrons with the nuclei, $\hat{J}$ and $\hat{K}$ are two-electron operators that arise from the electron-electron repulsion term, V_{nn} is the nuclear repulsion term, and *N* is the number of electrons. The variational principle states that given any arbitrary wavefunction (which is normalized, well-behaved, and satisfies

appropriate boundary conditions), the expectation value of the Hamiltonian with the arbitrary wavefunction will be less than or equal to the lowest-energy eigenvalue (ground state energy) of the Hamiltonian.[9]

Since the Slater determinant is a trial wavefunction, the variational principle can be applied to it. Thus, Eq. (8) is minimized with respect to the spin-orbitals so that the energy is as close to the true ground state energy as possible. A standard way of carrying out the minimization is by using Lagrange multipliers to minimize Eq. (8) under the constraint that the spin-orbitals remain orthonormal. Rearranging the Lagrange multiplier equations leads to the Hartree-Fock pseudo-eigenvalue equations:

$$F\phi_i = \sum_j^N \epsilon_{ij}\phi_j \tag{9}$$

where F is the Fock operator and ϵ_{ij} is a Lagrange multiplier.

The Fock operator is:

$$\hat{F}(1) = \hat{h}(1) + \sum_j^N \left(\hat{J}_j(1) - \hat{K}_j(1)\right) \tag{10}$$

Eq. (9) is the variational condition for the Hartree-Fock method. That is, if the orbitals are chosen such that they minimize the total energy, then Eq. (9) must be true. Since a unitary transformation of the spin-orbitals does not change the expectation value of a single-determinant wavefunction, the Lagrange multipliers can be chosen to be diagonal, as shown below.

$$F\phi_i(1) = \epsilon_i\phi_i(1) \tag{11}$$

The set of Lagrange multipliers that are diagonal, as shown in Eq. (11), are referred to as the canonical eigenvalues, and the orbitals that produce them are referred to

as the canonical orbitals. The canonical eigenvalues are interpreted as "orbital energies". Multiplying on the left side of Eq. (11) by orbital *j* and integrating gives:

$$\begin{aligned} \langle \phi_j | F | \phi_i \rangle &= \langle \phi_j | \epsilon_i | \phi_i \rangle \\ &= \epsilon_i \langle \phi_j | \phi_i \rangle \\ &= \epsilon_i \delta_{ij} \end{aligned} \tag{12}$$

Note that Eq. (12) is equivalent to Eq. (11), and is thus a different way of writing the variational condition. The orbital energies are the diagonal elements of the Fock operator:

$$\epsilon_i = \langle \phi_i | F | \phi_i \rangle \tag{13}$$

Eq. (11) is a pseudo-eigenvalue equation because the Fock operator depends on all spin-orbitals, not just orbital *i*. To compute orbital *i*, all other orbitals must be known, and thus an iterative method, called a self-consistent field (SCF) calculation, is used to solve the set of Hartree-Fock equations. The above equations are written in terms of spin-orbitals, which consist of a spatial molecular orbital and a spin function. It is often possible to integrate out the spin functions. For example, if the desired system has an even number of electrons and a singlet wavefunction, and if there are no spin-dependent terms in the Hamiltonian, the spin functions can be integrated out, and Eq. (8) rewritten terms of only spatial orbitals. A wavefunction as described above (with an even number of electrons and a singlet wavefunction) is referred to as a Restricted Hartree-Fock (RHF) wavefunction. The RHF energy can be written as

$$E_{elec} = 2\sum_{i}^{N/2} \langle \varphi_i | \hat{h}_i | \varphi_i \rangle + \sum_{ij}^{N/2} \left(2 \langle \varphi_i(1)\varphi_j(2) | \frac{1}{r_{12}} | \varphi_i(1)\varphi_j(2) \rangle - \langle \varphi_i(1)\varphi_i(2) | \frac{1}{r_{12}} | \varphi_j(1)\varphi_j(2) \rangle \right) \tag{14}$$

where φ_i is a spatial molecular orbital.

To make solving the Hartee-Fock equations more computationally feasible, the Linear Combination of Atomic Orbitals (LCAO) approximation is used. In the LCAO approximation, each molecular orbital is expanded in a set of atomic basis functions, as shown below:

$$\varphi_i(r) = \sum_{\mu}^{\text{basis functions}} c_{\mu i}\chi_\mu(r) \tag{15}$$

where *r* is the electronic coordinate, $c_{\mu i}$ is the coefficient of atomic basis function μ in the *i*th molecular orbital, and χ_μ is basis function μ. Re-writing the Hartee-Fock equations with the LCAO approximation leads to the Roothaan-Hall equations, where the coefficients of the atomic basis functions are solved for.[11]

Once the wavefunction is obtained, there is often still information desired. For instance, one might want to find the geometry of a molecule with the lowest energy, or see how the electronic density changes when perturbed by an electric field. To see how the wavefunction changes in the presence of a perturbation, gradients must be computed. The analytic gradient is composed of derivatives of the orbitals and derivatives of the operators. By Eq. (15), the orbitals are a sum of products of basis functions and coefficients that are calculated in the SCF procedure. The basis functions are typically Gaussian functions, so the derivatives of the basis functions should be straightforward. The derivatives of the coefficients are slightly more complicated, since they are solved variationally. If the derivative is with respect to nuclear geometry, then it is clear that the molecular orbital coefficients depend implicitly on the nuclear geometry. The molecular orbital derivative is typically expanded in the basis of the unpertubed molecular orbital coefficients:[12]

$$\frac{\partial c_{\mu i}}{\partial a} = \sum_{m}^{\text{molecular orbitals}} U_{mi}^{a} c_{\mu m} \tag{16}$$

The U^a matrix is called the response matrix. If the response matrix is known, the derivative of the molecular orbitals can be computed. Thus, the response matrix needs to be calculated somehow. Since the molecular orbital coefficients are determined variationally, the derivative of the molecular orbital coefficients can be determined by the derivative of the variational condition. For canonical Hartree-Fock orbitals, the variational condition is Eq. (12)—that the Fock matrix must be diagonal. Taking the derivative of Eq. (12) leads to a set of equations called the Coupled-Perturbed Hartree-Fock (CPHF) equations, which can be solved to compute the response matrix, and thus the derivative of the molecular orbital coefficients. For RHF wavefunctions, and other variational wavefunctions, the response matrix is not needed for the first-order derivative, since the variational condition (and for RHF, the orthonormal orbital constraint) can be used to remove the term with the response matrix in it. [12]

The Hartree-Fock method does not take into account electron correlation, since it is a single-determinant method. However, methods that include electron correlation are often much more computationally expensive than Hartree-Fock. For example, when N is the size of the basis set, Hartree-Fock calculations scale as ~ $O(N^4)$. That is, doubling the basis set leads to the time to solution increasing by 16 (2^4) times. MP2, a method that includes electron correlation through Raleigh-Schrodinger perturbation theory, scales as $O(N^5)$. Coupled-cluster singles and doubles with perturbative triples, a method that includes multiple determinants and is often considered the “gold-standard” of computational chemistry, scales as $O(N^7)$. There are multiple ways of dealing with the computational cost. One way is simply to improve the algorithm or hardware. Another

way is to simplify the energy method somehow. There are a few common ways of simplifying the energy method. One way includes starting from the *ab initio* expressions and then simplifying extensively so that there is no longer a wavefunction to be solved for. Force fields and intermolecular interaction methods often involve deriving a simplified functional form for the energy, and then fitting parameters to it. Certain intermolecular interaction methods, such as Sum of Interaction Between Fragments Ab initio computed (SIBFA)[13 14] and the EFP method, have functional forms that are derived from quantum chemistry and also have parameters that are computed from *ab initio* calculations. Another way of decreasing computational cost is by fragmentation methods, such as FMO. [1 15] The EFP and FMO methods are discussed briefly below.

In the EFP method, the interaction energy between the monomers in a system is computed. The general form for the EFP interaction energy is:

$$E_{EFP} = \sum_{A<B}^{monomers} \left(E_{AB}^{\text{Coulomb}} + E_{AB}^{\text{dispersion}} + E_{AB}^{\text{charge-transfer}} + E_{AB}^{\text{exchange-repulsion}} \right) + E^{\text{polarization}} \tag{17}$$

The Coulomb, polarization, and dispersion terms are considered “long-range” terms and can be derived from perturbation theory. The charge transfer and exchange repulsion terms are considered “short-range” terms, and can be derived by considering the intermolecular overlap. For the long-range terms, consider the interaction energy between two monomers A and B. A non-perturbed Hamiltonian is constructed by summing the individual Hamiltonians for A and B. The perturbation is the Coulomb interaction between A and B. The Coulomb interaction is typically written using a multipole moment expansion. Then, the first-order interaction energy is the Coulomb interaction energy. The second order energy is a sum of the polarization and dispersion energies. Since the

interaction energy is calculated from a simplified functional form, it is much less computationally expensive than an SCF calculation.

The FMO method begins with a many-body expansion. The system is first divided into monomers (fragments). The total energy is then written as a many-body expansion:

$$E = \sum_{A}^{monomers} E_A + \sum_{A>B}^{monomers} \left(E_{AB} - E_A - E_B\right) + \sum_{A>B>C}^{monomers} \left[\left(E_{ABC} - E_A - E_B - E_C\right) - \left(E_{AB} - E_A - E_B\right) - \left(E_{BC} - E_B - E_C\right) - \left(E_{CA} - E_A - E_C\right)\right] + \ldots \quad (18)$$

Eq. (18) adds the energy of the monomers, the interaction energy of the dimers (two-body energy), the interaction energy of the trimers (three-body energy), and so on. In the FMO method, the many-body expansion is typically truncated at the two-body or three-body term. The monomer energies are computed in the presence of a Coulomb electrostatic potential (ESP) of all the other monomers in the system. Since the electrostatic potential depends on the monomer charge densities, the monomer energies must be iterated to self-consistency. The dimer and trimer energies are calculated in the ESP, but are not iterated. The FMO method is a "nearly-linear" scaling method.[16]

Fragmentation methods lend themselves to efficient multi-level parallelization. Multi-level parallelization is important, since by itself, the speed-up due to parallelization is limited by the serial part of the code and communication overhead. With multi-level parallelization, if the problem is split up into many pieces that can be run in parallel, and each piece is parallelized itself, then scalability can be recovered. In FMO, multi-level

parallelization is formulated using the Generalized Distributed Data Interface (GDDI) library[17 18 19].

References

1. Gordon, M. S.; Fedorov, D. G.; Pruitt, S. R.; Slipchenko, L. V., Fragmentation Methods: A Route to Accurate Calculations on Large Systems. *Chemical Reviews* **2012,** *112* (1), 632-672.

2. Fedorov, D. G.; Kitaura, K., Extending the Power of Quantum Chemistry to Large Systems with the Fragment Molecular Orbital Method. *The Journal of Physical Chemistry A* **2007,** *111* (30), 6904-6914.

3. Steinmann, C.; Fedorov, D. G.; Jensen, J. H., Effective Fragment Molecular Orbital Method: A Merger of the Effective Fragment Potential and Fragment Molecular Orbital Methods. *The Journal of Physical Chemistry A* **2010,** *114* (33), 8705-8712.

4. Pruitt, S. R.; Steinmann, C.; Jensen, J. H.; Gordon, M. S., Fully Integrated Effective Fragment Molecular Orbital Method. *Journal of Chemical Theory and Computation* **2013,** *9* (5), 2235-2249.

5. Gordon, M. S.; Freitag, M. A.; Bandyopadhyay, P.; Jensen, J. H.; Kairys, V.; Stevens, W. J., The Effective Fragment Potential Method: A QM-Based MM Approach to Modeling Environmental Effects in Chemistry. *The Journal of Physical Chemistry A* **2001,** *105* (2), 293-307.

6. Hsu, P. Y.; Ge, L.; Li, X.; Stark, A. Y.; Wesdemiotis, C.; Niewiarowski, P. H.; Dhinojwala, A., Direct evidence of phospholipids in gecko footprints and spatula–

substrate contact interface detected using surface-sensitive spectroscopy. *Journal of The Royal Society Interface* **2012,** *9* (69), 657.

7. Day, P. N.; Jensen, J. H.; Gordon, M. S.; Webb, S. P.; Stevens, W. J.; Krauss, M.; Garmer, D.; Basch, H.; Cohen, D., An effective fragment method for modeling solvent effects in quantum mechanical calculations. *The Journal of Chemical Physics* **1996,** *105* (5), 1968-1986.

8. Levine, I. N., Quantum Chemistry. Third Edition ed.; Allyn and Bacon, Inc: Newton, MA, 1983.

9. Szabo, A.; Ostlund, N. S., *Modern Quantum Chemistry*. First Edition, Revised ed.; McGraw-Hill: New York, 1989.

10. Born, M.; Oppenheimer, R., On the quantum theory of molecules. *Ann. Phys* **1927,** *84* (4), 457-484.

11. Roothaan, C. C. J., New Developments in Molecular Orbital Theory. *Reviews of Modern Physics* **1951,** *23* (2), 69-89.

12. Yamaguchi, Y.; Schaefer, H. F.; Osamura, Y.; Goddard, J., *A New Dimension to Quantum Chemistry: Analytical Derivative Methods in Ab Initio Molecular Electronic Structure Theory*. Oxford University Press: New York, 1994.

13. Antony, J.; Piquemal, J.-P.; Gresh, N., Complexes of thiomandelate and captopril mercaptocarboxylate inhibitors to metallo-β-lactamase by polarizable molecular mechanics. Validation on model binding sites by quantum chemistry. *Journal of Computational Chemistry* **2005,** *26* (11), 1131-1147.

14. Nohad, G., Development, Validation, and Applications of Anisotropic Polarizable Molecular Mechanics to Study Ligand and Drug-Receptor Interactions. *Current Pharmaceutical Design* **2006,** *12* (17), 2121-2158.

15. Pruitt, S. R.; Bertoni, C.; Brorsen, K. R.; Gordon, M. S., Efficient and Accurate Fragmentation Methods. *Accounts of Chemical Research* **2014,** *47* (9), 2786-2794.

16. *Linear-Scaling Techniques in Computational Chemistry and Physics*. Springer Netherlands: 2011.

17. Fedorov, D. G.; Olson, R. M.; Kitaura, K.; Gordon, M. S.; Koseki, S., A new hierarchical parallelization scheme: Generalized distributed data interface (GDDI), and an application to the fragment molecular orbital method (FMO). *Journal of Computational Chemistry* **2004,** *25* (6), 872-880.

18. Fletcher, G. D.; Schmidt, M. W.; Bode, B. M.; Gordon, M. S., The Distributed Data Interface in GAMESS. *Computer Physics Communications* **2000,** *128* (1), 190-200.

19. Ryan, M. O.; Michael, W. S.; Mark, S. G.; Alistair, P. R., Enabling the Efficient Use of SMP Clusters: The GAMESS/DDI Model. *SC Conference* **2003**, 41-41.

CHAPTER 2. ANALYTIC GRADIENTS FOR THE EFFECTIVE FRAGMENT MOLECULAR ORBITAL METHOD

A paper published in

Journal of Chemical Theory and Computation **2016,** *12* (10), 4743-4767

Colleen Bertoni and Mark S. Gordon

Abstract

The analytic gradient for the Coulomb, polarization, exchange-repulsion, and dispersion terms of the fully integrated effective fragment molecular orbital (EFMO) method is derived and the implementation is discussed. The derivation of the EFMO analytic gradient is more complicated than that for the effective fragment potential (EFP) gradient, because the geometry of each EFP fragment is flexible (not rigid) in the EFMO approach. The accuracy of the gradient is demonstrated by comparing the EFMO analytic gradient with the numeric gradient for several systems, and by assessing the energy conservation during an EFMO NVE ensemble molecular dynamics simulation of water molecules. In addition to facilitating accurate EFMO geometry optimizations, this allows calculations with flexible EFP fragments to be performed.

Introduction

Many interesting chemical systems involve large molecules (such as protein-ligand complexes and enzyme catalysis) or many molecules (such as chemical reactions in solution). However, it is computationally expensive to perform *ab initio* calculations on large systems. Several methods have been developed to make such calculations feasible. These include using parameterized classical force fields to model interactions

between molecules, hybrid quantum mechanics (QM)/molecular mechanics (MM) methods, and fragmentation schemes that perform *ab initio* calculations on fragments of a system and then combine the fragment results.[1]

The effective fragment molecular orbital (EFMO) method was developed to combine the sophisticated semi-classical effective fragment potential (EFP) method[2] with the fragment molecular orbital (FMO) method[3], in order to take advantage of the computational efficiency of both[4]. The FMO method is a fragmentation method based on a many-body expansion of the energy that has been applied extensively to molecular clusters and biological systems.[5] The EFP method is a sophisticated model potential method that is derived from first principles, with no empirically fitted parameters. Fragment geometries in the EFP method are rigid. The EFP method decomposes the interaction energy into five terms: Coulomb, polarization, exchange-repulsion, dispersion, and charge-transfer. It has enabled many studies of intermolecular interactions, including solvent effects on chemical processes.[6] The original EFMO method combined the fragmentation scheme of the FMO method with just the Coulomb and polarization interaction energy terms of the EFP method. An approximate gradient for the original EFMO method was reported.[4]

The EFMO method has recently been greatly improved, by incorporating the EFP dispersion, exchange-repulsion, and charge-transfer interaction terms.[7] This improved method was called the fully integrated effective fragment molecular orbital (FIEFMO) method in Ref. 7. The gradient for the additional terms was not derived or implemented. Hereinafter the FIEFMO method will be referred to simply as the EFMO method, and the

original method with just the Coulomb and polarization terms will be referred to as the original EFMO method.

There are many motivations for the development of fully analytic gradients. Geometry optimizations of molecules are typically much more accurate, numerically stable and less time consuming with analytic, rather than numeric gradients. Transition state searches and reaction path following are enabled by analytic gradients, and fully analytic gradients are essential for molecular dynamics (MD) simulations.[8]

This work presents the derivation and implementation of the gradient terms that are needed to make the original EFMO gradient fully analytic, and the Coulomb, exchange-repulsion, polarization, and dispersion terms that are needed to make the fully integrated EFMO gradient fully analytic. The gradient of the charge-transfer term, usually the least important and most computationally demanding component of the EFP interaction energy,[43] has not been derived or implemented, as discussed further in Section 3.3. Since the EFMO analytic gradient involves EFP interaction energy derivatives without assuming the fragments are rigid, an added benefit of the derivation presented here is that it provides insight regarding which EFP interaction energy terms are most important with regard to fragment flexibility.

This paper is organized as follows. Section 2 introduces the notation used; Section 3 gives a brief overview of the EFMO energy expression; Section 4 presents the derivation of the EFMO gradient while noting the differences with the EFP gradient; Section 5 discusses the implementation of the EFMO analytic gradient; Section 6 presents test calculations on a variety of systems (a cluster of water molecules, a cluster of water molecules, methanol molecules, and dimethyl sulfoxide molecules, and an ionic

liquid pair) and discusses the consequent potential energy surfaces; Section 7 presents timing comparisons to FMO gradients. The final section concludes.

Notation and definitions

Much of the notation and definitions are adopted from Yamaguchi et al.[9] This work assumes a basis set that contains both contracted and uncontracted Gaussian functions.

2.1 Indices

-- *i,j,k* denote occupied canonical molecular orbital (occ CMO) indices

-- *l,m,n,o* denote localized molecular orbital (LMO) indices

-- *a,b,c* denote virtual molecular orbital (vir) indices

-- *p,q,r,s* denote any canonical molecular orbital (occ or vir) indices

-- *t,u* denote primitive Gaussian (PG) indices

-- μ, ν, ξ, σ denote atomic orbital (AO) indices

-- *A,B,C* denote fragment indices

-- *I,J,K* denote nuclei indices or multipole expansion points

-- $\alpha, \beta, \gamma, \kappa$ denote directions *x*, *y*, or *z*

2.2 Definitions

Z_I is the nuclear charge on atom *I*

S_{ps} is the overlap integral between orbitals *p* and *s*

$c_{\mu p}$ is the canonical or virtual MO coefficient of AO μ in MO *p*

$c_{\mu l}^{L}$ is the localized MO coefficient of AO μ in LMO *l*

$P_{\mu\nu}\left(=2\sum_{i}^{occ} c_{\mu i} c_{\nu i}\right)$ is the restricted Hartree-Fock (RHF) density matrix element for AOs μ and ν

2.3 Superscript Notation

A variable with a superscript in parentheses, e.g., $S_{pq}^{(x)}$, denotes that the derivative with respect to x is taken only of the AO terms, and any molecular orbital coefficients are considered to be constant. A variable with a fragment index as a superscript denotes the variable for that fragment. However, if the appropriate fragment is clear by context, the superscript might be omitted.

2.4 Derivative of a canonical MO coefficient with respect to a perturbation

The derivative of an MO coefficient can be written in terms of the orbital response matrix[9] U^x:

$$\frac{\partial c_{\mu p}}{\partial x} = \sum_{q}^{CMO} U_{qp}^{x} c_{\mu q} \tag{2.1}$$

U^x is the orbital response matrix to a perturbation x. In this work, there are nuclear perturbations, which will be denoted by an x, and field perturbations, which will be denoted by a Greek letter. U^x is an N_{MO} X N_{MO} matrix, where N_{MO} is the number of molecular orbitals. It is convenient to think about the response matrix in terms of sub-matrices; i.e., the occupied orbital-occupied orbital (occ-occ) block, virtual orbital-virtual orbital (vir-vir) block, and virtual orbital-occupied orbital (vir-occ) block.

2.5 Localized molecular orbital notation and definitions

Localized MOs $|I\rangle$ are related to canonical MOs by a unitary transformation L:

$$|l\rangle = \sum_{i}^{\substack{occ \\ CMO}} L_{li}|i\rangle$$

$$c_{\mu l}^{L} = \sum_{i}^{\substack{occ \\ CMO}} L_{li} c_{\mu i}$$

(2.2)

L is a unitary transformation matrix $(\sum_{m}^{LMO} L_{mn}L_{ml} = \delta_{\ln})$ calculated by a localization method, such as the Boys method[10], which was originally proposed by Edmiston and Ruedenberg[11,12].

2.6 Derivative of a localized MO coefficient with respect to a nuclear perturbation, written in terms of the canonical response matrix and localization response matrix

Following previous studies that considered perturbed localized molecular orbitals,[13,14,15,16] the nuclear derivative of the LMO coefficient is split into a term that includes a localization response matrix (which describes how the localization transform changes with geometry) and a term that includes the canonical response matrix (which describes how the canonical molecular orbitals change with geometry):

$$\frac{\partial c_{\mu l}^{L}}{\partial x} = \sum_{i}^{\substack{occ \\ CMO}} \frac{\partial}{\partial x}\left(L_{li} c_{\mu i}\right) = \sum_{n}^{LMO} c_{\mu n}^{L} v_{nl}^{x} + \sum_{i}^{\substack{occ \\ CMO}} L_{li} \sum_{q}^{\substack{occ+vir \\ CMO}} U_{qi}^{x} c_{\mu q}$$

(2.3)

where v_{nl}^{x} is the localization transform response matrix.

The EFMO method

The EFMO method is an integration of the FMO and EFP methods, designed to take advantage of the speed and accuracy of the two methods. The FMO and EFP

methods are described briefly in Sections 3.1 and 3.2, respectively. Since the EFMO method has been described previously[7,4], only a brief overview is given in Section 3.3.

3.1 The Fragment Molecular Orbital (FMO) Method

Ref. 5 provides an excellent review of the FMO method. In general, the system is divided into fragments (monomers) in a chemically sensible way, for example, using common functional groups. Then, the energy of each monomer is calculated in a Coulomb field due to the other monomers. Since the field depends on the electron density of the monomers, the Coulomb field is converged self-consistently. This level of theory is called FMO1. After it has converged, the dimer (pair of fragments) and trimer (set of three fragments) energy may be computed in the self-consistently converged monomer Coulomb field as well. The monomer, dimer, and possibly trimer energies are added together to obtain the total energy for the system. The computational expense increases when one adds all dimers (FMO2) and (especially) trimers (FMO3) to the monomer calculations.

The total FMO2 energy can be written as

$$\sum_{A}^{\text{fragments}} E_A + \sum_{A>B}^{\text{fragments}} \left(E_{AB} - E_A - E_B\right) \tag{3.1}$$

E_A and E_{AB} are the energies of the monomers and dimers, respectively. Approximations to the dimer energies can be used to decrease the computational cost. An additional advantage of the FMO method is that it is naturally parallelizable. The FMO method is parallelized with the general distributed data interface (GDDI)[17]. Because the FMO method is a generally applicable approach to dividing a system into smaller pieces, it can be combined with any electronic structure method. The usual notation is FMO/A, where

A is a specific quantum chemistry method, such as second order perturbation theory (MP2).

3.2 The Effective Fragment Potential (EFP) Method

The EFP method was initially developed to model aqueous solvent effects[2]. In the EFP method, the system is split into solute and solvent molecules. In this context the solute molecules are typically calculated using an *ab initio* electronic structure method. The one-electron term in the solute Hamiltonian is modified by an explicit EFP solvent model potential. An EFP is generated by performing a single *ab initio* calculation on a solvent molecule, and then using the wavefunction to generate the input for the potential. Thus, it contains no empirical or fitted parameters. EFP internal geometries are rigid. More broadly, the EFP method can be used to explore intermolecular (non-covalent) interactions, without the need for an *ab initio* component. In this case, the system is divided into fragments that are modeled with EFPs. The EFP only (no *ab initio* solute) method is considered in this work.

The EFP method decomposes the interaction energy of a system into the Coulomb energy, exchange repulsion energy, dispersion energy, charge-transfer energy, and many-body polarization energy terms. All terms are pairwise additive except for the polarization energy. The energy can be written as:

$$E_{AB}^{EFP} = E_{AB}^{Coul} + E_{AB}^{rep} + E_{AB}^{disp} + E_{AB}^{ct}$$
$$E_{total}^{EFP} = \sum_{A>B}^{\text{fragments}} E_{AB}^{EFP} + E_{total}^{pol} \qquad (3.2)$$

The EFMO method uses the interaction energy calculations, so they are considered in more detail below. Since the gradient involves taking the derivative of the

energy terms, it is important to first consider the details of the energy expressions. The charge-transfer term is not considered here.

3.2.1 Coulomb term

The Coulomb energy can be thought of as the energy produced from the interaction of the static charge density of two molecules. In the EFP method, the Coulomb energy is based on a Taylor series expansion of Coulomb's law, and a distributed multipole moment expansion using the Stone distributed multipole analysis (DMA)[18]. Multipole moment expansion sites are distributed across each fragment in the system. The Coulomb contribution to the interaction energy between two EFP fragments is the sum of the interaction energy between all pairs of multipole moments.

$$E_{AB}^{Coul} = \sum_{I}^{A}\sum_{J}^{B}\left[\begin{array}{l} q^J q^I T^{IJ} - \sum_{\alpha}^{x,y,z} q^J \mu_\alpha^I T_\alpha^{IJ} + \frac{1}{3}\sum_{\alpha,\beta}^{x,y,z} q^J \Theta_{\alpha\beta}^I T_{\alpha\beta}^{IJ} + \sum_{\alpha}^{x,y,z} \mu_\alpha^J q^I T_\alpha^{IJ} \\ -\sum_{\alpha,\beta}^{x,y,z} \mu_\alpha^J \mu_\beta^I T_{\alpha\beta}^{IJ} + \frac{1}{3}\sum_{\alpha,\beta,\gamma}^{x,y,z} \mu_\alpha^J \Theta_{\beta\gamma}^I T_{\alpha\beta\gamma}^{IJ} + \ldots \end{array}\right] \tag{3.3}$$

In Eq. (3.3) E_{AB}^{Coul} is the Coulomb interaction energy between fragments *A* and *B*, *I* (*J*) runs over all multipole moment expansion points in *A* (*B*), q^I is the monopole on site *I*, μ^I is the dipole on site *I*, Θ^I is the quadrupole on site *I*, $T_{\alpha\beta\ldots\nu}^{IJ} = \nabla_\alpha \nabla_\beta \ldots \nabla_\nu \frac{1}{R_{IJ}}$ is the multipole interaction tensor for sites *I* and *J*, and R_{IJ} is the distance between expansion points *I* and *J*.

The multipole moments on each site are calculated using the DMA. This is described in more detail in the Supporting Information. The multipole moments can be expressed as:

$$q^I = Z_I - \sum_{\mu\nu}^{AO\in A} P_{\mu\nu} \sum_{ut\ \text{nearest}\ I}^{\substack{PG\ u\in\mu \\ PG\ t\in\nu}} P'_{ut} \langle u \,|\, t \rangle$$

$$\mu_x^I = -\sum_{\mu\nu}^{AO\in A} P_{\mu\nu} \sum_{ut\ \text{nearest}\ I}^{\substack{PG\ u\in\mu \\ PG\ t\in\nu}} P'_{ut} \langle u \,|\, (x - x_I) \,|\, t \rangle$$

...

(3.4)

where x_I is the location of expansion center I and P'_{ut} is the primitive Gaussian cross term that contains the product of the contraction coefficients for PG u and t.

To account for charge penetration between interacting fragments A and B, an overlap-based damping term is computed, and added to the Coulomb interaction energy term[17]. The expression for this term is:

$$E_{AB}^{chgpen} = \sum_{l}^{LMO\in A} \sum_{m}^{LMO\in B} \frac{-2S_{lm}^2}{R_{lm}} \sqrt{\left(\frac{1}{-2\ln|S_{lm}|} \right)}$$

(3.5)

where R_{lm} is the distance between the LMO centroids of l and m, and $\langle l \,|\, x \,|\, l \rangle$ is the centroid in the x-direction for LMO l.

3.2.2 Exchange repulsion term

The exchange repulsion energy is a quantum mechanical contribution to the interaction energy that arises due to the Pauli exclusion principle. It is derived from approximations to the overlap of the wavefunctions of two isolated molecules[20]. The

exchange repulsion interaction energy between fragments *A* and *B* and can be expressed as

$$E_{AB}^{rep} = -2\sum_{l}^{LMO\in A}\sum_{m}^{LMO\in B} 2\sqrt{\frac{-2\ln S_{lm}}{\pi}}\frac{S_{lm}^2}{R_{lm}} - 2\sum_{l}^{LMO\in A}\sum_{m}^{LMO\in B} S_{lm}\left[\sum_{n}^{LMO\in A} F_{ln}^{A}S_{nm} + \sum_{n}^{LMO\in B} F_{mn}^{B}S_{nl} - 2T_{lm}\right]$$
$$+2\sum_{l}^{LMO\in A}\sum_{m}^{LMO\in B} S_{lm}^2\left[-\sum_{J}^{nuclei\in B}\frac{Z_J}{R_{lJ}} + 2\sum_{n}^{LMO\in B}\frac{1}{R_{ln}} - \sum_{I}^{nuclei\in A}\frac{Z_I}{R_{Im}} + 2\sum_{n}^{LMO\in A}\frac{1}{R_{nm}} - \frac{1}{R_{lm}}\right] \quad (3.6)$$

R_{lJ} is the distance between MO centroid *l* and atom *J,* T_{lm} is the kinetic energy integral between *l* and *m*, and F_{ln}^{A} is the Fock matrix element between *l* and *n* on fragment *A*.

3.2.3 Polarization term

The polarization energy (sometimes referred to as the induction interaction since it arises from multipole-induced multipole interactions) can be thought of as the interaction energy that occurs due to the change in the charge distribution of one molecule by the electric field due to the charge distribution of the other molecule.

In the EFP method, the polarization energy is calculated by placing localized molecular orbital dipole polarizability tensors, $\alpha_{\beta\gamma}$, on the LMO centroids of each fragment. The electric field of the other fragments (due to both the static multipole field and the induced dipoles on the other fragments) acts on the polarizability tensors and self-consistently generates induced dipoles, *p*, on the LMO centroids of the fragment[21]. The induced dipole on LMO centroid *l* in the β direction in fragment *A*, $p_{l,\beta}^{A}$, is:

$$p_{l,\beta}^{A} = \sum_{\gamma}^{\{x,y,z\}} \alpha_{l,\beta\gamma} E_{l,\gamma}^{tot,A} \quad (3.7)$$

where $\alpha_{l,\beta\gamma}$ is the dipole polarizability tensor on LMO l, γ,κ are field directions, and $E_{l,\gamma}^{tot,A}$ is the total field in the γ direction at LMO l. Since $E_{l,\gamma}^{tot,A}$ can be written in terms of a static electric field, $E_{l,\gamma}^{0,A}$, and a field due to induced dipoles, Eq. (3.7) can be rewritten as:

$$p_{l,\beta}^{A} = \sum_{\gamma}^{\{x,y,z\}} \alpha_{l,\beta\gamma} \left(E_{l,\gamma}^{0,A} + \sum_{B\neq A}^{\text{fragments}} \sum_{m}^{LMO\in B} \sum_{\kappa}^{\{x,y,z\}} T_{\gamma\kappa}^{lm} p_{m,\kappa}^{B} \right) \tag{3.8}$$

where $T_{\gamma\kappa}^{lm}$ is the dipole moment interaction tensor for sites l and m. $E_{l,\gamma}^{0,A}$ is the electric field at site l on fragment A due to the static DMA-calculated multipole moments, q^I, μ_β^I, $\Theta_{\beta\gamma}^I$, on all multipole expansion points I on fragments other than A in the system:

$$E_{l,\gamma}^{0,A} = \sum_{B\neq A}^{\text{fragments}} \sum_{I}^{B} E_{lI,\gamma}^{0} = \sum_{B\neq A}^{\text{fragments}} \sum_{I}^{B} \left(q^I T_\gamma^{lI} + \sum_{\alpha}^{\{x,y,z\}} \mu_\alpha^I T_{\gamma\alpha}^{lI} + \frac{1}{3} \sum_{\alpha\beta}^{\{x,y,z\}} \Theta_{\alpha\beta}^I T_{\gamma\alpha\beta}^{lI} \right) \tag{3.9}$$

As in the Coulomb term, in this work, the expansion sites are only on the nuclei.

Collecting the terms containing the induced dipoles, Eq. (3.7) can be written as

$$p_{l,\beta}^{A} = \sum_{B}^{\text{fragments}} \sum_{m}^{LMO\in B} \sum_{\alpha}^{\{x,y,z\}} (D^{-1})_{lm,\beta\alpha} E_{m,\alpha}^{0,B} \tag{3.10}$$

where:

$$D_{ll,\beta\gamma} = (\alpha_l)^{-1}{}_{\beta\gamma}$$
$$D_{lm,\beta\gamma} = 0 \text{ (when } l \text{ and } m \text{ are on the same fragment)}$$
$$= -T^{lm}_{\beta\gamma} \text{ (when } l \text{ and } m \text{ are on different fragments)}$$

After generating the converged induced dipoles, the polarization energy can be calculated as

$$E^{pol} = \sum_{A}^{\text{fragments}} \left[-\frac{1}{2} \sum_{n}^{LMO\in A} \sum_{\alpha}^{\{x,y,z\}} E^{0,A}_{n,\alpha} p^{A}_{n,\alpha} \right]$$
$$= \sum_{A}^{\text{fragments}} \left[-\frac{1}{2} \sum_{n}^{LMO\in A} \sum_{\alpha}^{\{x,y,z\}} E^{0,A}_{n,\alpha} \sum_{B}^{\text{fragments}} \sum_{m}^{LMO\in B} \sum_{\beta}^{\{x,y,z\}} (D^{-1})_{nm,\alpha\beta} E^{0,B}_{m,\beta} \right] \tag{3.11}$$

The dipole polarizability tensors on the LMO centroids of each fragment are calculated by decomposing the total dipole polarizability tensor for each fragment into contributions from each LMO[22,23]. The dipole polarizability tensor on LMO centroid n on fragment A is:

$$\alpha_{n,\beta\gamma} = -4 \sum_{jk}^{\substack{occ \\ CMO\in A}} \sum_{a}^{vir\in A} L_{nj} L_{nk} U^{\gamma A}_{aj} \langle a | \beta | k \rangle \tag{3.12}$$

In Eq. (3.12) γ is a field perturbation.

The multipole interaction tensors are multiplied by a damping function, $F^{pol}_{damp,lI} = 1 - \exp\left(-R^2_{lI}\sqrt{fg}\right)\left(1 + R^2_{lI}\sqrt{fg}\right)$.[24] (The terms f and g are constants usually set to 0.6.) The damped multipole interaction tensors can be written as $T^{lI,damped}_{\alpha\beta\ldots\nu} = F^{pol}_{damp,lI} T^{lI}_{\alpha\beta\ldots\nu}$. Substituting the damped multipole interaction tensors into the static electric field, the damped static electric fields become

$$E_{l,\gamma}^{0,A,damped} = \sum_{B\neq A}^{\text{fragments}} \sum_{I}^{B} E_{lI,\gamma}^{0,damped} = \sum_{B\neq A}^{\text{fragments}} \sum_{I}^{B} \left(q^I T_{\gamma}^{lI,damped} + \sum_{\alpha}^{\{x,y,z\}} \mu_{\alpha}^I T_{\gamma\alpha}^{lI,damped} + \frac{1}{3} \sum_{\alpha\beta}^{\{x,y,z\}} \Theta_{\alpha\beta}^I T_{\gamma\alpha\beta}^{lI,damped} \right)$$

(3.13)

and the damped induced dipoles, $p_{l,\beta}^{A,damped}$, can be written as:

$$p_{l,\beta}^{A,damped} = \sum_{\gamma}^{\{x,y,z\}} \alpha_{l,\beta\gamma} \left(E_{l,\gamma}^{0,A,damped} + \sum_{B\neq A}^{\text{fragments}} \sum_{m}^{LMO\in B} \sum_{\kappa}^{\{x,y,z\}} T_{\gamma\kappa}^{lm,damped} p_{m,\kappa}^{B,damped} \right)$$

(3.14)

3.2.4 Dispersion term

The dispersion energy can be thought of as the energy that arises from the interaction between induced multipoles on two molecules. The dispersion energy can be derived from Rayleigh-Schrodinger perturbation theory, starting from the sum of the Hamiltonians for two noninteracting molecules[18]. The second order correction to the energy contains the dispersion energy.

The dispersion energy between fragments *A* and *B* can be written in terms of inverse powers of the distance between the molecules.

$$E_{AB}^{disp} = \frac{C_{6,AB}}{R_{AB}^6} + \frac{C_{7,AB}}{R_{AB}^7} + \frac{C_{8,AB}}{R_{AB}^8} + \ldots$$

(3.15)

In the EFP method, the dispersion energy is calculated by distributing isotropic dynamic polarizabilty tensors on the LMO centroids of each fragment. For this work, the total dispersion energy between fragments *A* and *B* is approximated as[25]

$E_{AB}^{disp} = \frac{C_{6,AB}}{R_{AB}^6} + \frac{1}{3}\frac{C_{6,AB}}{R_{AB}^6}$, where all terms with higher order than the R^{-6} term have been approximated as $\frac{1}{3}\frac{C_{6,AB}}{R_{AB}^6}$. The R^{-7} term has recently been derived and implemented,[26,27] but is not used in this work.

The dispersion energy between fragments *A* and *B* can then be written in atomic units as

$$E_{AB}^{disp} = \frac{4}{3}\left(-\frac{3}{\pi} \sum_{l}^{LMO\in A} \sum_{m}^{LMO\in B} \frac{1}{R_{lm}^6} \left(\int_0^\infty \bar{\alpha}^l(i\omega)\bar{\alpha}^m(i\omega) d\omega \right) \right) \tag{3.16}$$

where $\bar{\alpha}^l = \frac{1}{3}\sum_{\beta}^{\{x,y,z\}} \alpha_{\beta\beta}^l(i\omega)$, and $\alpha_{\beta\gamma}^l(i\omega)$ is the distributed dynamic polarizability at LMO *l* for a frequency $i\omega$.

Using a 12-point Gauss-Legendre quadrature and substitution of variables, the integral can be rewritten as a sum:

$$E_{AB}^{disp} = \frac{4}{3}\left(-\frac{3}{\pi} \sum_{l}^{LMO\in A} \sum_{m}^{LMO\in B} \frac{1}{R_{lm}^6} \sum_{f}^{12} \left(w_f \frac{2v_0}{(1-t_f)^2} \bar{\alpha}^l(i\omega_f)\bar{\alpha}^m(i\omega_f) \right) \right) \tag{3.17}$$

where $w_f, v_0,$ and t_f are constants used in the numerical quadrature.

The distributed dynamic polarizability on a fragment at LMO *l* for a frequency $i\omega$, $\alpha_{\beta\gamma}^l(i\omega)$, can be calculated as follows:

$$\alpha_{\beta\gamma}^l(i\omega) = -2\sum_{a}^{vir} \left(\sum_{j}^{occ\ CMO} \langle a | \beta | j \rangle L_{lj} \right) \left(\sum_{i}^{occ\ CMO} Z_{ai}^{\gamma}(i\omega) L_{li} \right)$$

(3.18)

where $Z_{ai}^{\gamma}(i\omega)$ is the response vector that is calculated from solving the dynamic analog of the CPHF equations (time-dependent coupled perturbed Hartree-Fock theory)[28], and $\boldsymbol{\gamma}$ is a field perturbation. The TD CPHF equations are:

$$\sum_{b}^{vir}\sum_{j}^{occ\,CMO}\sum_{c}^{vir}\sum_{k}^{occ\,CMO}\left(H_{ai,bj}^{(2)}H_{bj,ck}^{(1)}Z_{ck}^{\gamma}(i\omega)\right)-(i\omega)^2 Z_{at}^{\gamma}(i\omega)=-2\sum_{b}^{vir}\sum_{j}^{occ\,CMO}H_{ai,bj}^{(2)}\langle b\,|\,\gamma\,|\,j\rangle$$

$$H_{ai,bj}^{(2)}=(aj\,|\,bi)-(ab\,|\,ij)+(\epsilon_a-\epsilon_i)\delta_{ab}\delta_{ij}$$

$$H_{ai,bj}^{(1)}=4(ai\,|\,bj)-(aj\,|\,bi)-(ab\,|\,ji)+(\epsilon_a-\epsilon_i)\delta_{ab}\delta_{ij}$$

(3.19)

ϵ_a,ϵ_i are virtual and occupied orbital energies, respectively.

The EFP method contains a multiplicative damping factor for the dispersion term[24]. Incorporating the damping term, the dispersion energy becomes:

$$E_{AB}^{disp,damped}=\frac{4}{3}\left(-\frac{3}{\pi}\sum_{l}^{LMO\in A}\sum_{m}^{LMO\in B}F_{lm}^{disp,damp}\frac{1}{R_{lm}^{6}}\left(\int_{0}^{\infty}\bar{\alpha}^{l}(i\omega)\bar{\alpha}^{m}(i\omega)d\omega\right)\right)$$

(3.20)

In the EFMO method, the damping function is an overlap-based formula

$$F_{lm}^{disp,damp}=1-|S_{lm}|^2\sum_{n=0}^{6}\left(\frac{-2\ln|S_{lm}|}{n!}\right)^{n/2}$$

(3.21)

The damping function in Eq. (3.21) is a recent improvement on the original EFP damping function[29].

3.3 General EFMO energy expression

The EFMO energy expression is a many-body expansion, similar to the FMO energy expression. As with the FMO method, the EFMO method begins by dividing the system into fragments. However, the monomer and dimer energy calculations differ: the EFMO method contains a many-body EFP polarization term, generated from all of the fragments and does not require the self-consistent convergence of the monomer Coulomb field. Importantly, the EFMO method inherits the GDDI parallelization of the FMO method.

The general EFMO energy expression is:

$$E^{EFMO} = \sum_{A}^{\text{fragments}} E_A^0 + \sum_{A>B}^{R_{A,B}\le R_{cut}} (\Delta E_{AB}^0 - E_{AB}^{pol}) + \sum_{A>B}^{R_{A,B}>R_{cut}} (E_{AB}^{EFP}) + E_{tot}^{pol} \tag{3.22}$$

E_A^0 is the gas phase energy of fragment A

$\Delta E_{AB}^0 = E_{AB}^0 - E_A^0 - E_B^0$ (the dimer 2-body interaction energy)

E_{AB}^{EFP} is the long-range EFP energy between fragments *A* and *B*

E_{tot}^{pol} is the EFP polarization energy for the entire system

E_{AB}^{pol} is the EFP polarization energy for fragments *A* and *B*

EFMO dimer calculations are performed with the chosen *ab initio* method (e.g., MP2) unless the two fragments in the dimer are farther apart than a predetermined cutoff R_{cut}. In the latter case, the dimer calculation is done using the EFP method. The inter-fragment distance $R_{A,B} = \min_{I\in A, J\in B} \frac{|\mathbf{r}_I - \mathbf{r}_J|}{V_I + V_J}$ is the relative minimum interatomic distance

between atoms *I* on fragment *A* and atoms *J* on fragment *B*, weighted by the sum of the van der Waals radii, V_I and V_J. $R_{A,B}$ is compared to R_{cut} to determine if the EFP method is to be used to calculate the dimer energy.

The EFMO energy is calculated by summing the gas phase *ab initio* energy of each monomer (fragment). Then, one loops over all pairs of monomers, and the dimer energy is added to the monomer energy. If the distance between two monomers is less than R_{cut}, the dimer energy is calculated with the chosen gas phase *ab initio* method (subtracting out the EFP polarization energy of the dimer to avoid double counting). If the distance is greater than R_{cut}, the dimer energy is approximated by the EFP interaction energy. The EFP polarization energy of the entire system is then added to the dimer and monomer energies.

For this work, the long-range EFP energy is:

$$E_{AB}^{EFP} = E_{AB}^{Coul} + E_{AB}^{rep} + E_{AB}^{disp} \tag{3.23}$$

The charge-transfer term is not included in this work. As noted above, the charge transfer term is the most computationally expensive component of the EFP energy, and it is usually the smallest term in the EFP interaction energy. Charged systems are an exception.[24] Additionally, since charge transfer is a short-range interaction[18], most of the charge transfer interaction energy will be captured by the *ab initio* dimer interaction. Therefore, it is not necessary to have charge transfer in the long-range EFP interaction energy.

Substituting Eq. (3.23) into Eq. (3.22), the energy expression becomes:

$$E^{EFMO} = \sum_{A}^{\text{fragments}} E_A^0 + \sum_{A>B}^{R_{A,B}\le R_{cut}} (\Delta E_{AB}^0 - E_{AB}^{pol}) + \sum_{A>B}^{R_{A,B}>R_{cut}} (E_{AB}^{Coul} + E_{AB}^{rep} + E_{AB}^{disp}) + E_{tot}^{pol} \tag{3.24}$$

This can be written as

$$E^{EFMO} = E_{ab\ initio}^{EFMO} + E_{EFP}^{EFMO} \tag{3.25}$$

where $E_{ab\ initio}^{EFMO} = \sum_{A}^{\text{fragments}} E_A^0 + \sum_{A>B}^{R_{A,B}\le R_{cut}} \Delta E_{AB}^0$ and

$$E_{EFP}^{EFMO} = \sum_{A>B}^{R_{A,B}\le R_{cut}} \left(-E_{AB}^{pol}\right) + \sum_{A>B}^{R_{A,B}>R_{cut}} (E_{AB}^{Coul} + E_{AB}^{rep} + E_{AB}^{disp}) + E_{tot}^{pol}$$

Analytic EFMO gradient

The expression for the EFMO gradient is:

$$\frac{\partial E^{EFMO}}{\partial x_K} = \sum_{A}^{\text{fragments}} \frac{\partial E_A^0}{\partial x_K} + \sum_{A>B}^{R_{A,B}\le R_{cut}} \left(\frac{\partial \Delta E_{AB}^0}{\partial x_K} - \frac{\partial E_{AB}^{pol}}{\partial x_K} \right) + \sum_{A>B}^{R_{A,B}>R_{cut}} \left(\frac{\partial E_{AB}^{Coul}}{\partial x_K} + \frac{\partial E_{AB}^{rep}}{\partial x_K} + \frac{\partial E_{AB}^{disp}}{\partial x_K} \right) + \frac{\partial E_{tot}^{pol}}{\partial x_K} \tag{4.1}$$

Each term in Eq. (3.24) is differentiated with respect to the *x*-coordinate of atom *K* (x_K). The EFMO energy expression is a combination of gas phase *ab initio* energy terms ($E_A^0, \Delta E_{AB}^0$) and EFP interaction energy terms ($E_{AB}^{pol}, E_{AB}^{Coul}, E_{AB}^{rep}, E_{AB}^{disp}, E_{tot}^{pol}$). Thus, the EFMO gradient is derived from *ab initio* gradient terms and EFP interaction energy gradient terms.

To make the different types of terms clear, Eq. (3.25) can be used to write Eq. (4.1) as:

$$\frac{\partial E^{EFMO}}{\partial x_K} = \frac{\partial E^{EFMO}_{ab\ initio}}{\partial x_K} + \frac{\partial E^{EFMO}_{EFP}}{\partial x_K} \tag{4.2}$$

4.1 Gas phase gradient terms

Two *ab initio* gas phase terms ($\frac{\partial E^0_A}{\partial x_K}, \frac{\partial \Delta E^0_{AB}}{\partial x_K}$) are computed using standard methodology[30], so they are not discussed here. Note that if the gas-phase *ab initio* method chosen has response terms (e.g., MP2), response equations for the monomers and dimers must be solved. For the monomer terms, the responses can be added to the response equations that arise from the EFP interaction energy gradient terms (formulated in later sections) and solved without additional cost. For the dimer terms, the response equations are solved separately, and added into the gradient.

4.2 EFP interaction energy gradient terms

The gradient terms for the EFP method were derived and implemented previously[2]. However, the EFP gradient terms cannot be used in EFMO directly, because the EFP method has rigid fragments while the EFMO method has flexible fragments. In the EFMO method, the internal geometry can change during a geometry optimization or molecular dynamics simulation, so the gradient must take this flexibility into account.

For each term in the EFP interaction energy, a general formula for the nuclear gradient is presented below. The EFP terms in the EFMO gradient and the EFP translational gradient in the EFP method can both be derived from the general formula for the EFP nuclear gradient. After presenting the general formula for the nuclear gradient, the terms needed for the EFP method will be briefly discussed, since they are already

implemented and can be reused in the EFMO method. Then, the remaining terms needed for the EFMO method will be discussed.

To compare the EFP and EFMO gradient terms, it is useful to note the following points:

1) The translational gradient of the EFP interaction energy between fragments *A* and *B* with respect to the coordinates of fragment *A* can be derived by summing over the nuclear gradient of the EFP interaction energy with respect to the coordinates of each atom on fragment *A*:

$$\frac{\partial(E_{AB}^{EFP})}{\partial x_A} = \sum_K^A \frac{\partial(E_{AB}^{EFP})}{\partial x_{K\in A}} \tag{4.3}$$

where x_A is the translational motion of fragment *A* in the *x*-direction.

2) The derivative of an LMO centroid appears in the exchange-repulsion, polarization, and dispersion gradient terms. The derivative of an LMO centroid with respect to the translational motion of a rigid fragment is a delta function. That is, when a fragment translates, the LMO centroids move with it.

$$\sum_K^A \frac{\partial\langle l|\beta|l\rangle}{\partial x_K} = \delta_{\beta x}: \quad \beta = x,y,z \tag{4.4}$$

If bond midpoints are used as multipole expansion points, a similar expression applies for the derivative of the position of the bond midpoints.

3) Since the EFMO fragments are not rigid, the gradient with respect to each atom is calculated.

Each EFP interaction energy gradient term between fragments *A* and *B* in the EFMO method can be written in the form

$$\frac{\partial}{\partial x_{K\in A}} E_{AB}^{X} = \mathrm{NR}_{AB,x_K}^{X} + \sum_{i}^{\substack{\mathrm{occ}\\ \mathrm{CMO}\in \mathrm{A}}} \sum_{a}^{\mathrm{vir}\in \mathrm{A}} U_{ai}^{x_K A} L_{X,ai}^{A,B} + \sum_{ij}^{\substack{\mathrm{occ}\\ \mathrm{CMO}\in \mathrm{A}}} U_{ij}^{x_K A} L_{X,ij}^{A,B} + \sum_{ab}^{\mathrm{vir}\in \mathrm{A}} U_{ab}^{x_K A} L_{X,ab}^{A,B}$$
$$+ \sum_{l}^{\mathrm{LMO}\in \mathrm{A}} \sum_{m}^{\mathrm{LMO}\in \mathrm{A}} v_{mi}^{x_K A} M_{X,ml}^{A,B} + \sum_{\beta}^{\{x,y,z\}} \sum_{i}^{\substack{\mathrm{occ}\\ \mathrm{CMO}\in \mathrm{A}}} \sum_{a}^{\mathrm{vir}\in \mathrm{A}} \frac{\partial U_{ai}^{\beta A}}{\partial x_K} N_{X,ai}^{\beta,A,B}$$
$$+ \sum_{f}^{12} \sum_{\beta}^{\{x,y,z\}} \sum_{a}^{\mathrm{vir}\in \mathrm{A}} \sum_{i}^{\substack{\mathrm{occ}\\ \mathrm{CMO}\in \mathrm{A}}} \frac{\partial Z_{ai}^{\beta A}(i\omega_f)}{\partial x_{K\in A}} N_{X,ai}^{\beta,\omega_f,A,B} \tag{4.5}$$

In Eq. (4.5) the superscript/subscript *X* represents one of the EFP components *Coul*, *rep*, *pol*, or *disp*, corresponding to Coulomb, exchange-repulsion, polarization or dispersion. NR_{AB,x_K}^{X} contains all "non-response" terms that do not contain a first- or second-order CMO response or a localization response. The response matrices ($U^{x_K A}$ / $U^{\beta A}, v^{x_K A}, Z^{\beta A}(i\omega)$) are defined in Sections 2.4, 2.6, and 3.2.4, respectively. The superscript *A* indicates response matrices for fragment *A*.

Using the Z-vector method (see Appendix A), the last three terms in Eq. (4.5) can be replaced with non-response terms and terms involving the canonical MO response matrix. The CMO response term can then be obtained using the Z-vector method. Throughout the following, the gradient for each term will be written in a manner that is consistent with Eq. (4.5).

Since the EFP terms are based on MOs obtained from a separate gas phase *ab initio* calculation on a particular monomer, the response equations for each monomer depend only on that monomer. Thus, in contrast to the FMO method[31], there is no response equation with the dimension of the entire system.

4.2.1. Coulomb gradient term

The gradient of the Coulomb interaction energy between fragments *A* and *B* can be written as

$$\frac{\partial E_{AB}^{Coul}}{\partial x_{K\in A}} = \sum_{I}^{A}\sum_{J}^{B}\Bigg[q^J \frac{\partial\left(q^I T^{IJ}\right)}{\partial x_{K\in A}} - \sum_{\alpha}^{x,y,z} q^J \frac{\partial\left(\mu_\alpha^I T_\alpha^{IJ}\right)}{\partial x_{K\in A}} + \frac{1}{3}\sum_{\alpha,\beta}^{x,y,z} q^J \frac{\partial\left(\Theta_{\alpha\beta}^I T_{\alpha\beta}^{IJ}\right)}{\partial x_{K\in A}} + \sum_{\alpha}^{x,y,z}\mu_\alpha^J \frac{\partial\left(q^I T_\alpha^{IJ}\right)}{\partial x_{K\in A}} - \sum_{\alpha,\beta}^{x,y,z}\mu_\alpha^J \frac{\partial\left(\mu_\beta^I T_{\alpha\beta}^{IJ}\right)}{\partial x_{K\in A}} + \frac{1}{3}\sum_{\alpha,\beta,\gamma}^{x,y,z}\mu_\alpha^J \frac{\partial\left(\Theta_{\beta\gamma}^I T_{\alpha\beta\gamma}^{IJ}\right)}{\partial x_{K\in A}} + \ldots \Bigg] \tag{4.6}$$

Each term in Eq.(3.3) is differentiated with respect to the *x*-coordinate of atom *K* in fragment *A*. The multipole moments on fragment *B* are constant with respect to atoms on fragment *A*, so those terms are not included in the derivative. For this work, the expansion in Eq. (4.6) is terminated at the quadrupole-quadrupole term, and multipole expansion points are only on atomic centers.

The gradient terms are derivatives of products, so the product rule can be used. Then, Eq. (4.6) can be written as:

$$\frac{\partial E_{AB}^{Coul}}{\partial x_{K\in A}} = F_{AB}^{Coul}\left(\left\{\frac{\partial T_{\alpha\beta\ldots\gamma}^{IJ}}{\partial x_{K\in A}}\right\},\{m^I\},\{m^J\}\right) + F_{AB}^{Coul}\left(\{T_{\alpha\beta\ldots\gamma}^{IJ}\},\left\{\frac{\partial m^I}{\partial x_{K\in A}}\right\},\{m^J\}\right) \tag{4.7}$$

where m^I is an arbitrary multipole moment, $T_{\alpha\beta\ldots\gamma}^{IJ}$ is a multipole moment interaction tensor of the appropriate rank, $F_{AB}^{Coul}\left(\left\{\frac{\partial T_{\alpha\beta\ldots\gamma}^{IJ}}{\partial x_{K\in A}}\right\},\{m^I\},\{m^J\}\right)$ is the sum of all terms involving derivatives of interaction tensors, and $F_{AB}^{Coul}\left(\{T_{\alpha\beta\ldots\gamma}^{IJ}\},\left\{\frac{\partial m^I}{\partial x_{K\in A}}\right\},\{m^J\}\right)$ is the sum

of all terms involving the derivative of multipole moments. These terms are expanded in Appendix B.

For the EFP method, the gradient of the EFP Coulomb term was derived by Day et al.[2]. In the EFP method, only the first term in Eq. (4.7) is included in the translational gradient, since the multipole moments depend only on the internal geometry of the fragment, and do not change as the fragment translates. The net Coulomb translational gradient on the fragment is calculated by summing the derivatives of the Coulomb energy with respect to each atom center on the fragment. The EFP implementation of the first term in Eq. (4.7) can be reused for the EFMO gradient, with the gradient stored separately for each atom.

As shown in Eq. (3.4), the multipole moments are a sum of the product of a density matrix and a Gaussian function integral. The gradient of a multipole moment can therefore be calculated using the product rule. Consequently, each multipole moment derivative gives rise to a term involving AO-derivatives and a term involving the CMO response matrix.

The final EFMO Coulomb gradient can be written as

$$\frac{\partial E_{AB}^{Coul}}{\partial x_{K\in A}} = \mathrm{NR}_{AB,x_K}^{Coul} + \sum_{i}^{\substack{occ \\ CMO}} \sum_{a}^{\in A \; vir \in A} U_{ai}^{x_K A} L_{Coul,ai}^{A,B} \tag{4.8}$$

The details of the non-response term, $\mathrm{NR}_{AB,x_K}^{Coul}$, and the coefficient of the CMO response matrix, $L_{Coul,ai}^{A,B}$, are presented in Appendix B.

In Section 4.3, Eq. (4.8) will be combined with the other EFP interaction energy gradient terms, and the Z-vector method will be applied to give the form of the EFMO gradient that was implemented in GAMESS.

Coulomb damping term

The derivative of Eq. (3.5) can be easily added to the exchange repulsion gradient, so it is briefly discussed in the following subsection.

4.2.2 Exchange repulsion energy term

The gradient of the EFMO exchange repulsion term can be expressed by taking the nuclear derivative of each term in Eq. (3.6), as follows.

$$\frac{\partial E_{AB}^{rep}}{\partial x_{K\in A}} = -2\sum_{l}^{LMO\in A}\sum_{m}^{LMO\in B}\frac{\partial S_{lm}}{\partial x_K}\left[\begin{array}{l}\dfrac{S_{lm}}{R_{lm}}\left(-\sqrt{\dfrac{2}{-\pi\ln S_{lm}}}+4\sqrt{\dfrac{-2\ln S_{lm}}{\pi}}\right)+2\sum_{n}^{LMO\in A}F_{nl}^{A}S_{nm}+2\sum_{n}^{LMO\in B}F_{nm}^{B}S_{nl}-2T_{lm}\\ -2S_{lm}\left(-\sum_{J}^{nuclei\in B}\dfrac{Z_J}{R_{lJ}}+2\sum_{n}^{LMO\in B}\dfrac{1}{R_{ln}}-\sum_{I}^{nuclei\in A}\dfrac{Z_I}{R_{Im}}+2\sum_{n}^{LMO\in A}\dfrac{1}{R_{nm}}-\dfrac{1}{R_{lm}}\right)\end{array}\right]$$

$$-2\sum_{l}^{LMO\in A}\sum_{m}^{LMO\in A}\frac{\partial F_{lm}^{A}}{\partial x_K}\left[\sum_{n}^{LMO\in B}S_{ln}S_{mn}\right]-2\sum_{l}^{LMO\in A}\sum_{m}^{LMO\in B}\frac{\partial T_{lm}}{\partial x_K}\left[-2S_{lm}\right]+2\sum_{l}^{LMO\in A}\sum_{m}^{LMO\in B}\frac{\partial R_{lm}}{\partial x_K}\left[\begin{array}{l}2\sqrt{\dfrac{-2\ln S_{lm}}{\pi}}\dfrac{S_{lm}^2}{R_{lm}^2}+\dfrac{S_{lm}^2}{R_{lm}^2}\\ +\sum_{n}^{LMO\in B}-2\dfrac{S_{ln}^2}{R_{lm}^2}+\sum_{n}^{LMO\in A}-2\dfrac{S_{nm}^2}{R_{lm}^2}\end{array}\right]$$

$$+2\sum_{l}^{LMO\in A}\sum_{J}^{nuclei\in B}\frac{\partial R_{lJ}}{\partial x_K}\left[\sum_{m}^{LMO\in B}S_{lm}^2\frac{Z_J}{R_{lJ}^2}\right]+2\sum_{I}^{nuclei\in A}\sum_{m}^{LMO\in B}\frac{\partial R_{Im}}{\partial x_K}\left[\sum_{n}^{LMO\in A}S_{nm}^2\frac{Z_I}{R_{Im}^2}\right] \tag{4.9}$$

Each term in Eq.(4.9) is differentiated with respect to the *x*-coordinate of atom *K* in fragment *A*. This means that gradient terms that depend only on the geometry of fragment *B* will be zero.

In the EFP method, the internal geometries of the fragments do not change when the fragments translate, so the MO coefficients and Fock matrices do not change, and the LMO centroids move with the fragments. Thus, the kinetic energy and overlap integral

derivatives (the first and third terms in Eq. (4.9)) are computed by only taking the derivative of the AO integrals (ignoring the MO coefficient derivatives), and the Fock matrix derivative is not computed. Since the net translational gradient is calculated by summing over the nuclear gradients of the exchange repulsion energy with respect to each atom on the fragment, by Eq. (4.4) there is no need to explicitly calculate the derivative of each LMO centroid. The implementation of the first, third, fourth, fifth, and sixth terms in Eq. (4.9) for the EFP method can be reused for the EFMO gradient, but with additional terms added for the derivative of the LMO centroids and the canonical MO coefficients, and with the gradient stored separately for each atom.

For the EFMO gradient, the LMO centroid derivatives in the fourth and fifth terms of Eq. (4.9) can be collected. The explicit expressions are shown in Appendix C. Eq. (4.9) can then be written as:

$$\frac{\partial E_{AB}^{rep}}{\partial x_{K\in A}} = -2\sum_{l}^{LMO\in A}\sum_{m}^{LMO\in B}\frac{\partial S_{lm}}{\partial x_K}\left[\mathrm{W}_{lm}^{S}\right] - 2\sum_{l}^{LMO\in A}\sum_{m}^{LMO\in A}\frac{\partial F_{lm}^{A}}{\partial x_K}\left[\sum_{n}^{\mathrm{LMO}\in B} S_{ln}S_{mn}\right]$$
$$-2\sum_{l}^{LMO\in A}\sum_{m}^{LMO\in B}\frac{\partial T_{lm}}{\partial x_K}\left[\mathrm{W}_{lm}^{T}\right] + 2\sum_{l}^{LMO\in A}\sum_{\alpha}^{\{x,y,z\}} < \frac{\partial l}{\partial x_K} | \alpha | l > \left[W_{l\alpha}^{R}\right]$$
$$+2\sum_{l}^{LMO\in B}(x_K - < l | x | l >)\left[\sum_{m}^{LMO\in A} S_{ml}^{2}\frac{Z_K}{R_{Kl}^{3}}\right] \tag{4.10}$$

where W_{lm}^{S} holds all the terms in the coefficient of $\frac{\partial S_{lm}}{\partial x_K}$, W_{lm}^{T} holds all the terms in the coefficient of $\frac{\partial T_{lm}}{\partial x_K}$, and $W_{l\alpha}^{R}$ holds all the terms in the coefficient of $< \frac{\partial l}{\partial x_K} | \alpha | l >$.

It is important to note that the MO coefficient derivatives are derivatives of LMO coefficients, so the derivative results in a term with a canonical MO response matrix and a term with a localization response matrix, as shown in Eq. (2.3). Appendix C provides the details that lead from Eq. (4.10) to Eq. (4.11).

Combing all non-response terms into NR_{AB}^{rep}, and writing out the response terms one obtains

$$\frac{\partial E_{AB}^{rep}}{\partial x_{K\in A}} = \mathrm{NR}_{AB,x_K}^{rep} + \sum_{i}^{\substack{occ \\ CMO\in A}} \sum_{a}^{vir\in A} U_{ai}^{x_K A} L_{rep,ai}^{A,B} + \sum_{i,j}^{\substack{occ \\ CMO\in A}} U_{ji}^{x_K A} O_{rep,ji}^{A,B} + \sum_{l}^{LMO\in A} \sum_{m}^{LMO\in A} v_{ml}^{x_K A} M_{rep,ml}^{A,B} \tag{4.11}$$

In Section 4.3 Eq. (4.11) will be combined with the other EFP terms and the Z-vector method will be applied to give the form of the EFMO gradient that was implemented.

Coulomb damping function

The derivative of Eq. (3.5) can easily be added to the exchange repulsion term, since it only involves LMO dipole and overlap integrals. Since the derivative is derived in a similar manner to the exchange repulsion gradient, it is not shown here.

4.2.3 Polarization energy term

The EFMO polarization energy gradient can be derived beginning with Eq. (26) in Ref. 21 (written in the notation of this paper):

$$\frac{\partial E_{tot}^{pol}}{\partial x_{K\in A}} = -\sum_{B}^{\text{fragments}} \sum_{n}^{LMO\in B} \sum_{\alpha}^{\{x,y,z\}} \left(\frac{\partial E_{n,\alpha}^{0,B}}{\partial x_{K\in A}} \right) \left(\frac{p_{n,\alpha}^{B} + \tilde{p}_{n,\alpha}^{B}}{2} \right) + \frac{1}{2} \sum_{BC}^{\text{fragments}} \sum_{m}^{LMO\in B} \sum_{n}^{LMO\in C} \sum_{\alpha,\beta}^{\{x,y,z\}} (\tilde{p}_{n,\alpha}^{C}) \left(\frac{\partial D_{nm,\alpha\beta}}{\partial x_{K\in A}} \right) p_{m,\beta}^{B}$$

(4.12)

The derivative in Eq. (4.12) is taken with respect to atom *K* on fragment *A*. As in Ref. 21,

$\tilde{p}^{A}_{l,\beta} = \sum_{B}^{\text{fragments}} \sum_{m}^{LMO\in B} \sum_{\alpha}^{\{x,y,z\}} (D^{-1})^{T}_{lm,\beta\alpha} E^{0,B}_{m,\alpha}$. All other terms are defined in Section 3.2.3.

The dimer polarization energy term, $\frac{\partial E^{pol}_{AB}}{\partial x_{K\in A}}$, can be derived in a similar fashion, so the details are only shown for the total polarization energy term.

The static electric field in the first term in Eq. (4.12) is represented by the multipole moment expansion as in the Coulomb term. The derivative is handled in a similar manner here as in the Coulomb term: It is split into a term with the sum of all multipole moment interaction tensors ($F^{P}_{A}(\{\frac{\partial T^{nI}_{\alpha\beta\ldots\gamma}}{\partial x_{K\in A}}\},\{m^{I}\},\{p_{n}\})$) and a term with the sum of all multipole moment derivatives ($F^{P}_{A}(\{T^{nI}_{\alpha\beta\ldots\gamma}\},\{\frac{\partial m^{I}}{\partial x_{K\in A}}\},\{p_{n}\})$). The second term in Eq. (4.12) can be expanded using the definition in Eq. (3.10).

The expansion of Eq. (4.12) is shown in more detail in Appendix D. Then, Eq. (4.12) can be written as:

$$\frac{\partial E_{tot}^{pol}}{\partial x_{K\in A}} = \left[-\sum_{n}^{LMO\in A}\sum_{\beta}^{\{x,y,z\}} \frac{\partial \langle n|\beta|n\rangle}{\partial x_{K\in A}} \left[\sum_{\alpha}^{\{x,y,z\}}\sum_{B\neq A}^{\text{fragments}}\sum_{l}^{B} \left(\frac{\partial E^{0}_{nl,\alpha}}{\partial \langle n|\beta|n\rangle} \right) \left(\frac{p^{A}_{n,\alpha} + \tilde{p}^{A}_{n,\alpha}}{2} \right) \right] \right]$$
$$- \left[F_A^P(\{\frac{\partial T^{nl}_{\alpha\beta\ldots\gamma}}{\partial x_{K\in A}}\},\{m^l\},\{p_n\}) \right]$$
$$- \left[F_A^P(\{T^{nl}_{\alpha\beta\ldots\gamma}\},\{\frac{\partial m^l}{\partial x_{K\in A}}\},\{p_n\}) \right]$$
$$+ \left[\frac{1}{2}\sum_{n}^{LMO\in A}\sum_{\beta,\gamma}^{\{x,y,z\}} (\tilde{p}^{A}_{n,\beta}) \left(\frac{\partial \left(\alpha^{-1}_{n,\beta\gamma}\right)}{\partial x_{K\in A}} \right) p^{A}_{n,\gamma} \right]$$
$$+ \left[\frac{1}{2}\sum_{n}^{LMO\in A}\sum_{\gamma}^{\{x,y,z\}} \frac{\partial \langle n|\gamma|n\rangle}{\partial x_{K\in A}} \sum_{B\neq A}^{\text{fragments}}\sum_{m}^{LMO\in B}\sum_{\alpha,\beta}^{\{x,y,z\}} \left[(\tilde{p}^{A}_{n,\alpha}) \left(\frac{\partial D_{nm,\alpha\beta}}{\partial \langle n|\gamma|n\rangle} \right) p^{B}_{m,\beta} + (\tilde{p}^{B}_{m,\alpha}) \left(\frac{\partial D_{mn,\alpha\beta}}{\partial \langle n|\gamma|n\rangle} \right) p^{A}_{n,\beta} \right] \right] \tag{4.13}$$

The EFP polarization gradient for the EFP method was derived by Li et al.[21] and Day et al.[2]. As in the Coulomb and exchange-repulsion gradient, the net polarization translational gradient with respect to fragment *A* can be calculated by summing the nuclear derivatives with respect to each atom on fragment *A*. Only the first, second, and fifth terms in Eq. (4.13) are needed for the EFP translational gradient. The third and fourth terms have derivatives of the multipole moments and the dipole polarizability tensor, respectively, which depend only on the internal geometry. As with the exchange repulsion term, the terms in Eq. (4.13) that contain derivatives of the LMO centroids can be expressed without explicitly calculating $\frac{\partial \langle l|\beta|l\rangle}{\partial x_K}$, by using Eq. (4.4) instead. The EFP implementation of the first, second, and fifth terms can be used for the EFMO method, with additional terms added for the derivative of the LMO centroids, and the gradient stored separately for each atom.

The LMO centroid derivatives in Eq. (4.13) can be combined. The third term can be replaced with two terms arising from the derivative of the multipole moments, as in

the Coulomb term. Since this involves the derivative of the canonical MO density matrix, a canonical MO response matrix term is necessary.

The fourth term in Eq. (4.13) can be manipulated using matrix derivative operations[21] and the defintion in Eq. (3.7)

$$\frac{1}{2}\sum_{n}^{LMO\in A}\sum_{\beta,\gamma}^{\{x,y,z\}}(\tilde{p}^{A}_{n,\beta})\left(\frac{\partial\left(\alpha^{-1}_{n,\beta\gamma}\right)}{\partial x_{K\in A}}\right)p^{A}_{n,\gamma}=-\frac{1}{2}\sum_{n}^{LMO\in A}\sum_{\beta,\gamma}^{\{x,y,z\}}\tilde{E}^{tot,A}_{n,\beta}\left(\frac{\partial\left(\alpha_{n,\beta\gamma}\right)}{\partial x_{K\in A}}\right)E^{tot,A}_{n,\gamma} \tag{4.14}$$

where $\tilde{E}^{tot,A}_{l,\beta}=\sum_{\kappa}^{\{x,y,z\}}\alpha^{-1}_{l,\kappa\beta}\tilde{p}^{A}_{l,\kappa}$

The LMO dipole polarizability tensor in Eq. (4.14) is expanded as[22]

$$\begin{aligned}&-\frac{1}{2}\sum_{n}^{LMO\in A}\sum_{\beta,\gamma}^{\{x,y,z\}}\tilde{E}^{tot,A}_{n,\beta}\left(\frac{\partial\left(\alpha_{n,\beta\gamma}\right)}{\partial x_{K\in A}}\right)E^{tot,A}_{n,\gamma}\\&=-\frac{1}{2}\sum_{n}^{LMO\in A}\sum_{\beta,\gamma}^{\{x,y,z\}}\tilde{E}^{tot,A}_{n,\beta}\left(\frac{\partial}{\partial x_{K\in A}}\left(-4\sum_{jk}^{\substack{occ\\CMO\in A}}\sum_{a}^{vir\in A}L_{nj}L_{nk}U^{\gamma A}_{aj}\langle a\,|\,\beta\,|\,k\rangle\right)\right)E^{tot,A}_{n,\gamma}\end{aligned} \tag{4.15}$$

The RHS of Eq. (4.15) results in three terms: one term with the derivative of the LMO transforms, one term with the derivative of the canonical MO field response $\left(\frac{\partial}{\partial x_{K\in A}}U^{\gamma A}_{aj}\right)$, and one term with the derivative of the dipole $\left(\frac{\partial}{\partial x_{K\in A}}\langle a\,|\,\beta\,|\,k\rangle\right)$. Once Eq. (4.15) has been expanded in terms of non-response terms, localization transform derivative terms, and second order canonical MO field response terms, the polarization energy gradient can be rewritten as

$$\frac{\partial E_{tot}^{pol}}{\partial x_{K\in A}} = \mathrm{NR}_{A,tot,x_K}^{pol} + \sum_{i}^{\substack{occ \\ CMO\in A}} \sum_{a}^{vir\in A} U_{ai}^{x_c A} L_{pol,ai}^{A,tot} + \sum_{ij}^{\substack{occ \\ CMO\in A}} U_{ij}^{x_K A} O_{pol,ij}^{A,tot} + \sum_{ab}^{vir\in A} U_{ab}^{x_K A} V_{pol,ab}^{A,tot}$$
$$+ \sum_{m}^{LMO\in A} \sum_{l}^{LMO\in A} v_{ml}^{x_K A} M_{pol,ml}^{A,tot} + \sum_{\beta}^{\{x,y,z\}} \sum_{i}^{\substack{occ \\ CMO\in A}} \sum_{a}^{vir\in A} \frac{\partial U_{ai}^{\beta A}}{\partial x_K} N_{pol,ai}^{\beta,A,tot} \tag{4.16}$$

The terms in Eq. (4.16) (such as $\mathrm{NR}_{A,tot,x_K}^{pol}$, $L_{pol,ai}^{A,tot}$, $O_{pol,ij}^{A,tot}$, $V_{pol,ab}^{A,tot}$, $M_{pol,ml}^{A,tot}$, $N_{pol,ai}^{\beta,A,tot}$) are similar to those in Eq. (4.5), but with a *tot* superscript/subscript instead of a *B* superscript/subscript, to denote that this is a gradient contribution from the total polarization energy instead of a gradient contribution from a dimer interaction energy between fragments *A* and *B*. The canonical MO response terms and the localization response terms can also be removed using the Z-vector method. This will be done in Section 4.3 for all EFP interaction energy terms.

Polarization damping function

The polarization energy derivative can be modified to include damping. The damping term is a function of the distance between two LMO centroids or an LMO centroid and an atom center, so the derivative is straightforward. Using the expression for polarization damping in Section 3.2.3:

$$\frac{\partial T_{\alpha\beta\ldots\gamma}^{lm,damped}}{\partial x} = \frac{\partial F_{damp,lm}^{pol}}{\partial x} T_{\alpha\beta\ldots\gamma}^{lm} + F_{damp,lm}^{pol} \frac{\partial T_{\alpha\beta\ldots\gamma}^{lm}}{\partial x} \tag{4.17}$$

All multipole interaction tensor derivatives can be replaced with the above, and the gradient can be evaluated in the same way.

4.2.4 Dispersion energy term

The EFMO dispersion gradient can be expressed by taking the derivative of Eq. (3.17).

$$\frac{\partial E_{AB}^{disp}}{\partial x_{K\in A}} = \frac{\partial}{\partial x_{K\in A}}\left(-\frac{4}{\pi}\sum_{l}^{LMO\in A}\sum_{m}^{LMO\in B}\frac{1}{R_{lm}^{6}}\sum_{f}^{12}\left(w_f\frac{2v_0}{(1-t_f)^2}\bar{\alpha}^{l}(i\omega_f)\bar{\alpha}^{m}(i\omega_f)\right)\right)$$
$$= \sum_{l}^{LMO\in A}\sum_{m}^{LMO\in B}\frac{\partial\left(R_{lm}^{-6}\right)}{\partial x_{K\in A}}\left(-\frac{4}{\pi}\sum_{f}^{12}\left(w_f\frac{2v_0}{(1-t_f)^2}\bar{\alpha}^{l}(i\omega_f)\bar{\alpha}^{m}(i\omega_f)\right)\right)$$
$$+\sum_{l}^{LMO\in A}\sum_{f}^{12}\frac{\partial\bar{\alpha}^{l}(i\omega_f)}{\partial x_{K\in A}}\left(-\frac{4}{\pi}\left(w_f\frac{2v_0}{(1-t_f)^2}\right)\sum_{m}^{LMO\in B}\frac{1}{R_{lm}^{6}}\bar{\alpha}^{m}(i\omega_f)\right) \tag{4.18}$$

The first term in Eq. (4.18) can be written in terms of an LMO centroid derivative as in the polarization energy gradient. Eq. (4.18) can then be expressed as:

$$\frac{\partial E_{AB}^{disp}}{\partial x_{K\in A}} = \sum_{l}^{LMO\in A}\sum_{\beta}^{\{x,y,z\}}\frac{\partial\langle l|\beta|l\rangle}{\partial x_{K\in A}}\left(\sum_{m}^{LMO\in B}\frac{-6(<l|\beta|l>-<m|\beta|m>)}{R_{lm}^{8}}\left(-\frac{4}{\pi}\sum_{f}^{12}\left(w_f\frac{2v_0}{(1-t_f)^2}\bar{\alpha}^{l}(i\omega_f)\bar{\alpha}^{m}(i\omega_f)\right)\right)\right)$$
$$+\sum_{l}^{LMO\in A}\sum_{f}^{12}\frac{\partial\bar{\alpha}^{l}(i\omega_f)}{\partial x_{K\in A}}\left(-\frac{4}{\pi}\left(w_f\frac{2v_0}{(1-t_f)^2}\right)\sum_{m}^{LMO\in B}\frac{1}{R_{lm}^{6}}\bar{\alpha}^{m}(i\omega_f)\right) \tag{4.19}$$

In the EFP method, only the first term in Eq. (4.19) is needed for the translational gradient. As in the exchange repulsion and polarization terms, there is no need to calculate the nuclear derivative of the LMO centroids explicitly to get the EFP translational dispersion gradient. The second term contains the derivative of the dynamic polarizability tensor, which only depends on the internal geometry of the fragment, and does not change as the fragment translates. For the EFMO gradient, the first term in Eq. (4.19) can be calculated using the implementation from the EFP method, but with additional terms added for the derivative of the LMO centroids, and the gradient stored separately for each atom.

The first term in Eq. (4.19) is a LMO centroid derivative. The LMO centroid derivative has been discussed in the subsections on the exchange-repulsion and polarization gradient previously. The second term in Eq. (4.19) contains the derivative of the dynamic polarizability tensor. This is derived in a similar manner as the derivative of the static polarizability tensor, and is discussed in Appendix E, Section 2.

The dispersion energy gradient can then be written as

$$\frac{\partial E_{AB}^{disp}}{\partial x_{K\in A}} = \mathrm{NR}_{AB,x_K}^{disp} + \sum_{i}^{\substack{occ \\ CMO\in A}} \sum_{a}^{\text{vir}\in \text{A}} U_{ai}^{x_K A} L_{disp,ai}^{A,B} + \sum_{ji}^{\substack{occ \\ CMO\in A}} U_{ij}^{x_K A} O_{disp,ij}^{A,B} + \sum_{ab}^{vir\in A} U_{ab}^{x_K A} V_{disp,ab}^{A,B}$$
$$+ \sum_{l}^{LMO\in A} \sum_{m}^{LMO\in A} v_{ml}^{x_K A} M_{disp,ml}^{A,B} + \sum_{f}^{12} \sum_{\beta}^{\{x,y,z\}} \sum_{a}^{vir\in A} \sum_{i}^{\substack{occ \\ CMO\in A}} \frac{\partial Z_{ai}^{\beta A}(i\omega_f)}{\partial x_{K\in A}} N_{disp,ai}^{\beta,\omega_f,A,B} \tag{4.20}$$

As shown in Section 4.3, Eq. (4.20) can be combined with the other EFMO gradient terms, and the Z-vector method can be used to calculate the canonical MO response terms and the localization response terms.

Dispersion damping function

The damping function, shown in Eq. (3.21) adds a factor that depends only on the overlap. The energy and gradient then become

$$E_{AB}^{disp,damped} = \sum_{l}^{LMO\in A} \sum_{m}^{LMO\in B} F_{lm}^{disp,damp} \left[-\frac{4}{\pi} \frac{1}{R_{lm}^6} \left(\int_0^\infty \bar{\alpha}^l(i\omega) \bar{\alpha}^m(i\omega) d\omega \right) \right]$$

$$\frac{\partial E_{AB}^{disp,damped}}{\partial x} = \sum_{l}^{LMO\in A} \sum_{m}^{LMO\in B} \frac{\partial F_{lm}^{disp,damp}}{\partial x} \left[-\frac{4}{\pi} \frac{1}{R_{lm}^6} \left(\int_0^\infty \bar{\alpha}^l(i\omega) \bar{\alpha}^m(i\omega) d\omega \right) \right]$$
$$+ \sum_{l}^{LMO\in A} \sum_{m}^{LMO\in B} F_{lm}^{disp,damp} \frac{\partial \left[-\frac{4}{\pi} \frac{1}{R_{lm}^6} \left(\int_0^\infty \bar{\alpha}^l(i\omega) \bar{\alpha}^m(i\omega) d\omega \right) \right]}{\partial x} \tag{4.21}$$

The damping function only depends on the overlap, and the damping function gradient can be computed in a similar manner to the LMO overlap derivatives in the exchange-repulsion energy term.

4.3 The Combined Gradient

The terms in Eq. (4.1) (and likewise, Eq. (4.2)) that are EFP interaction energy derivatives can be expressed using Eq. (4.8), (4.11), (4.16), and (4.20):

$$\begin{aligned}
\frac{\partial E_{EFP}^{EFMO}}{\partial x_K} = & \sum_{A>B}^{R_{A,B}\le R_{cut}} \left(-\mathrm{NR}_{AB,x_K}^{pol}\right) + \sum_{A>B}^{R_{A,B}>R_{cut}} \left(\mathrm{NR}_{AB,x_K}^{Coul} + \mathrm{NR}_{AB,x_K}^{rep} + \mathrm{NR}_{AB,x_K}^{disp}\right) + \mathrm{NR}_{A,tot,x_K}^{pol} \\
& + \sum_{i}^{CMO\in A} \sum_{a}^{vir\in A} U_{ai}^{x_K A} \left(\sum_{A>B}^{R_{A,B}\le R_{cut}} \left(-L_{pol,ai}^{A,B}\right) + \sum_{A>B}^{R_{A,B}>R_{cut}} (L_{Coul,ai}^{A,B} + L_{rep,ai}^{A,B} + L_{disp,ai}^{A,B}) + L_{pol,ai}^{A,tot} \right) \\
& + \sum_{ij}^{CMO\in A} U_{ij}^{x_K A} \left(\sum_{A>B}^{R_{A,B}\le R_{cut}} \left(-O_{pol,ij}^{A,B}\right) + \sum_{A>B}^{R_{A,B}>R_{cut}} (O_{rep,ij}^{A,B} + O_{disp,ij}^{A,B}) + O_{pol,ij}^{A,tot} \right) \\
& + \sum_{ab}^{vir\in A} U_{ab}^{x_K A} \left(\sum_{A>B}^{R_{A,B}\le R_{cut}} \left(-V_{pol,ab}^{A,B}\right) + \sum_{A>B}^{R_{A,B}>R_{cut}} (V_{disp,ab}^{A,B}) + V_{pol,ab}^{A,tot} \right) \\
& + \sum_{l}^{LMO\in A} \sum_{m}^{LMO\in A} v_{ml}^{x_K A} \left(\sum_{A>B}^{R_{A,B}\le R_{cut}} \left(-M_{pol,ml}^{A,B}\right) + \sum_{A>B}^{R_{A,B}>R_{cut}} (M_{rep,ml}^{A,B} + M_{disp,ml}^{A,B}) + M_{pol,ml}^{A,tot} \right) \\
& + \sum_{f}^{12} \sum_{\beta}^{\{x,y,z\}} \sum_{a}^{vir\in A} \sum_{i}^{CMO\in A} \frac{\partial Z_{ai}^{\beta A}(i\omega_f)}{\partial x_{K\in A}} \left(\sum_{A>B}^{R_{A,B}>R_{cut}} N_{disp,ai}^{\beta,\omega_f,A,B} \right) \\
& + \sum_{\beta}^{\{x,y,z\}} \sum_{i}^{CMO\in A} \sum_{a}^{vir\in A} \frac{\partial U_{ai}^{\beta A}}{\partial x_K} \left(\sum_{A>B}^{R_{A,B}\le R_{cut}} \left(-N_{pol,ai}^{\beta,A,B}\right) + N_{pol,ai}^{\beta,A,tot} \right)
\end{aligned} \tag{4.22}$$

where the derivative is taken with respect to atom K on fragment A.

Then, the non-response terms and the coefficients of the response terms can be collected and combined into terms with the superscript/subscript *tot*, as shown below:

$$\frac{\partial E_{EFP}^{EFMO}}{\partial x_K} = \mathrm{NR}_{A,x_K}^{tot} + \sum_{i}^{\substack{occ \\ CMO\in A}} \sum_{a}^{vir\in A} U_{ai}^{x_K A} L_{ai,tot}^{A} + \sum_{ij}^{\substack{occ \\ CMO\in A}} U_{ij}^{x_K A}\left(L_{ij,tot}^{A}\right) + \sum_{ab}^{vir\in A} U_{ab}^{x_K A}\left(L_{ab,tot}^{A}\right)$$
$$+ \sum_{l}^{LMO\in A} \sum_{m}^{LMO\in A} v_{ml}^{x_K A}\left(M_{ml,tot}^{A}\right) + \sum_{f}^{12} \sum_{\beta}^{\{x,y,z\}} \sum_{a}^{vir\in A} \sum_{i}^{\substack{occ \\ CMO\in A}} \frac{\partial Z_{ai}^{\beta A}(i\omega_f)}{\partial x_{K\in A}} N_{ai,tot}^{\beta,\omega_f,A}$$
$$+ \sum_{\beta}^{\{x,y,z\}} \sum_{i}^{\substack{occ \\ CMO\in A}} \sum_{a}^{vir\in A} \frac{\partial U_{ai}^{\beta A}}{\partial x_K} N_{ai,tot}^{\beta,A} \tag{4.23}$$

The Z-vector method can be used to replace the term that involves the derivative of the canonical MO response (the last term in Eq. (4.23)), the derivative of the time-dependent response term (the second to last term in Eq. (4.23)), and the localization response term (the third to last term in Eq. (4.23)). After solving the Z-vector equations, the second order canonical response term, second order time-dependent response term, and localization response term are replaced with first order canonical response terms and non-response terms. The first order canonical response terms can then be collected with the other first order canonical response terms. Using details given in Appendix D, Section 3, Appendix E, Section 1, and Appendix A, Section 8, Eq. (4.23) can be written as:

$$\frac{\partial E_{EFP}^{EFMO}}{\partial x_K} = \mathrm{NR}_{A,x_K}^{tot,3} + \sum_{i}^{\substack{occ \\ CMO\in A}} \sum_{a}^{vir\in A} U_{ai}^{x_K A}\left(L_{ai,tot}^{A,3}\right) + \sum_{ij}^{\substack{occ \\ CMO\in A}} U_{ij}^{x_K A}\left(L_{ij,tot}^{A,3}\right) + \sum_{ab}^{vir\in A} U_{ab}^{x_K A}\left(L_{ab,tot}^{A,2}\right) \tag{4.24}$$

$\mathrm{NR}_{A,x_K}^{tot,3}$ is a non-response term resulting from the Z-vector methods, and $L_{ai,tot}^{A,3}$, $L_{ij,tot}^{A,3}$ are the coefficients of the occ-occ and vir-occ CMO response matrices after the terms from the Z-vector methods have been added in.

Next, the terms that involve the vir-vir and occ-occ parts of the canonical MO response matrix are considered. More details are provided in Appendix A, Section 6. Eq. (4.24) becomes

$$\frac{\partial E_{EFP}^{EFMO}}{\partial x_K} = \mathrm{NR}_{\Lambda,x_K}^{tot,3} + \sum_{i}^{\substack{occ \\ CMO\in A}} \sum_{a}^{vir\in A} U_{ai}^{x_K A} \left(L_{ai,tot}^{A,3} + \sum_{k}^{\substack{core \\ CMO\in A}} \sum_{j}^{\substack{act \\ CMO\in A}} \left(\frac{A'_{kj,ai} L_{kj,tot}^{A,3}}{(\epsilon_j - \epsilon_k)} + \frac{A'_{jk,ai} L_{jk,tot}^{A,3}}{(\epsilon_k - \epsilon_j)} \right) \right)$$
$$+ \sum_{ij}^{\substack{core \\ CMO\in A}} \left(-\frac{1}{2} S_{ij}^{(x_K)A} \right) \left(L_{ij,tot}^{A,3} \right) + \sum_{ij}^{\substack{act \\ CMO\in A}} \left(-\frac{1}{2} S_{ij}^{(x_K)A} \right) \left(L_{ij,tot}^{A,3} \right) + \sum_{ab}^{vir\in A} \left(-\frac{1}{2} S_{ab}^{(x_K)A} \right) \left(L_{ab,tot}^{A,2} \right)$$
$$+ \sum_{i}^{\substack{core \\ CMO\in A}} \sum_{j}^{\substack{act \\ CMO\in A}} \left(\left(\frac{B_{ij}^{x_K A} L_{ij,tot}^{A,3}}{(\epsilon_j - \epsilon_i)} \right) + \left(\frac{B_{ji}^{x_K A} L_{ji,tot}^{A,3}}{(\epsilon_i - \epsilon_j)} \right) \right) \tag{4.25}$$

$A'_{kj,ai}$, $B_{ji}^{x_K A}$ and ϵ_q are defined in Eq. (A.1).

The non-response terms in Eq. (4.25) can be combined, and then Eq. (4.25) becomes:

$$\frac{\partial E_{EFP}^{EFMO}}{\partial x_K} = \mathrm{NR}_{A,x_K}^{tot,4} + \sum_{i}^{\substack{occ \\ CMO\in A}} \sum_{a}^{vir\in A} U_{ai}^{x_K A} \left(L_{ai,tot}^{A,3} + \sum_{k}^{\substack{core \\ CMO\in A}} \sum_{j}^{\substack{act \\ CMO\in A}} \left(\frac{A'_{kj,ai} L_{kj,tot}^{A,3}}{(\epsilon_j - \epsilon_k)} + \frac{A'_{jk,ai} L_{kj,tot}^{A,3}}{(\epsilon_k - \epsilon_j)} \right) \right) \tag{4.26}$$

where $\mathrm{NR}_{A,x_K}^{tot,4}$ is the sum of the non-response terms in Eq. (4.25).

Finally, all canonical MO response terms are collected, and the Z-vector method can be used to replace the canonical MO response matrices. This gives the EFP interaction energy part of the EFMO gradient:

$$\frac{\partial E_{EFP}^{EFMO}}{\partial x_K} = \mathrm{NR}_{A,x_K}^{tot,3} + \sum_{i}^{\substack{occ \\ CMO\in A}} \sum_{a}^{vir\in A} B_{ai}^{x_K A} Z_{ai}^{A,cphf}$$

$$\text{where } \sum_{b}^{vir\in A} \sum_{j}^{occ\in A} A_{bj,ai} Z_{bj}^{A,cphf} = \left(L_{ai,tot}^{A,3} + \sum_{k}^{\substack{core \\ CMO\in A}} \sum_{j}^{\substack{act \\ CMO\in A}} \left(\frac{A'_{kj,ai} L_{kj,tot}^{A,3}}{(\epsilon_j - \epsilon_k)} + \frac{A'_{jk,ai} L_{jk,tot}^{A,3}}{(\epsilon_k - \epsilon_j)} \right) \right)$$

(4.27)

5. Implementation

The EFMO gradient has been implemented in the GAMESS quantum chemistry software package[33]. The coefficients of the LMO centroid derivative term, Fock matrix derivative term, canonical MO response matrix term, localization response matrix term, and second-order response matrix terms are collected separately. The Z-vector equation for the localization response, second-order canonical MO response, and second-order time-dependent canonical MO response are solved. The Z-vectors that result from solving the Z-vector equations are summed with a non-response term and a term that involves the canonical MO response matrix. Since the application of the Z-vector method to the localization response, second-order canonical MO response, and second-order time-dependent canonical MO response terms contributes to the coefficient of the canonical MO response matrix, these Z-vector equations must be solved first. Then the Z-vector equation for the canonical MO response matrix is solved.

6. Test Calculations

To evaluate the accuracy of the gradient, two methods were used. First, the analytic gradient was compared to the numeric gradient for several systems (Section 6.1). Second, the EFMO method and analytic gradient were used in MD simulations to test energy conservation in a Velocity-Verlet NVE ensemble[34,8] (Section 6.2). Again, note

that neither the energy expression used in the numeric gradient nor the analytic gradient contain the EFP charge-transfer term. Although the charge-transfer term might make a significant contribution to the ionic liquid dimer, it is stressed that this section is meant only to assess the accuracy of the analytic gradient.

6.1 Analytic to numeric comparison

For the comparisons, the analytic gradient was computed for several systems and compared to the numeric gradient. A 6-31++G(d,p) basis set was used for all calculations, and R_{cut} was set to 0.3, forcing all dimer interaction energies to be evaluated as EFP interaction energies. The multipole moments are only expanded through the quadrupole-quadrupole term, and all multipole moment expansion points are exclusively on atomic centers, in contrast to the EFP method in which bond midpoints are also expansion centers. The numeric gradient was calculated using a two-point formula.

For the three systems, the maximum absolute difference and root mean square deviation (RMSD) are presented. The RMSD, for N gradient elements, is calculated as

$$\sqrt{\frac{\sum_{i}^{N}\left(\text{analytic gradient element } i - \text{numeric gradient element } i\right)^2}{N}} \tag{6.1}$$

The max interaction gradient value is the maximum contribution to the analytic gradient from the EFP interaction energy gradient. The interaction gradient is calculated by subtracting the one-body (*ab initio*) gradient from the total gradient for each gradient element.

6.1.1. 64 water molecules

The numeric gradient for the system of 64 water molecules (shown in Fig.1) was calculated using a 0.005 Å step size. Table 1 shows the maximum interaction analytic gradient value, the maximum analytic gradient value, the RMSD, and the maximum absolute difference between the numeric and analytic gradients.

Table 1: Comparison of analytic and numeric gradient (Hartree/Bohr) for a system of 64 water molecules

Max interaction analytic gradient value	**Max absolute analytic gradient value**	**RMSD**	**Max absolute difference**
0.026037	0.025670	$8.1*10^{-6}$	$3.7*10^{-5}$

The RMSD and maximum absolute difference values are small and comparable to the RMSDs for other analytic gradients.[31,34] The values in Table 1 demonstrate that the gradient is accurate for the system of 64 water molecules.

6.1.2. Five dimethyl sulfoxide (DMSO) molecules, five methanol molecules, and 10 water molecules

The numeric gradient for the system of five dimethyl sulfoxide (DMSO) molecules, five methanol molecules, and 10 water molecules (shown in Fig. 2) was calculated using a 0.005 Å step size and a 0.001 Å step size.

Using a 0.005 Å step size for the numeric gradient resulted in instances for which the forward and backward steps in the two energy calculations for each numeric gradient element had slightly different allocations of charge density in the multipole moment calculation. That is, some charge density components were allocated to different

expansion centers. In some cases, this led to large enough energy differences in the calculation of the numeric gradient that the numeric and analytic gradient elements differed by ~10^{-3} Hartree/Bohr. These differences, which are not observed for the water cluster discussed in the previous subsection, are too large to be considered accurate.

Reducing the step size to 0.001 Å removed all of the instances in which the forward and backward energy calculations allocated charge density to different expansion points. The analytic and numeric gradients match well, as shown in Table 2. These results show that the analytic gradient is accurate.

Table 2: Comparison of analytic and numeric gradient (Hartree/Bohr) for a system of five dimethyl sulfoxide (DMSO) molecules, five methanol molecules, and 10 water molecules

Max interaction analytic gradient value	**Max absolute analytic gradient value**	**RMSD**	**Max absolute difference**
0.213522	0.208892	$2.8*10^{-7}$	$1.2*10^{-6}$

6.1.3 Ionic liquid dimer

The numeric gradient for the system of two hexafluorophosphate $(PF_6)^-$ anions and two 1-N-butyl-3-methylimidazolium $(bmim)^+$ cations (shown in Fig. 3) was calculated using a 0.005, 0.001, 0.0005, 0.0001, and 0.00005 Å step size.

The differences between elements of the numeric and analytic gradient are large (10^{-2} to 10^{-4}) until the step size is decreased to 0.0001 Å or below. Using a 0.0001 or 0.00005 Å step size results in fewer instances in which the numeric gradient forward and backward steps have density components allocated to different expansion points. Once the step size decreases to 0.0001 Å, the RMSD and maximum gradient difference

between the numeric and analytic gradient were both on the order of 10^{-6} or 10^{-7} Hartree/Bohr. Similar to the previous case, this suggests that there may be discontinuities in the potential energy surface. Small step sizes in numeric gradients can be suspect, so in this case, the there is not an accurate numeric to analytic gradient comparison. However, when the multipole moment allocation algorithm is modified to always allocate to the same expansion points[1], the RMSD between the numeric and analytic gradient is on the order of 10^{-6} Hartree/Bohr and the maximum gradient difference between the numeric and analytic gradient is on the order of 10^{-5} Hartree/Bohr, both in the acceptable range.

6.1.4 Discussion of potential energy surface

In two of the above cases, the numeric and analytic gradients did not match until the step size was decreased or when the allocation algorithm for the multipole moments was changed to always allocate density components to the same expansion point for forward and backward displacements. This can be understood by considering how the multipole moments are calculated. To calculate the multipole moments, the nearest-site allocation algorithm is used to place multipole moments on expansion centers. The nearest-site allocation algorithm involves evaluating multipole moments at every Gaussian basis function overlap center (that is, at each piece of charge density), and then shifting the multipole moments to the nearest expansion center. In the EFMO method, all expansion centers are atom centers. If, during a MD simulation or geometry optimization, atoms in a single fragment move in such a way that the multipole moments at a Gaussian basis function overlap center are suddenly closer to a different atom center, then the

[1] This was done by modifying the nearest-site allocation algorithm to choose not the nearest atom, but rather the nearest of the two atoms upon which the two Gaussian basis functions that comprise the piece of charge density are centered.

multipole moments on the atoms are calculated differently, and thus the final energy is different. If the energy is significantly different, the PES will not be smooth. As noted above, one way to solve this problem is to require the energy calculations to use the same set of expansion centers. Although this is useful for testing the gradient, this is not an ideal solution since it changes the energy calculation. Alternatively, it is possible that including bond midpoints as expansion centers in the EFMO multipole expansion (as is done in the EFP method) might decrease or eliminate the problem. This possibility will be explored.

Currently, for the systems studied, the maximum difference between the numeric and analytic gradient is on the order of 10^{-5} Hartree/Bohr or less, and the RMSD is on the order of 10^{-6} Hartree/Bohr or less once the numeric gradient step size is small enough or if the allocation algorithm is modified so that the same expansion points are always used for the forward and backward steps in the numerical gradient procedure. The small differences between the analytic and numerical gradients imply that the analytic gradient is accurate. In addition, for small molecules such as water, displacing the atoms by 0.005 Å in the forward and backward directions generally uses the same expansion points. The problem discussed here is most likely to arise for larger molecules.

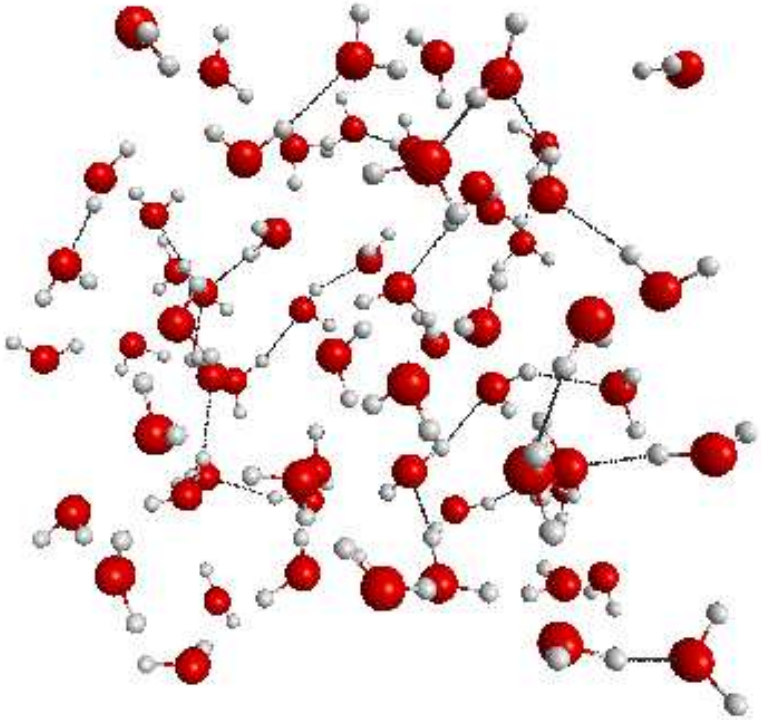

Figure 1: Geometry of 64 water molecules used in the numeric and analytic gradient comparison. Hydrogen atoms are light gray and oxygen atoms are red.

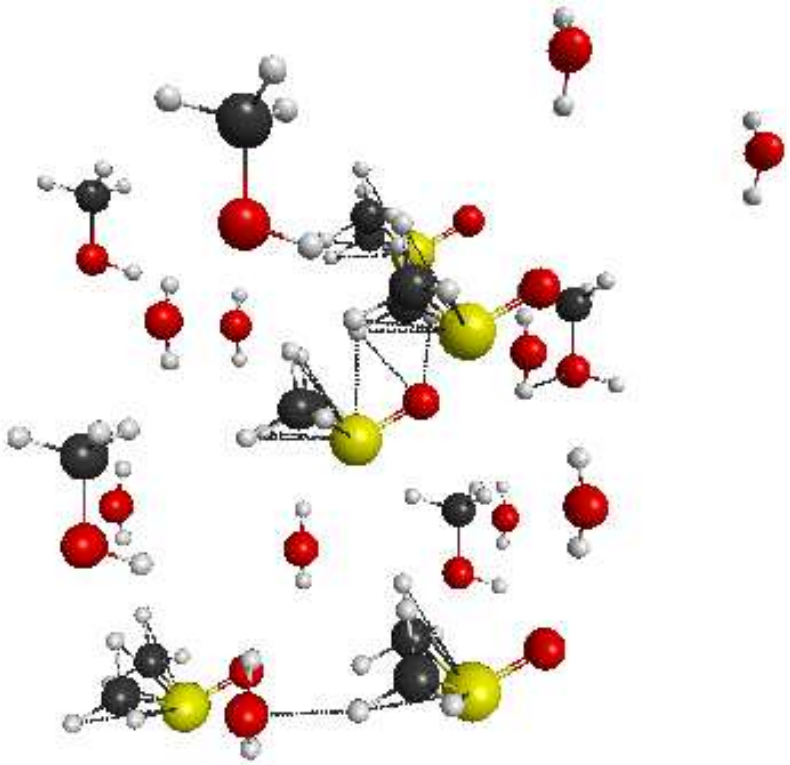

Figure 2: Geometry of a cluster of 5 DMSO, 5 methanol, 10 water molecules used in the numeric and analytic gradient comparison. Hydrogen atoms are light gray, carbon atoms are dark gray, oxygen atoms are red, and sulfur atoms are yellow.

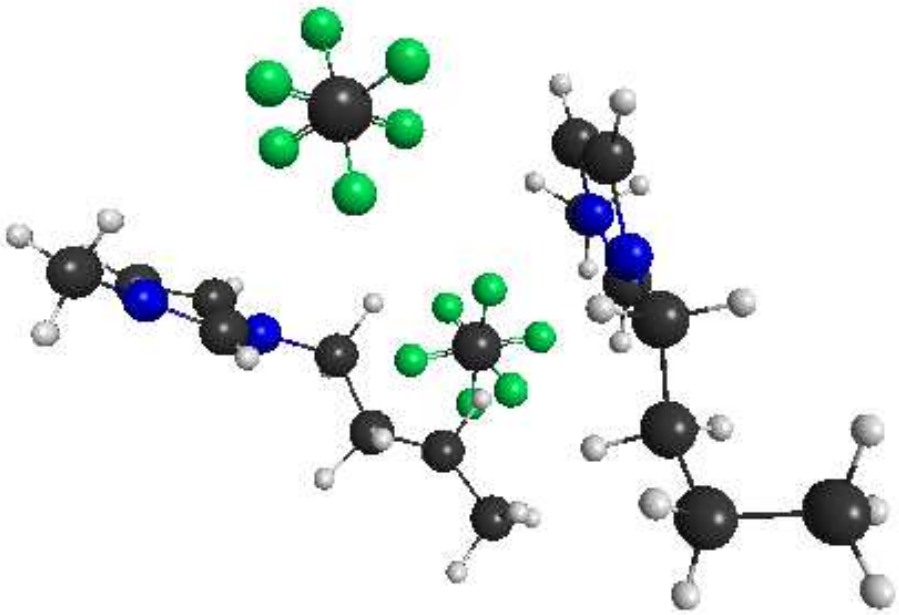

Figure 3: Geometry of 2[bmim]PF_6 used in the numeric and analytic gradient comparison. Hydrogen atoms are light gray, carbon atoms are dark gray, nitrogen atoms are blue, and fluorine atoms are green.

6.2 MD simulations

A system of 32 water molecules was equilibrated before each production run, as summarized below. For several of the steps, a Nose/Hoover thermostat that randomly reassigns the velocities to a Maxwell-Boltzman distribution every N fs, denoted Nose/Hoover (N) was used. The details of the simulations are as follows:

1. The initial configuration was generated by randomly placing 32 water molecules in a box with a volume that matches the density of water at 300 K.

2. A 6 ps NVT classical MD simulation of the water molecules was performed with the EFP method. The temperature was set to 300K and the time step size to 0.5 fs. A Nose/Hoover (500) thermostat was used to regulate the temperature.

3. The last configuration of the previous run was used as the initial configuration for a 500 fs NVT equilibration run performed with the EFMO method, with a 1.0 fs time step size and a Nose/Hoover (100) thermostat, at 300 K. The 6-31++G(d,p) basis set and R_{cut}=0.3 was used.

This set of equilibration runs was done to match previous MD simulations used to check energy conservation[8]. Periodic boundary conditions were not used, since this work is a test of the gradient, not a production simulation.

As discussed by Nakata et al.[34] and Brorsen et al. [8], the energy conservation in an NVE simulation using the Velocity-Verlet algorithm can be tested by comparing the RMSD(E) to the time step size. The RMSD(E), for M steps, is calculated as

$$\sqrt{\frac{\sum_{j}^{M}\left(\text{Energy at step } j - \text{Average energy of all steps}\right)^2}{M}} \tag{6.2}$$

For the Velocity-Verlet algorithm the relationship between the MD simulation time step size and the RMSD(E) for NVE ensembles should be

$$RMSD(E) \propto (\text{time step size})^2 \tag{6.3}$$

Eq. (6.3) can be rewritten as:

$$\log(RMSD(E)) \propto 2\log(\text{time step size}) \tag{6.4}$$

Thus, a log-log plot should show a straight line with a slope of about 2.

To check that the EFMO MD simulation using the analytic energy gradient closely follows Eq. (6.3), seven NVE EFMO MD simulations were run for 50 fs each. The initial configuration and velocity were taken from the last step of the equilibration runs. The seven runs had time step sizes of 0.1, 0.2, 0.25, 0.35, 0.5, 0.6, and 0.75 fs and R_{cut}=0.3. Figure 4 shows a log-log plot of the time step size vs. the RMSD(E) for the 7 runs. The plot shows a straight line with a slope of about 2.03, close to that which is expected when the energy is conserved. This suggests that for the seven time step sizes, EFMO MD simulations using the analytic gradient properly conserve energy in NVE ensembles.

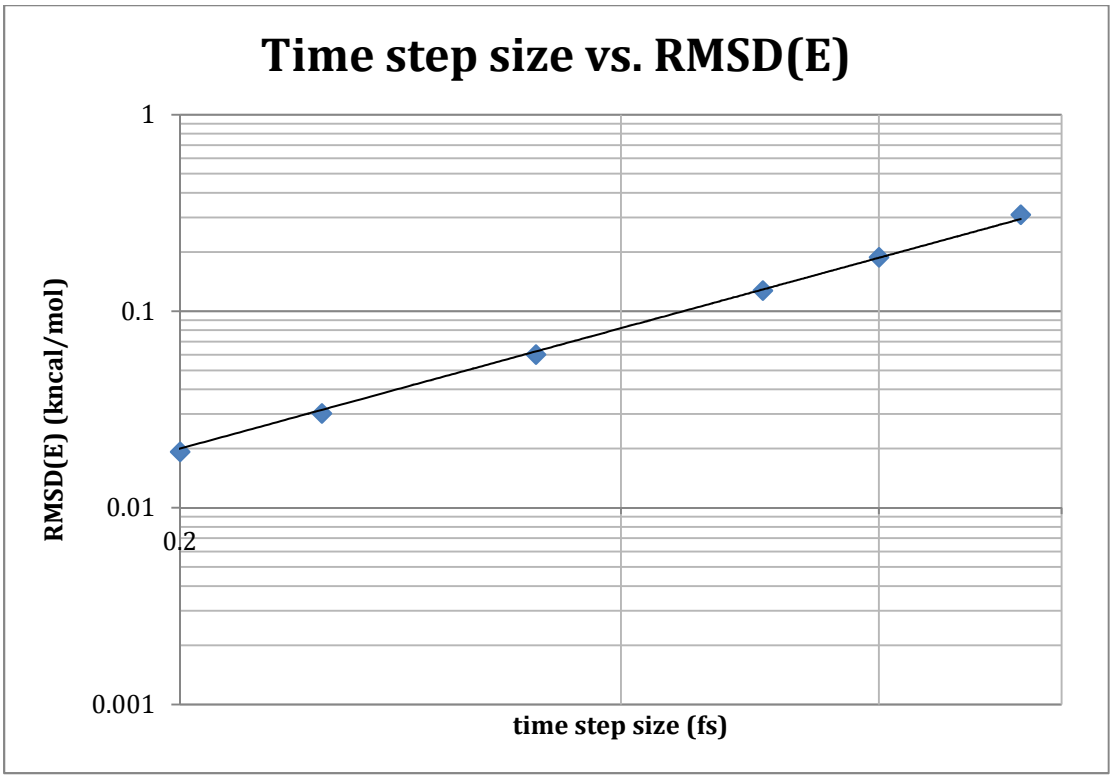

Figure 4: A log-log plot of six EFMO MD simulations of a 32-water cluster in the NVE ensemble using six different time step sizes vs. the RMSD(E) of the energy.

7. Timings

Timing comparisons between EFMO/MP2 and FMO2/MP2 gradient calculations, with the 6-31++G(d,p) basis set are presented in Table 3. All calculations were done on 4 compute nodes. Each compute node has two quad-core 3.0 GHz Intel Xenon E5450 CPUs connected by Mellanox 4X DDR Infiniband. Multi-level parallelism with GDDI was used to split each calculation into 4 groups. The timings were done for R_{cut}=1 and R_{cut}=2.

Table 3: Timing comparison for EFMO/MP2 and FMO2/MP2 gradient calculations on water clusters

	R_{cut}=1			R_{cut}=2		
	EFMO wall clock time (s)	**FMO wall clock time (s)**	**FMO time/ EFMO time**	**EFMO wall clock time (s)**	**FMO wall clock time (s)**	**FMO time/ EFMO time**
20 water molecules	20.00	33.00	1.65	35.90	61.30	1.71
30 water molecules	30.20	52.20	1.73	62.60	122.50	1.96
40 water molecules	42.30	69.80	1.65	74.20	138.30	1.86
64 water molecules	64.40	101.50	1.58	134.90	277.60	2.06

As can be seen in the table, the EFMO/MP2 method gives a speed up ranging from 1.58x to 2.06x compared to FMO2/MP2. Recall that EFMO includes explicit many-body interactions via the self-consistent EFP polarizability, whereas FMO2 does not. As seen in Ref. 7, EFMO can attain the same level as accuracy as FMO but with a smaller R_{cut} value. Thus it is possible that the speed up might be greater.

As mentioned above, the dimension of the largest response equation is the dimension of the largest monomer. In this work, the timings were obtained for systems in which the largest monomer is a water molecule. Since the dimension of the largest response equation in one iteration of the self-consistent Z-vector method in the FMO gradient[31] is also the dimension of the largest monomer, the comparison should hold for larger molecules.

Conclusions

As shown in Section 6, the current implementation of the EFMO gradient is fully analytic for the Coulomb, exchange-repulsion, polarization, and dispersion terms. For the

EFP interaction energy part of the gradient, response equations must be solved, but the response equations are separable, so there is no response equation with the dimension of the full system. That is, for the EFP interaction energy part of the gradient, the dimension of the largest response equation is the dimension of the largest monomer. If the gradient of the chosen *ab initio* method has response terms, then the gas phase monomer and dimer energy gradients will have response terms. The monomer response terms can be combined with the EFP interaction energy response terms, but the dimer response terms must be solved separately. As demonstrated in Section 7, the EFMO gradient is up to 2.06x faster than the FMO gradient.

In testing the analytic gradient, it was discovered that the allocation of charge density in the multipole moment calculation during a numeric gradient calculation for a large molecule can differ for the forward and backward steps, thereby causing the numeric and analytic gradient to differ by too much. It is anticipated that adding bond-midpoints as expansion points should decrease the impact of the allocation difference. This will be explored in a future paper. Future work will also include the derivation and implementation of the gradient of the charge-transfer term.

Acknowledgments

This research was supported by the U.S. Department of Energy, Office of Basic Energy Sciences, Division of Chemical Sciences, Geosciences, and Biosciences, through the Ames Laboratory Chemical Physics program. The Ames Laboratory is operated for the U.S. Department of Energy by Iowa State University under Contract No. DE-AC02-07CH11358. The authors thank Drs. Mike Schmidt, Aaron West, Peng Xu, and Federico Zahariev and Professor Hui Li for helpful discussions.

Appendix and Supporting Information

Appendix Section A: Response Equations, discussion of responses, and the Z-vector method

A1: Coupled Perturbed Hartree-Fock Equation

Since the molecular orbital coefficients are calculated using a variational minimization, the derivative of the molecular orbital coefficients can be calculated using the derivative of the variational conditional. For the RHF SCF equation, the variational condition is that $F_{ia} = F_{ai} = 0$ where *i* is an occupied orbital and *a* is virtual orbital.

For canonical molecular orbitals, the variational condition becomes $F_{pq} = F_{qp} = 0$ where $p \neq q$. This is described in detail previously[9], and results in the Coupled Perturbed Hartree-Fock Equation:

$$\sum_{c}^{vir}\sum_{k}^{occ} A_{pq,ck}U_{ck}^{x} = B_{pq}^{x} \tag{A.1}$$

where

$$A'_{pq,ck} = 4(pq\,|\,ck) - (pc\,|\,qk) - (pk\,|\,qc)$$
$$A_{pq,ck} = (\epsilon_q - \epsilon_p)\delta_{pc}\delta_{qk} - A'_{pq,ck}$$
$$B_{pq}^{x} = F_{pq}^{(x)} - S_{pq}^{(x)}\epsilon_q - \sum_{kj}^{occ} S_{kj}^{(x)}\left(2(pq\,|\,kj) - (pk\,|\,qj)\right)$$

and ϵ_q is the orbital energy of MO *q*.

Only the virtual-occupied block of the response matrix is uniquely defined. For the RHF energy, unitary transformations between occupied-occupied (occ-occ) and virtual-virtual (vir-vir) MOs do not change the energy (but must still follow the

orthonormality constraint on orbitals), and are not uniquely defined. They are often referred to as “non-independent”, while the vir-occ block is “independent”[9].

If it is assumed that the canonical MOs are used ($F_{ij} = F_{ji} = \delta_{ij}\epsilon_i$ where *i* is an occupied orbital and *j* is an occupied orbital), then the occ-occ part of the response matrix can be written as

$$U_{ij}^{x} = \frac{1}{(\epsilon_j - \epsilon_i)}\left(\sum_{c}^{vir}\sum_{k}^{occ} A'_{ij,ck}U_{ck}^{x} + B_{ij}^{x} \right) \tag{A.2}$$

although it is undefined when there is a degeneracy in orbital energy.

Alternately, if the energy expression is invariant to unitary transformations among the CMO occupied orbitals or the virtual orbitals then[35,36]

$$U_{ij}^{x} = -\frac{1}{2}S_{ij}^{(x)}$$
$$U_{ab}^{x} = -\frac{1}{2}S_{ab}^{(x)} \tag{A.3}$$

for the occ-occ or vir-vir part of the response matrix. This can only be used in certain formulations of gradients. For example, Eq. (A.3) is valid if the gradient is directly derived from an energy formula that does not assume a particular unitary transform of the MOs.

The CPHF equation can be solved for each canonical response matrix element. In practice, this is avoided, as described in the Z-vector method.

A2: Derivative of the orthonormality constraint with respect to a nuclear perturbation

$S_{pq} = \delta_{pq}$ implies $U^x_{pq} + U^x_{qp} = -S^{(x)}_{pq}$ when *x* is a nuclear perturbation (and the basis set depends on nuclear coordinates). For a field perturbation, α, $U^\alpha_{pq} + U^\alpha_{qp} = 0$ since the basis set does not depend on the field.

A3: Coupled Perturbed Localization (CPL) Equation

Since the LMO transform matrix is determined using the localization condition (which depends on the localization method used), the derivative of the LMO transform matrix can be determined from the derivative of the localization expression. (This is similar to how the CPHF equations are derived, where the MO coefficients are determined from the variational condition, and the derivative of the MO coefficients can be determined from the derivative of the variational condition). For this work, only Boys localization[10] has been considered. Other localization methods can be used, but the CPL equation would be different.

First, Eq. (2.3) is written in more detail:

$$\begin{aligned}
\frac{\partial c_{\mu l}^{L}}{\partial x} &= \sum_{i}^{\substack{occ \\ CMO}} \frac{\partial}{\partial x}\left(L_{li} c_{\mu i}\right) \\
&= \sum_{i}^{\substack{occ \\ CMO}} \frac{\partial L_{li}}{\partial x} c_{\mu i} + \sum_{i}^{\substack{occ \\ CMO}} L_{li} \frac{\partial c_{\mu i}}{\partial x} \\
&= \sum_{i}^{\substack{occ \\ CMO}} \frac{\partial L_{li}}{\partial x} c_{\mu i} + \sum_{i}^{\substack{occ \\ CMO}} L_{li} \sum_{q}^{\substack{occ+vir \\ CMO}} U_{qi}^{x} c_{\mu q} \\
&= \sum_{i}^{\substack{occ \\ CMO}} \frac{\partial L_{li}}{\partial x} \sum_{n}^{LMO} L_{ni} c_{\mu n}^{L} + \sum_{i}^{\substack{occ \\ CMO}} L_{li} \sum_{q}^{\substack{occ+vir \\ CMO}} U_{qi}^{x} c_{\mu q} \\
&= \sum_{n}^{LMO} c_{\mu n}^{L} \left[\sum_{i}^{\substack{occ \\ CMO}} L_{ni} \frac{\partial L_{li}}{\partial x} \right] + \sum_{i}^{\substack{occ \\ CMO}} L_{li} \sum_{q}^{\substack{occ+vir \\ CMO}} U_{qi}^{x} c_{\mu q} \\
&= \sum_{n}^{LMO} c_{\mu n}^{L} v_{nl}^{x} + \sum_{i}^{\substack{occ \\ CMO}} L_{li} \sum_{q}^{\substack{occ+vir \\ CMO}} U_{qi}^{x} c_{\mu q}
\end{aligned}$$

As previously known[16], the localization condition for Boys LMOs is

$$\mathbf{r}_{lm} \cdot (\mathbf{r}_{ll} - \mathbf{r}_{mm}) = 0 \tag{A.4}$$

where $\mathbf{r}_{lm} = (r_{lm,x}, r_{lm,y}, r_{lm,z})$ and $r_{lm,\alpha} = < l \mid \alpha \mid m >$.

for all *l,m* pairs of localized occupied orbitals. The bold notation indicates that the term is a vector.

Eq. (A.4) must be true at any geometry, so

$$\frac{\partial\left(\mathbf{r}_{lm} \cdot (\mathbf{r}_{ll} - \mathbf{r}_{mm})\right)}{\partial x} = 0 \tag{A.5}$$

This is the starting point for the Boys CPL equation. Other studies have presented the derivation of the equation for Boys (or similar localization methods) in detail[13,15,16,37], so the result is presented here. An overview of the derivation used in the code implemented for this study is below.

Eq. (A.5) is expanded and rearranged to form an equation for the localization response matrix (as is similarly done in the CPHF equation derivation).
The derivative of the LMO coefficient as shown in Eq. (2.3) is used throughout. Note also that v_{nl}^{x} is antisymmetric. Using

$\left\langle \frac{\partial l}{\partial x} \middle| \alpha \middle| m \right\rangle = \sum_{n}^{LMO} v_{nl}^{x} r_{nm,\alpha} + \sum_{i}^{\substack{occ \\ CMO}} L_{li} \sum_{q}^{\substack{all \\ CMO}} U_{qi}^{x} r_{qm,\alpha} + \sum_{\mu}^{AO} c_{\mu l}^{L} \left\langle \frac{\partial \mu}{\partial x} \middle| \alpha \middle| m \right\rangle$, the left-hand side of Eq. (A.5) becomes

$$\left(\mathbf{r}_{ll} - \mathbf{r}_{mm}\right)\left(\sum_{n}^{LMO} \left(v_{nl}^{x} \mathbf{r}_{nm} + v_{nm}^{x} \mathbf{r}_{nl} \right) + \sum_{j}^{\substack{occ \\ CMO}} \sum_{q}^{\substack{occ+vir \\ CMO}} U_{qj}^{x} \left(L_{lj} \mathbf{r}_{qm} + L_{mj} \mathbf{r}_{ql} \right) + \sum_{\mu}^{AO} c_{\mu l}^{L} \left\langle \frac{\partial \mu}{\partial x} \middle| \alpha \middle| m \right\rangle + \sum_{\mu}^{AO} c_{\mu m}^{L} \left\langle \frac{\partial \mu}{\partial x} \middle| \alpha \middle| l \right\rangle \right)$$
$$+2\mathbf{r}_{lm}\left(\sum_{n}^{LMO} \left(v_{nl}^{x} \mathbf{r}_{nl} - v_{nm}^{x} \mathbf{r}_{nm} \right) + \sum_{j}^{\substack{occ \\ CMO}} \sum_{q}^{\substack{occ+vir \\ CMO}} U_{qj}^{x} \left(L_{lj} \mathbf{r}_{ql} - L_{mj} \mathbf{r}_{qm} \right) + \sum_{\mu}^{AO} c_{\mu l}^{L} \left\langle \frac{\partial \mu}{\partial x} \middle| \alpha \middle| l \right\rangle - \sum_{\mu}^{AO} c_{\mu m}^{L} \left\langle \frac{\partial \mu}{\partial x} \middle| \alpha \middle| m \right\rangle \right) = 0 \tag{A.6}$$

After rearranging, and separating out the response matrices, Eq. (A.6) can be written as

$$\left(\mathbf{r}_{ll} - \mathbf{r}_{mm}\right)\left(\sum_{\mu}^{AO} c_{\mu l}^{L} \left\langle \frac{\partial \mu}{\partial x} \middle| \alpha \middle| m \right\rangle + \sum_{\mu}^{AO} c_{\mu m}^{L} \left\langle \frac{\partial \mu}{\partial x} \middle| \alpha \middle| l \right\rangle \right) + 2\mathbf{r}_{lm}\left(\sum_{\mu}^{AO} c_{\mu l}^{L} \left\langle \frac{\partial \mu}{\partial x} \middle| \alpha \middle| l \right\rangle - \sum_{\mu}^{AO} c_{\mu m}^{L} \left\langle \frac{\partial \mu}{\partial x} \middle| \alpha \middle| m \right\rangle \right)$$
$$+ \sum_{o<n}^{LMO} v_{no}^{x} \begin{pmatrix} \delta_{ol}\mathbf{r}_{nm}\left(\mathbf{r}_{oo} - \mathbf{r}_{mm}\right) + \delta_{om}\mathbf{r}_{nl}\left(\mathbf{r}_{ll} - \mathbf{r}_{oo}\right) + 2\mathbf{r}_{no}\left(\delta_{ol}\mathbf{r}_{om} - \delta_{om}\mathbf{r}_{lo}\right) \\ -\delta_{nl}\mathbf{r}_{om}\left(\mathbf{r}_{nn} - \mathbf{r}_{mm}\right) - \delta_{nm}\mathbf{r}_{ol}\left(\mathbf{r}_{ll} - \mathbf{r}_{nn}\right) - 2\mathbf{r}_{on}\left(\delta_{nl}\mathbf{r}_{nm} - \delta_{nm}\mathbf{r}_{ln}\right) \end{pmatrix}$$
$$+ \sum_{j}^{\substack{occ \\ CMO}} \sum_{q}^{\substack{occ+vir \\ CMO}} U_{qj}^{x} \left(\left(\mathbf{r}_{ll} - \mathbf{r}_{mm}\right)\left(L_{lj}\mathbf{r}_{qm} + L_{mj}\mathbf{r}_{ql} \right) + 2\mathbf{r}_{lm}\left(L_{lj}\mathbf{r}_{ql} - L_{mj}\mathbf{r}_{qm} \right) \right) = 0 \tag{A.7}$$

By the localization condition, Eq. (A.4),

$$\mathbf{r}_{lm} \cdot (\mathbf{r}_{ll} - \mathbf{r}_{mm}) = 0$$
$$\text{---} >$$
$$\mathbf{r}_{lm} \cdot \mathbf{r}_{ll} = \mathbf{r}_{lm} \cdot \mathbf{r}_{mm}$$

Using this, Eq. (A.7) can be rewritten:

$$-\sum_{o<n}^{LMO} v_{no}^{x} \left(\left(-\delta_{ol} \mathbf{r}_{mm} + \delta_{om} \mathbf{r}_{ml} - \delta_{nl} \mathbf{r}_{mm} + \delta_{nm} \mathbf{r}_{ml} \right) \left(\mathbf{r}_{nn} - \mathbf{r}_{oo} \right) + 2\mathbf{r}_{no} \left(\delta_{ol} \mathbf{r}_{om} - \delta_{om} \mathbf{r}_{lo} - \delta_{nl} \mathbf{r}_{nm} + \delta_{nm} \mathbf{r}_{ln} \right) \right)$$
$$= \left(\mathbf{r}_{ll} - \mathbf{r}_{mm} \right) \left(\sum_{\mu}^{AO} c_{\mu l}^{L} < \frac{\partial \mu}{\partial x} \mid \boldsymbol{\alpha} \mid m > + \sum_{\mu}^{AO} c_{\mu m}^{L} < \frac{\partial \mu}{\partial x} \mid \boldsymbol{\alpha} \mid l > \right) + 2\mathbf{r}_{lm} \left(\sum_{\mu}^{AO} c_{\mu l}^{L} < \frac{\partial \mu}{\partial x} \mid \boldsymbol{\alpha} \mid l > - \sum_{\mu}^{AO} c_{\mu m}^{L} < \frac{\partial \mu}{\partial x} \mid \boldsymbol{\alpha} \mid m > \right)$$
$$+ \sum_{j}^{CMO} \sum_{q}^{CMO} U_{oj}^{x} \left(\left(\mathbf{r}_{ll} - \mathbf{r}_{mm} \right) \left(L_{lj} \mathbf{r}_{qm} + L_{mj} \mathbf{r}_{ql} \right) + 2\mathbf{r}_{lm} \left(L_{lj} \mathbf{r}_{ql} - L_{mj} \mathbf{r}_{qm} \right) \right)$$

(A.8)

To simplify Eq. (A.8), the terms in front of the response matrices v and U can be collected into terms C^{cpl} and B^{cpl}, respectively. The remaining terms can be combined into the term A^{cpl}. Then Eq. (A.8) can be written as

$$\sum_{o<n}^{LMO} v_{no}^{x} C_{lm,no}^{cpl} = -A_{lm}^{cpl} + -\sum_{j}^{occ} \sum_{q}^{occ+vir} U_{qj}^{x} B_{lm,qj}^{cpl}$$

(A.9)

Above is the CPL equation. If the canonical MO response matrix (U^x) is known, Eq. (A.9) can be solved for each v^x. In practice, this is avoided, as shown in the Z-vector section.

A4: Second order Coupled Perturbed Hartree-Fock Equation

The variational condition for the RHF SCF equation is $F_{ia} = F_{ai} = 0$. This must be zero regardless of the fragment geometry. This means that $\frac{\partial^2 F_{ia}}{\partial x_1 \partial x_2} = \frac{\partial^2 F_{ai}}{\partial x_1 \partial x_2} = 0$ (where x_1 and x_2 are coordinates of two arbitrary atoms).

For this work, a nuclear derivative of the canonical response matrix to a field perturbation is needed. That is, $\frac{\partial U^{\alpha}}{\partial x}$ where α is an electric field in the x-, y-, or z-direction, and x is the coordinate of an atom. An expression for $\frac{\partial U^{\alpha}}{\partial x}$ can be derived as shown below:

$$\frac{\partial}{\partial x}\left(\frac{\partial F_{ia}}{\partial \alpha}\right) = 0 = \frac{\partial}{\partial x}\left(F_{ia}^{(\alpha)}\right) + \frac{\partial U_{ai}^{\alpha}}{\partial x} F_{aa} + \sum_{b}^{vir}\left(U_{bi}^{\alpha}\frac{\partial F_{ba}}{\partial x}\right) + \frac{\partial U_{ia}^{\alpha}}{\partial x} F_{ii} + \sum_{j}^{occ}\left(U_{ja}^{\alpha}\frac{\partial F_{ji}}{\partial x}\right) + \sum_{b}^{vir}\sum_{j}^{occ}\left(\frac{\partial U_{bj}^{\alpha}}{\partial x} A'_{ia,bj} + U_{bj}^{\alpha}\frac{\partial A'_{ia,bj}}{\partial x}\right) \tag{A.10}$$

Using $\left(\frac{\partial U_{pj}^{\alpha}}{\partial x} = -\frac{\partial U_{jp}^{\alpha}}{\partial x}\right)$ and $F_{ia}^{(\alpha)} = \langle i \,|\, \alpha \,|\, a \rangle$[8] (since α is a field derivative), Eq. (A.10) can be rewritten as:

$$\begin{aligned}
&\frac{\partial U_{ai}^{\alpha}}{\partial x}(F_{ii} - F_{aa}) - \sum_{b}^{vir}\sum_{j}^{occ}\left(\frac{\partial U_{bj}^{\alpha}}{\partial x} A'_{ai,bj}\right) \\
&= \frac{\partial}{\partial x}\left(\langle i \,|\, \alpha \,|\, a \rangle\right) + \sum_{b}^{vir}\left(U_{bi}^{\alpha}\frac{\partial F_{ba}}{\partial x}\right) + \sum_{j}^{occ}\left(U_{ja}^{\alpha}\frac{\partial F_{ji}}{\partial x}\right) + \sum_{b}^{vir}\sum_{j}^{occ}\left(U_{bj}^{\alpha}\frac{\partial A'_{ai,bj}}{\partial x}\right)
\end{aligned} \tag{A.11}$$

Eq. (A.11) only solves for the vir-occ block of $\frac{\partial U^{\alpha}}{\partial x}$, but that is all that is needed for this work.

A5: Second-order Time-Dependent Coupled Perturbed Hartree-Fock Equation

The second-order time-dependent coupled perturbed Hartree-Fock equation can be derived in a manner similar to the first order equation[38,39,28].

The first order TD CPHF equation can be derived by using time dependent Hartree-Fock theory and time dependent variational conditions. The interaction between a molecule and a time-dependent oscillating electric field with frequency ω and direction γ is considered, and the MO coefficients, Fock matrix, and energy can be expanded in terms of the perturbation. This can be written as

$$\langle a|\gamma|i\rangle + \sum_{b}^{vir}\sum_{j}^{occ}[2(ai|bj)-(ab|ij)]U_{bj}^{\gamma}(\pm\omega) + \sum_{b}^{vir}\sum_{j}^{occ}[2(ai|bj)-(aj|ib)]U_{bj}^{\gamma}(\pm\omega)$$
$$+\sum_{p}^{MO}U_{pi}^{\gamma}(\pm\omega)F_{pa} - \sum_{p}^{MO}U_{ap}^{\gamma}(\pm\omega)F_{pi} \pm \omega U_{ai}^{\gamma} = F_{ai}^{\gamma}(\pm\omega) \qquad \text{(A.12)}$$

The variational condition is $F_{ai}^{\gamma}(\pm\omega) = 0$, resulting in the first order TD CPHF equations. If the definition $Z_{ai}^{\gamma}(\omega) \equiv U_{ai}^{\gamma}(\omega) + U_{ai}^{\gamma}(-\omega)$ is used, and canonical MOs are assumed, then this can be rewritten as Eq. (3.19).

Since $F_{ai}^{\gamma}(\pm\omega) = 0$ regardless of the geometry, $\frac{\partial}{\partial x}F_{ai}^{\gamma}(\pm\omega) = 0$. Then the second-order TD CPHF equation can be derived by taking the nuclear derivative of Eq. (A.12), and using the variational condition. The resulting equation can be written as

$$\sum_{b}^{vir}\sum_{j}^{CMO}\sum_{c}^{vir}\sum_{k}^{CMO}\Big(H^{(2)}_{ai,bj}H^{(1)}_{bj,ck}\frac{\partial Z^{\gamma}_{ck}(i\omega)}{\partial x}\Big)-(i\omega)^2\frac{\partial Z^{\gamma}_{ai}(i\omega)}{\partial x}$$
$$=-2\sum_{b}^{vir}\sum_{j}^{CMO}H^{(2)}_{ai,bj}\frac{\partial\langle b|\gamma|j\rangle}{\partial x}+-\sum_{bc}^{vir}\sum_{jk}^{occ}H^{(2)}_{ai,bj}Z^{\gamma}_{ck}(i\omega)\frac{\partial A'_{bj,ck}}{\partial x}$$
$$+-\sum_{bc}^{vir}\sum_{j}^{occ}H^{(2)}_{ai,bj}Z^{\gamma}_{cj}(i\omega)\frac{\partial F_{bc}}{\partial x}+\sum_{b}^{vir}\sum_{jk}^{occ}H^{(2)}_{ai,bj}Z^{\gamma}_{bk}(i\omega)\frac{\partial F_{jk}}{\partial x}$$
$$+-\sum_{b}^{vir}\sum_{j}^{occ}\left[2\langle b|\gamma|j\rangle+\sum_{c}^{vir}\sum_{k}^{occ}H^{(1)}_{bj,ck}Z^{\gamma}_{ck}(i\omega)\right]\frac{\partial}{\partial x}((aj|bi)-(ab|ij))$$
$$+-\sum_{b}^{vir}\left[2\langle b|\gamma|i\rangle+\sum_{c}^{vir}\sum_{k}^{occ}H^{(1)}_{bi,ck}Z^{\gamma}_{ck}(i\omega)\right]\frac{\partial F_{ab}}{\partial x}$$
$$+\sum_{j}^{occ}\left[2\langle a|\gamma|j\rangle+\sum_{c}^{vir}\sum_{k}^{occ}H^{(1)}_{aj,ck}Z^{\gamma}_{ck}(i\omega)\right]\frac{\partial F_{ij}}{\partial x}$$

(A.13)

A6: The occupied-occupied and virtual-virtual canonical response matrix

The exchange repulsion, polarization, and dispersion EFP energy expressions involve sums over LMOs. As shown in Section 4, the use of LMOs results in gradient terms involving the occ-occ canonical response matrix due to the occ-occ canonical response matrix that is in the last term of Eq. (2.3).

If all occupied molecular orbitals are localized, then the energy is invariant to unitary transformations of the molecular orbitals that are used to initiate the localization procedure. This is not strictly true when the LMOs are not unique (e.g., the π orbitals in benzene)[41] but is true for all cases tested. Since the energy is invariant to rotations among the canonical molecular orbitals (which are the molecular orbitals that are used to initiate the localization procedure), Eq. (A.3) can be used to replace the occ-occ and vir-vir portion of the response matrix with a non-response term.

However, the EFP method by default is implemented with frozen chemical core occupied molecular orbitals. Thus, only the active (non chemical core) occupied molecular orbitals are localized, and used in the energy calculation. If only the active occupied MOs are localized, then the energy is only invariant to unitary rotations among the active occupied molecular orbitals. The act-act and core-core blocks of the response matrix can be replaced using Eq. (A.3), but the act-core part of the response matrix cannot. It can, however, be calculated using Eq. (A.2). This means that there could be singularities if a chemical core orbital energy and an active occupied orbital energy are the same. As noted in a derivation of the frozen core second order MP2 gradient[40], usually the chemical core orbital energies and active occupied orbital energies should not be degenerate.

Additionally, one can think of the Z-vector contributions to the final Lagrangian in Eq. (4.24) as contributions that correct for non-variational character[42] to make the expression appear variational in terms of orbital rotations.

The virtual-virtual block of the canonical response matrix is replaced with Eq. (A.3) as well. The difference between using Eq. (A.3) and using Eq. (A.2) is negligible for all cases tested. The final implementation uses Eq. (A.3) for the relevant blocks of the response matrix to avoid singularities.

A7: Z-Vector method

Once all terms with response matrices in them have been collected, the Z-vector method is used to avoid solving for all nuclear perturbations[9]. As an example, let $\sum_{i}^{occ}\sum_{a}^{vir} U_{ai}^{x} L_{ai}$ be one term of the gradient. By Eq. (A.1), $\sum_{a}^{vir}\sum_{i}^{occ} A_{pq,ai} U_{ai}^{x} = B_{pq}^{x}$. Then the contribution to the gradient can be rewritten as shown below.

$$\sum_{i}^{occ}\sum_{a}^{vir} U_{ai}^{x} L_{ai} = \sum_{i}^{occ}\sum_{a}^{vir}\left(\sum_{c}^{vir}\sum_{j}^{occ} (A)_{ai,cj}^{-1} B_{cj}^{x} \right) L_{ai}$$
$$= \sum_{c}^{vir}\sum_{j}^{occ} B_{cj}^{x}\left(\sum_{a}^{vir}\sum_{i}^{occ} (A)_{ai,cj}^{-1} L_{ai} \right)$$

(A.14)

Defining Z as the solution to $L_{ai} = \sum_{c}^{vir}\sum_{j}^{occ} A_{cj,ai} Z_{cj}$, then $\sum_{i}^{occ}\sum_{a}^{vir} U_{ai}^{x} L_{ai} = \sum_{c}^{vir}\sum_{j}^{occ} B_{cj}^{x} Z_{cj}$.

A8: Applying the Z-Vector method to the localization response term

This section discusses the details of using the Z-vector technique on the localization response term in Eq. (4.40)

First, the localization response matrix term can be modified, noting that $v_{ml}^{X_K,A}$ is antisymmetric, and defining $M_{ml,tot}^{A,2} = M_{ml,tot}^{A} - M_{lm,tot}^{A}$ as shown below

$$\sum_{l}^{LMO\in A}\sum_{m}^{LMO\in A} v_{ml}^{x_K A} M_{ml,tot}^{A} = \sum_{l<m}^{LMO\in A} v_{ml}^{x_K A}\left(M_{ml,tot}^{A} - M_{lm,tot}^{A} \right)$$
$$= \sum_{l<m}^{LMO\in A} v_{ml}^{x_K A} M_{ml,tot}^{A,2}$$

(A.15)

Then, using Sections A3 and A7,

$$\sum_{l<m}^{LMO\in A} v_{ml}^{x_K A} M_{ml,tot}^{A,2} = \sum_{l<m}^{LMO\in A} Z_{ml}^{cpl,A}\left(-A_{ml}^{cpl,A} + - \sum_{i}^{\substack{occ \\ CMO\in A}} \sum_{q}^{\substack{occ+vir \\ CMO\in A}} U_{qi}^{x_K A} B_{ml,qi}^{cpl,A} \right)$$

(A.16)

where Z comes from solving the Z-vector equation, $\sum_{o<n}^{LMO} C_{ml,no}^{cpl,A} Z_{ml}^{cpl,A} = M_{ml,tot}^{A,2}$.

Terms in Eq. (A.16) can be rearranged and combined with Eq. (4.40) to result in Eq. (4.24).

Appendix Section B: Coulomb gradient derivation details

To simplify subsequent equations, define a function, $F_{AB}^{Coul}(\{T_{\alpha\beta\ldots\gamma}^{IJ}\},\{m^I\},\{m^J\})$. Given a set of multipole moments on fragment *A*, multipole moments on fragment *B*, and multipole moment interaction tensors between all pairs of multipole moments on fragments *A* and *B*, $F_{AB}^{Coul}(\{T_{\alpha\beta\ldots\gamma}^{IJ}\},\{m^I\},\{m^J\})$ contains the EFP Coulomb energy as in Eq. (3.3):

$$F_{AB}^{Coul}(\{T_{\alpha\beta\ldots\gamma}^{IJ}\},\{m^I\},\{m^J\}) \equiv \sum_I^A \sum_J^B \left[\begin{array}{l} q^J q^I T^{IJ} - \sum_\alpha^{x,y,z} q^J \mu_\alpha^I T_\alpha^{IJ} + \frac{1}{3}\sum_{\alpha,\beta}^{x,y,z} q^J \Theta_{\alpha\beta}^I T_{\alpha\beta}^{IJ} + \sum_\alpha^{x,y,z} \mu_\alpha^J q^I T_\alpha^{IJ} \\ -\sum_{\alpha,\beta}^{x,y,z} \mu_\alpha^J \mu_\beta^I T_{\alpha\beta}^{IJ} + \frac{1}{3}\sum_{\alpha,\beta,\gamma}^{x,y,z} \mu_\alpha^J \Theta_{\beta\gamma}^I T_{\alpha\beta\gamma}^{IJ} + \ldots \end{array} \right] \tag{B.1}$$

$\{T_{\alpha\beta\ldots\gamma}^{IJ}\}$ represents the set of all multipole moment tensors on the RHS of Eq. (B.1). $\{m^I\}$ represents the set of all the multipole moments on *A* on the RHS of Eq. (B.1) and $\{m^J\}$ represents the set of all the multipole moments on *B* on the RHS of Eq. (B.1).

Noting that the multipole moments are products of a density matrix and a integral involving primitive Gaussians, Eq. (4.7) can be rewritten as

$$\begin{aligned} \frac{\partial E_{AB}^{Coul}}{\partial x_{K\in A}} &= F_{AB}^{Coul}(\{\frac{\partial T_{\alpha\beta\ldots\gamma}^{IJ}}{\partial x_{K\in A}}\},\{m^I\},\{m^J\}) + F_{AB}^{Coul}(\{T_{\alpha\beta\ldots\gamma}^{IJ}\},\{m_{PG-deriv}^{I,x_K}\},\{m^J\}) \\ &+ F_{AB}^{Coul}(\{T_{\alpha\beta\ldots\gamma}^{IJ}\},\{m_{density-deriv}^{I,x_K}\},\{m^J\}) \end{aligned} \tag{B.2}$$

Where $m^{I,x_K}_{PG-deriv}$ is the contribution from the PG integral derivatives and $m^{I,x_K}_{density-deriv}$ is the contribution from the density matrix derivatives.

The second term in Eq. (B.2) involves only derivatives of Gaussian integrals, which depend explicitly on the atom positions, and can be implemented in a straightforward manner. Care must be taken to properly account for the derivative of the expansion point in the dipole and quadrupole terms.

The third term in Eq. (B.2) involves the derivative of the density matrix, which has an implicit dependence on the atom positions. The third term is expanded:

$$
\begin{aligned}
&F^{Coul}_{AB}(\{T^{IJ}_{\alpha\ldots}\},\{m^{I,x_K}_{density-deriv}\},\{m^{J}\}) = \\
&= \sum_{I\in A}\sum_{J\in B}\sum_{\mu\nu}^{AO\in A}\frac{\partial P_{\mu\nu}}{\partial x_{K\in A}}\sum_{ut}^{\substack{PG\ u\in\mu \\ PG\ t\in\nu}}\sum_{\text{nearest } I}\left(-P'_{ut}\right)
\begin{bmatrix}
T^{IJ}q^{J}\langle u\,|\,t\rangle + \sum_{\alpha}^{\{x,y,z\}} T^{IJ}_{\alpha}\mu^{J}_{\alpha}\langle u\,|\,t\rangle + \sum_{\alpha,\beta}^{\{x,y,z\}} T^{IJ}_{\alpha\beta}\Theta^{J}_{\alpha\beta}\langle u\,|\,t\rangle - \sum_{\alpha}^{\{x,y,z\}} T^{IJ}_{\alpha}q^{J}_{\alpha}\langle u\,|\,\alpha-\alpha_I\,|\,t\rangle \\
-\sum_{\alpha,\beta}^{\{x,y,z\}} T^{IJ}_{\alpha\beta}\mu^{J}_{\beta}\langle u\,|\,\alpha-\alpha_I\,|\,t\rangle - \frac{1}{3}\sum_{\alpha,\beta,\gamma}^{\{x,y,z\}} T^{IJ}_{\alpha\beta\gamma}\Theta^{J}_{\beta\gamma}\langle u\,|\,\alpha-\alpha_I\,|\,t\rangle \\
+\frac{1}{3}\sum_{\alpha,\beta}^{\{x,y,z\}} T^{IJ}_{\alpha\beta}q^{J}\left\langle u\,|\,\hat{\Theta}_{\alpha\beta}-\hat{\Theta}_{\alpha\beta,I}\,|\,t\right\rangle + \frac{1}{3}\sum_{\alpha,\beta,\gamma}^{\{x,y,z\}} T^{IJ}_{\alpha\beta\gamma}\mu^{J}_{\gamma}\left\langle u\,|\,\hat{\Theta}_{\alpha\beta}-\hat{\Theta}_{\alpha\beta,I}\,|\,t\right\rangle \\
+\frac{1}{9}\sum_{\alpha,\beta,\gamma,\kappa}^{\{x,y,z\}} T^{IJ}_{\alpha\beta\gamma\kappa}\Theta^{J}_{\gamma\kappa}\left\langle u\,|\,\hat{\Theta}_{\alpha\beta}-\hat{\Theta}_{\alpha\beta,I}\,|\,t\right\rangle
\end{bmatrix} \\
&= \sum_{I\in A}\sum_{J\in B}\sum_{\mu\nu}^{AO\in A}\frac{\partial P_{\mu\nu}}{\partial x_{K\in A}}\sum_{ut}^{\substack{PG\ u\in\mu \\ PG\ t\in\nu}}\sum_{\text{nearest } I}\left[K^{IJ}_{ut}\right]
\end{aligned}
\tag{B.3}
$$

where $\alpha-\alpha_I$ and $\hat{\Theta}_{\alpha\beta}-\hat{\Theta}_{\alpha\beta,I}$ denote that the integral is being calculated around *I*, and K^{IJ} contains the terms that are summed over PGs.

The derivatives of the MO coefficients are replaced with expansions in terms of the canonical MO response matrix. The terms involving the response matrix are separated into the occupied-occupied terms and the virtual-occupied terms. The definitions in Section 2 and Appendix A are used.

$$
\begin{aligned}
&= \sum_{I\in A}\sum_{J\in B}\sum_{\mu\nu}^{AO\in A}\frac{\partial P_{\mu\nu}}{\partial x_{K\in A}}\sum_{ut\ \text{nearest}\ I}^{\substack{PG\ u\in\mu\\ PG\ t\in\nu}}\left[K_{ut}^{IJ}\right] \\
&= \sum_{I\in A}\sum_{J\in B}\sum_{\mu\nu}^{AO\in A}\left[\frac{\partial}{\partial x_{K\in A}}\left[2\sum_{i}^{occ\in A}c_{\mu i}c_{\nu i}\right]\right]_{ut\ \text{nearest}\ I}\sum^{\substack{PG\ u\in\mu\\ PG\ t\in\nu}}\left[K_{ut}^{IJ}\right] \\
&= 2\sum_{I\in A}\sum_{J\in B}\sum_{\mu\nu}^{AO\in A}\left[\sum_{i}^{occ\in A}\sum_{a}^{vir\in A}U_{ai}^{x_K A}(c_{\mu a}c_{\nu i}+c_{\nu a}c_{\mu i})\right]_{ut\ \text{nearest}\ I}\sum^{\substack{PG\ u\in\mu\\ PG\ t\in\nu}}\left[K_{ut}^{IJ}\right] \\
&+\sum_{I\in A}\sum_{J\in B}\sum_{\mu\nu}^{AO\in A}\left[\sum_{i}^{occ\in A}\sum_{j}^{occ\in A}(c_{\mu j}c_{\nu i}+c_{\nu j}c_{\mu i})(U_{ij}^{x_K A}+U_{ji}^{x_K A})\right]_{ut\ \text{nearest}\ I}\sum^{\substack{PG\ u\in\mu\\ PG\ t\in\nu}}\left[K_{ut}^{IJ}\right] \\
&= \sum_{i}^{occ\in A}\sum_{a}^{vir\in A}U_{ai}^{x_K A}\left[2\sum_{I\in A}\sum_{J\in B}\sum_{\mu\nu}^{AO\in A}\left[(c_{\mu a}c_{\nu i}+c_{\nu a}c_{\mu i})\right]\sum_{ut\ \text{nearest}\ I}^{\substack{PG\ u\in\mu\\ PG\ t\in\nu}}\left[K_{ut}^{IJ}\right]\right] \\
&+\sum_{I\in A}\sum_{J\in B}\sum_{\mu\nu}^{AO\in A}\left[\sum_{i}^{occ\in A}\sum_{j}^{occ\in A}(c_{\mu j}c_{\nu i}+c_{\nu j}c_{\mu i})(-S_{ij}^{(x_K)})\right]_{ut\ \text{nearest}\ I}\sum^{\substack{PG\ u\in\mu\\ PG\ t\in\nu}}\left[K_{ut}^{IJ}\right]
\end{aligned}
\tag{B.4}
$$

Then, noting the definition of K_{ut}^{IJ}, eq. (B.4) can be written as

$$
= \sum_{i}^{occ\in A}\sum_{a}^{vir\in A}U_{ai}^{x_K A}\left[F^{Coul}(\{T_{\alpha\beta\ldots\gamma}^{IJ}\},\{m_{U-weighted,ai}^{I}\},\{m^{J}\})\right]_{ai}+F^{Coul}(\{T_{\alpha\beta\ldots\gamma}^{IJ}\},\{m_{occ\text{-}weighted}^{I,x_K}\},\{m^{J}\})
\tag{B.5}
$$

where $\{m_{U-weighted,ai}^{I}\}\equiv\{q_{U-weighted,ai}^{I},\mu_{U-weighted,ai}^{I},\Theta_{U-weighted,ai}^{I}\}$ with

$$
q_{U-weighted,ai}^{I}\equiv-\sum_{\mu\nu}^{AO\in A}\sum_{ut\ \text{nearest}\ I}^{PG\in\mu\nu}2(c_{\mu a}c_{\nu i}+c_{\nu a}c_{\mu i})P'_{ut}\langle u\,|\,t\rangle
$$

and $\{m_{occ-weighted}^{I,x_K}\}\equiv\{q_{occ-weighted}^{I,x_K},\mu_{occ-weighted}^{I,x_K},\Theta_{occ-weighted}^{I,x_K}\}$ with

$$
q_{occ-weighted}^{I,x_K}\equiv-\sum_{\mu\nu}^{AO\in A}\sum_{ut\ \text{nearest}\ I}^{\substack{PG\ u\in\mu\\ PG\ t\in\nu}}\left[\sum_{i}^{occ\in A}\sum_{j}^{occ\in A}(c_{\mu j}c_{\nu i}+c_{\nu j}c_{\mu i})(-S_{ij}^{(x_K)})\right]P'_{ut}\langle u\,|\,t\rangle
$$

Then, using Eq. (B.5),

$$F_{AB}^{Coul}(\{T_{\alpha\ldots}^{IJ}\},\{m_{density-deriv}^{I,x_K}\},\{m^J\}) = \sum_{I\in A}\sum_{J\in B}\sum_{\mu\nu}^{AO\in A}\frac{\partial P_{\mu\nu}}{\partial x_{K\in A}}\sum_{ut\ \text{nearest}\ I}^{\substack{PG\ u\in\mu\\ PG\ t\in\nu}}\left[K_{ut}^{IJ}\right]$$

$$= \sum_{i}^{occ\in A}\sum_{a}^{vir\in A} U_{ai}^{x_K A}\left[F^{Coul}(\{T_{\alpha\beta\ldots\gamma}^{IJ}\},\{m_{U-weighted,ai}^{I}\},\{m^J\})\right]_{ai}$$

$$+F^{Coul}(\{T_{\alpha\beta\ldots\gamma}^{IJ}\},\{m_{occ\text{-}weighted}^{I,x_K}\},\{m^J\})$$

(B.6)

Eq. (B.6) can be combined with Eq. (B.2) to produce Eq. (B.7).

$$\frac{\partial E_{AB}^{Coul}}{\partial x_{K\in A}} = F_{AB}^{Coul}(\{\frac{\partial T_{\alpha\beta\ldots\gamma}^{IJ}}{\partial x_{K\in A}}\},\{m^I\},\{m^J\}) + F_{AB}^{Coul}(\{T_{\alpha\beta\ldots\gamma}^{IJ}\},\{m_{PG-deriv}^{I,x_K}\},\{m^J\}) + F_{AB}^{Coul}(\{T_{\alpha\beta\ldots\gamma}^{IJ}\},\{m_{density-deriv}^{I,x_K}\},\{m^J\})$$

$$= F_{AB}^{Coul}(\{\frac{\partial T_{\alpha\beta\ldots\gamma}^{IJ}}{\partial x_{K\in A}}\},\{m^I\},\{m^J\}) + F_{AB}^{Coul}(\{T_{\alpha\beta\ldots\gamma}^{IJ}\},\{m_{PG-deriv}^{I,x_K}\},\{m^J\})$$

$$+\sum_{i}^{\text{occ in A}}\sum_{a}^{\text{virt in A}} U_{ai}^{x_K A}\left[F_{AB}^{Coul}(\{T_{\alpha\beta\ldots\gamma}^{IJ}\},\{m_{U-weighted,ai}^{I}\},\{m^J\})\right]_{ai} + F_{AB}^{Coul}(\{T_{\alpha\beta\ldots\gamma}^{IJ}\},\{m_{occ\text{-}weighted}^{I,x_K}\},\{m^J\})$$

$$= F_{AB}^{Coul}(\{\frac{\partial T_{\alpha\beta\ldots\gamma}^{IJ}}{\partial x_{K\in A}}\},\{m^I\},\{m^J\}) + F_{AB}^{Coul}(\{T_{\alpha\beta\ldots\gamma}^{IJ}\},\{m_{PG-deriv}^{I,x_K}+m_{occ\text{-}weighted}^{I,x_K}\},\{m^J\})$$

$$+\sum_{i}^{\text{occ in A}}\sum_{a}^{\text{virt in A}} U_{ai}^{x_K A}\left[F_{AB}^{Coul}(\{T_{\alpha\beta\ldots\gamma}^{IJ}\},\{m_{U-weighted,ai}^{I}\},\{m^J\})\right]_{ai}$$

(B.7)

Appendix Section C: Exchange-repulsion gradient derivation details

This section presents the details of the derivation between Eq. (4.9) and Eq. (4.11). Expanding each derivative in Eq. (4.9) generates six terms (A-F)) that correspond to the six terms in Eq. (4.9):

$$(A)\quad \frac{\partial S_{lm}}{\partial x_K} = \sum_{\mu}^{AO\in A}\sum_{\nu}^{AO\in B} \frac{\partial c_{\mu l}^{L}}{\partial x_K} c_{\nu m}^{L} \langle \mu \mid \nu \rangle + S_{lm}^{(x)}$$

$$(B)\quad \frac{\partial F_{lm}^{A}}{\partial x_K} = \sum_{\mu}^{AO\in A} \frac{\partial c_{\mu l}^{L}}{\partial x_K} F_{\mu m}^{A} + \sum_{\mu}^{AO\in A} \frac{\partial c_{\mu m}^{L}}{\partial x_K} F_{\mu l}^{A} + \sum_{i}^{\substack{occ \\ CMO\in A}} \sum_{\mu}^{AO\in A} \frac{\partial c_{\mu i}}{\partial x_K} A'_{lm,\mu i} + F_{lm}^{A,(x)}$$

$$(C)\quad \frac{\partial T_{lm}}{\partial x_K} = \sum_{\mu}^{AO\in A}\sum_{\nu}^{AO\in B} \frac{\partial c_{\mu l}^{L}}{\partial x_K} c_{\nu m}^{L} \left\langle \mu \left| \frac{-\nabla^2}{2} \right| \nu \right\rangle + T_{lm}^{(x)}$$

$$(D)\quad \frac{\partial R_{lm}}{\partial x_K} = \frac{1}{R_{lm}} \sum_{\alpha}^{\{x,y,z\}} \left[(< l \mid \alpha \mid l > - < m \mid \alpha \mid m >) \frac{\partial < l \mid \alpha \mid l >}{\partial x_K} \right]$$

$$(E)\quad \frac{\partial R_{lJ}}{\partial x_K} = \frac{1}{R_{lJ}} \sum_{\alpha}^{\{x,y,z\}} \left[(< l \mid \alpha \mid l > - \alpha_J) \frac{\partial < l \mid \alpha \mid l >}{\partial x_K} \right]$$

$$(F)\quad \frac{\partial R_{lm}}{\partial x_K} = \frac{\left(x_I - \langle m \mid x \mid m \rangle\right)}{R_{lm}} \delta_{IK}$$

(C.1)

$A'_{lm,\mu i}$ is defined in Eq. (A.1). For the EFP method, the gradient of the EFP exchange repulsion term was derived by Li et al.[32] (See Eq. (2) in Ref. 32 in particular). The expansions in Eq. (C.1) can be substituted into Eq. (4.9) to rewrite the expression as Eq. (4.10).

The AO-derivative terms in Eq. (4.10), shown below, are straightforward to compute:

$$\sum_{\mu}^{AO\in A}\sum_{\nu}^{AO\in B}\frac{\partial S_{\mu\nu}}{\partial x_K}\left[-2\sum_{l}^{LMO\in A}\sum_{m}^{LMO\in B}c_{\mu l}^{L}c_{\nu m}^{L}\left[\mathrm{W}_{lm}^{S}\right]\right]$$
$$+\sum_{\mu,\nu}^{AO\in A}\frac{\partial F_{\mu\nu}^{A}}{\partial x_K}\left[-2\sum_{l}^{LMO\in A}\sum_{m}^{LMO\in A}c_{\mu l}^{L}c_{\nu m}^{L}\left[\sum_{n}^{\mathrm{LMO}\in B}S_{\mathrm{ln}}S_{mn}\right]\right]$$
$$+\sum_{\mu}^{AO\in A}\sum_{\nu}^{AO\in B}\frac{\partial T_{\mu\nu}}{\partial x_K}\left[-2\sum_{l}^{LMO\in A}\sum_{m}^{LMO\in B}c_{\mu l}^{L}c_{\nu m}^{L}\left[\mathrm{W}_{lm}^{T}\right]\right]$$
$$+\sum_{\mu,\nu}^{AO\in A}\sum_{\alpha}^{\{x,y,z\}}<\frac{\partial\mu}{\partial x_K}|\alpha|\nu>\left[2\sum_{l}^{LMO\in A}\sum_{\alpha}^{\{x,y,z\}}c_{\mu l}^{L}c_{\nu l}^{L}\left[W_{l\alpha}^{R}\right]\right] \tag{C.2}$$

The MO-coefficient derivatives in Eq. (4.10) can be expressed as

$$-2\sum_{l}^{LMO\in A}\sum_{m}^{LMO\in B}\sum_{\mu}^{AO\in A}\sum_{\nu}^{AO\in B}\left[\frac{\partial c_{\mu l}^{L}}{\partial x_K}c_{\nu m}^{L}S_{\mu\nu}\mathrm{W}_{lm}^{S}\right]$$
$$+-2\sum_{l}^{LMO\in A}\sum_{m}^{LMO\in A}\left[\sum_{\mu}^{AO\in A}\frac{\partial c_{\mu l}^{L}}{\partial x_K}F_{\mu m}^{A}+\sum_{\mu}^{AO\in A}\frac{\partial c_{\mu m}^{L}}{\partial x_K}F_{\mu l}^{A}+\sum_{i}^{\mathrm{CMO}\in \mathrm{A}}\sum_{\mu}^{AO\in A}\frac{\partial c_{\mu i}}{\partial x_K}A'_{lm,\mu i}\right]\left[\sum_{n}^{\mathrm{LMO}\in B}S_{ln}S_{mn}\right]$$
$$+-2\sum_{l}^{LMO\in A}\sum_{m}^{LMO\in B}\sum_{\mu}^{AO\in A}\sum_{\nu}^{AO\in B}\frac{\partial c_{\mu l}^{L}}{\partial x_K}c_{\nu m}^{L}T_{\mu\nu}\left[\mathrm{W}_{lm}^{T}\right]$$
$$+2\sum_{l}^{LMO\in A}\sum_{\alpha}^{\{x,y,z\}}\sum_{\mu}^{AO\in A}\sum_{\nu}^{AO\in A}\frac{\partial c_{\mu l}^{L}}{\partial x_K}c_{\nu l}^{L}<\mu|\alpha|\nu>\left[W_{l\alpha}^{R}\right] \tag{C.3}$$

where the Fock matrix derivative is expanded[9]. Eq. (C.3) can be rewritten using Eq. (2.3) to expand LMO coefficient derivatives into terms with localization and canonical MO response matrices:

$$
\begin{aligned}
&= \left[-2 \sum_{l}^{LMO\in A} \sum_{m}^{LMO\in A} v_{ml}^{x_K A} \left[\sum_{n}^{LMO\in B} S_{mn} \left[\mathrm{W}_{ln}^{S} \right] \right] + -2 \sum_{i}^{\substack{occ \\ CMO\in A}} \sum_{q}^{\substack{occ+vir \\ CMO\in A}} U_{qi}^{x_K A} \left[\sum_{l}^{LMO\in A} \sum_{m}^{LMO\in B} L_{li} S_{qm} \left[\mathrm{W}_{lm}^{S} \right] \right] \right] \\
&+ \left[\begin{array}{l} -4 \sum_{l}^{LMO\in A} \sum_{m}^{LMO\in A} v_{ml}^{x_K A} \left[\sum_{o}^{LMO\in A} F_{mo}^{A} \sum_{n}^{LMO\in B} S_{ln} S_{on} \right] + -4 \sum_{i}^{\substack{occ \\ CMO\in A}} \sum_{j}^{\substack{occ \\ CMO\in A}} U_{ji}^{x_K A} \left[\sum_{l}^{LMO\in A} \sum_{m}^{LMO\in A} L_{li} F_{jm}^{A} \sum_{n}^{LMO\in B} S_{ln} S_{mn} \right] \\ + -2 \sum_{i}^{\substack{occ \\ CMO\in A}} \sum_{p}^{\substack{occ+vir \\ CMO\in A}} U_{pi}^{x_K A} \left[\sum_{m}^{LMO\in A} \sum_{l}^{LMO\in A} A'_{ml,pi} \sum_{n}^{LMO\in B} S_{mn} S_{ln} \right] \end{array} \right] \\
&+ \left[-2 \sum_{l}^{LMO\in A} \sum_{m}^{LMO\in A} v_{ml}^{x_K A} \left[\sum_{n}^{LMO\in B} T_{mn} \mathrm{W}_{ln}^{T} \right] + -2 \sum_{i}^{\substack{occ \\ CMO\in A}} \sum_{q}^{\substack{occ+vir \\ CMO\in A}} U_{qi}^{x_K A} \left[\sum_{l}^{LMO\in A} \sum_{m}^{LMO\in B} L_{li} T_{qm} \mathrm{W}_{lm}^{T} \right] \right] \\
&+ \left[\begin{array}{l} 2 \sum_{l}^{LMO\in A} \sum_{m}^{LMO\in A} v_{ml}^{x_K A} \left[\sum_{\alpha}^{\{x,y,z\}} < m \mid \alpha \mid l > W_{l\alpha}^{R} \right] \\ +2 \sum_{i}^{\substack{occ \\ CMO\in A}} \sum_{q}^{\substack{occ+vir \\ CMO\in A}} U_{qi}^{x_K A} \left[\sum_{l}^{LMO\in A} L_{li} \sum_{\alpha}^{\{x,y,z\}} < q \mid \alpha \mid l > W_{l\alpha}^{R} \right] \end{array} \right]
\end{aligned}
\tag{C.4}
$$

The fifth term can be simplified using Section A2 to remove the occ-occ canonical response matrix.

$$
\begin{aligned}
&= \left[-2 \sum_{l}^{LMO\in A} \sum_{m}^{LMO\in A} v_{ml}^{x_K A} \left[\sum_{n}^{LMO\in B} S_{mn} \left[\mathrm{W}_{ln}^{S} \right] \right] + -2 \sum_{i}^{\substack{occ \\ CMO\in A}} \sum_{q}^{\substack{occ+vir \\ CMO\in A}} U_{qi}^{x_K A} \left[\sum_{l}^{LMO\in A} \sum_{m}^{LMO\in B} L_{li} S_{qm} \left[\mathrm{W}_{lm}^{S} \right] \right] \right] \\
&+ \left[\begin{array}{l} -4 \sum_{l}^{LMO\in A} \sum_{m}^{LMO\in A} v_{ml}^{x_K A} \left[\sum_{o}^{LMO\in A} F_{mo}^{A} \sum_{n}^{LMO\in B} S_{ln} S_{on} \right] + -4 \sum_{i}^{\substack{occ \\ CMO\in A}} \sum_{j}^{\substack{occ \\ CMO\in A}} U_{ji}^{x_K A} \left[\sum_{l}^{LMO\in A} \sum_{m}^{LMO\in A} L_{li} F_{jm}^{A} \sum_{n}^{LMO\in B} S_{ln} S_{mn} \right] \\ + \sum_{i,j}^{\substack{occ \\ CMO\in A}} S_{ji}^{(x_K)} \left[\sum_{m}^{LMO\in A} \sum_{l}^{LMO\in A} A'_{ml,ji} \sum_{n}^{LMO\in B} S_{mn} S_{ln} \right] + -2 \sum_{i}^{\substack{occ \\ CMO\in A}} \sum_{a}^{vir\in A} U_{ai}^{x_K A} \left[\sum_{m}^{LMO\in A} \sum_{l}^{LMO\in A} A'_{ml,ai} \sum_{n}^{LMO\in B} S_{mn} S_{ln} \right] \end{array} \right] \\
&+ \left[-2 \sum_{l}^{LMO\in A} \sum_{m}^{LMO\in A} v_{ml}^{x_K A} \left[\sum_{n}^{LMO\in B} T_{mn} \mathrm{W}_{ln}^{T} \right] + -2 \sum_{i}^{\substack{occ \\ CMO\in A}} \sum_{q}^{\substack{occ+vir \\ CMO\in A}} U_{qi}^{x_K A} \left[\sum_{l}^{LMO\in A} \sum_{m}^{LMO\in B} L_{li} T_{qm} \mathrm{W}_{lm}^{T} \right] \right] \\
&+ \left[\begin{array}{l} 2 \sum_{l}^{LMO\in A} \sum_{m}^{LMO\in A} v_{ml}^{x_K A} \left[\sum_{\alpha}^{\{x,y,z\}} < m \mid \alpha \mid l > W_{l\alpha}^{R} \right] \\ +2 \sum_{i}^{\substack{occ \\ CMO\in A}} \sum_{q}^{\substack{occ+vir \\ CMO\in A}} U_{qi}^{x_K A} \left[\sum_{l}^{LMO\in A} L_{li} \sum_{\alpha}^{\{x,y,z\}} < q \mid \alpha \mid l > W_{l\alpha}^{R} \right] \end{array} \right]
\end{aligned}
\tag{C.5}
$$

Combining Eq. (C.5), Eq. (C.2), and the last term in Eq. (4.10) results in Eq. (4.11). Note that since $v^{x_K A}$ is antisymmetric, certain terms can be simplified.

Appendix Section D: Polarization gradient derivation details

D1: Eq. (4.12) is expanded to the form in Eq. (4.13):

Eq. (4.12) can be rewritten by splitting the first term into a sum over the LMOs on fragment *A* and a sum over the LMOs on all the other fragments; using Eq. (3.10), $E_{n,\alpha}^{0,B}$ can be expanded.

Then, the first term in Eq. (4.12) is:

$$-\sum_{B}^{\text{fragments}}\sum_{n}^{LMO\in B}\sum_{\alpha}^{\{x,y,z\}}\left(\frac{\partial E_{n,\alpha}^{0,B}}{\partial x_{K\in A}}\right)\left(\frac{p_{n,\alpha}^{B}+\tilde{p}_{n,\alpha}^{B}}{2}\right)=-\sum_{n}^{LMO\in A}\sum_{\alpha}^{\{x,y,z\}}\sum_{B\neq A}^{\text{fragments}}\sum_{I}^{B}\left(\frac{\partial E_{nI,\alpha}^{0}}{\partial x_{K\in A}}\right)\left(\frac{p_{n,\alpha}^{A}+\tilde{p}_{n,\alpha}^{A}}{2}\right)$$
$$-\sum_{B\neq A}^{\text{fragments}}\sum_{n}^{LMO\in B}\sum_{\alpha}^{\{x,y,z\}}\sum_{C\neq B}^{\text{fragments}}\sum_{I}^{C}\left(\frac{\partial E_{nI,\alpha}^{0}}{\partial x_{K\in A}}\right)\left(\frac{p_{n,\alpha}^{B}+\tilde{p}_{n,\alpha}^{B}}{2}\right) \tag{D.1}$$

In the first term in Eq. (D.1), $E_{nI,\alpha}^{0}$ is a function of the LMO centroid *n* on *A*, the atom center $I \in B$, and the multipole moments on *I*. Since the derivative is with respect to an atom in fragment *A*, and $B \neq A$, the derivative only affects $E_{nI,\alpha}^{0}$ through the LMO centroid *n* on *A*. The LMO centroid *n*, $\langle n|\beta|n\rangle$, is a function of the atom position through the LMO coefficients (with an implicit dependence) and the AO integrals (with an explicit dependence). Since $E_{nI,\alpha}^{0}$ is a function of LMO centroid *n*, and LMO centroid *n* is a function of the atom position, the chain rule can be used to obtain the derivative of $E_{nI,\alpha}^{0}$ with respect to the atom position, as shown in the first term in Eq. (D.2) below.

In the second term in Eq. (D.1), $E^0_{nI,\alpha}$ is a function of the LMO centroid *n* on *B*, the atom center $I \in C$, and the multipole moments on *I*. The derivative is with respect to an atom on *A*, so the only nonzero term will be for *C*=*A*. Then Eq. (D.1) can be rewritten as:

$$
\begin{aligned}
&-\sum_{B}^{\text{fragments}} \sum_{n}^{LMO\in B} \sum_{\alpha}^{\{x,y,z\}} \left(\frac{\partial E^{0,B}_{n,\alpha}}{\partial x_{K\in A}} \right) \left(\frac{p^B_{n,\alpha} + \tilde{p}^B_{n,\alpha}}{2} \right) = \\
&-\sum_{n}^{LMO\in A} \sum_{\beta}^{\{x,y,z\}} \frac{\partial \langle n \,|\, \beta \,|\, n \rangle}{\partial x_{K\in A}} \left[\sum_{\alpha}^{\{x,y,z\}} \sum_{B\neq A}^{\text{fragments}} \sum_{I}^{B} \left(\frac{\partial E^0_{nI,\alpha}}{\partial \langle n \,|\, \beta \,|\, n \rangle} \right) \left(\frac{p^A_{n,\alpha} + \tilde{p}^A_{n,\alpha}}{2} \right) \right] \\
&-\sum_{B\neq A}^{\text{fragments}} \sum_{n}^{LMO\in B} \sum_{\alpha}^{\{x,y,z\}} \sum_{I}^{A} \left(\frac{\partial E^0_{nI,\alpha}}{\partial x_{K\in A}} \right) \left(\frac{p^B_{n,\alpha} + \tilde{p}^B_{n,\alpha}}{2} \right)
\end{aligned}
\tag{D.2}
$$

The second term in Eq. (D.2) can be expanded in a similar fashion as the gradient of the Coulomb term in Section 4.3.1. That is,

$$
\begin{aligned}
&\sum_{B\neq A}^{\text{fragments}} \sum_{n}^{LMO\in B} \sum_{\alpha}^{\{x,y,z\}} \sum_{I}^{A} \left(\frac{\partial E^0_{nI,\alpha}}{\partial x_{K\in A}} \right) \left(\frac{p^B_{n,\alpha} + \tilde{p}^B_{n,\alpha}}{2} \right) \\
&= \sum_{B\neq A}^{\text{fragments}} \sum_{n}^{LMO\in B} \sum_{I}^{A} \left(\begin{aligned} &\sum_{\alpha}^{\{x,y,z\}} \frac{\partial \left(q^I T^{nI}_{\alpha} \right)}{\partial x_{K\in A}} \left(\frac{p^B_{n,\alpha} + \tilde{p}^B_{n,\alpha}}{2} \right) + \sum_{\alpha\beta}^{\{x,y,z\}} \frac{\partial \left(\mu^I_{\beta} T^{nI}_{\alpha\beta} \right)}{\partial x_{K\in A}} \left(\frac{p^B_{n,\alpha} + \tilde{p}^B_{n,\alpha}}{2} \right) \\ &+ \frac{1}{3} \sum_{\alpha\beta\gamma}^{\{x,y,z\}} \frac{\partial \left(\Theta^I_{\beta\gamma} T^{nI}_{\alpha\beta\gamma} \right)}{\partial x_{K\in A}} \left(\frac{p^B_{n,\alpha} + \tilde{p}^B_{n,\alpha}}{2} \right) \end{aligned} \right)
\end{aligned}
\tag{D.3}
$$

To simplify Eq. (D.3), let

$$
F^P_A(\{T^{nI}_{\alpha\beta\ldots\gamma}\},\{m^I\},\{p_n\}) \equiv \sum_{B\neq A}^{\text{fragments}} \sum_{n}^{LMO\in B} \sum_{I}^{A} \left(\begin{aligned} &\sum_{\alpha}^{\{x,y,z\}} q^I T^{nI}_{\alpha} \left(\frac{p^B_{n,\alpha} + \tilde{p}^B_{n,\alpha}}{2} \right) + \sum_{\alpha\beta}^{\{x,y,z\}} \mu^I_{\beta} T^{nI}_{\alpha\beta} \left(\frac{p^B_{n,\alpha} + \tilde{p}^B_{n,\alpha}}{2} \right) \\ &+ \frac{1}{3} \sum_{\alpha\beta\gamma}^{\{x,y,z\}} \Theta^I_{\beta\gamma} T^{nI}_{\alpha\beta\gamma} \left(\frac{p^B_{n,\alpha} + \tilde{p}^B_{n,\alpha}}{2} \right) \end{aligned} \right)
$$

As in Eq. (B.1), $\{T^{nI}_{\alpha\beta\ldots\gamma}\}$ represents the set of all multipole moment tensors on the RHS of the above expression. $\{m^I\}$ represents the set of all the multipole moments on A on the RHS of the above expression and $\{p_n\}$ represents the set of all the induced dipoles on in the RHS of the above expression.

Then, Eq. (D.3) can be written as:

$$\sum_{B\neq A}^{\text{fragments}}\sum_{n}^{LMO\in B}\sum_{\alpha}^{\{x,y,z\}}\sum_{I}^{A}\left(\frac{\partial E^0_{nI,\alpha}}{\partial x_{K\in A}}\right)\left(\frac{p^B_{n,\alpha}+\tilde{p}^B_{n,\alpha}}{2}\right)=F^P_A(\{\frac{\partial T^{nI}_{\alpha\beta\ldots\gamma}}{\partial x_{K\in A}}\},\{m^I\},\{p_n\})$$
$$+F^P_A(\{T^{nI}_{\alpha\beta\ldots\gamma}\},\{\frac{\partial m^I}{\partial x_{K\in A}}\},\{p_n\}) \qquad \text{(D.4)}$$

The second term in Eq. (4.12) can be expanded and split into terms involving the derivative of LMO centroids and a term involving the dipole polarizability tensor:

$$\frac{1}{2}\sum_{BC}^{\text{fragments}}\sum_{m}^{LMO\in B}\sum_{n}^{LMO\in C}\sum_{\alpha,\beta}^{\{x,y,z\}}(\tilde{p}^C_{n,\alpha})\left(\frac{\partial D_{nm,\alpha\beta}}{\partial x_{K\in A}}\right)p^B_{m,\beta}=$$
$$\frac{1}{2}\sum_{n}^{LMO\in A}\sum_{\alpha,\beta}^{\{x,y,z\}}(\tilde{p}^A_{n,\alpha})\left(\frac{\partial D_{nn,\alpha\beta}}{\partial x_{K\in A}}\right)p^A_{n,\beta}+\frac{1}{2}\sum_{B\neq A}^{\text{fragments}}\sum_{m}^{LMO\in B}\sum_{n}^{LMO\in A}\sum_{\alpha,\beta}^{\{x,y,z\}}(\tilde{p}^A_{n,\alpha})\left(\frac{\partial D_{nm,\alpha\beta}}{\partial x_{K\in A}}\right)p^B_{m,\beta}$$
$$+\frac{1}{2}\sum_{C\neq A}^{\text{fragments}}\sum_{m}^{LMO\in A}\sum_{n}^{LMO\in C}\sum_{\alpha,\beta}^{\{x,y,z\}}(\tilde{p}^C_{n,\alpha})\left(\frac{\partial D_{nm,\alpha\beta}}{\partial x_{K\in A}}\right)p^A_{m,\beta} \qquad \text{(D.5)}$$

Eq. (D.5) can be rewritten in terms of LMO centroid derivatives and dipole polarizability tensor derivatives, as shown below.

$$
\begin{aligned}
&= \frac{1}{2}\sum_{n}^{LMO\in A}\sum_{\beta,\gamma}^{\{x,y,z\}}(\tilde{p}^{A}_{n,\beta})\left(\frac{\partial\left(\alpha^{-1}_{n,\beta\gamma}\right)}{\partial x_{K\in A}}\right)p^{A}_{n,\gamma} + \frac{1}{2}\sum_{B\neq A}^{\text{fragments}}\sum_{m}^{LMO\in B}\sum_{n}^{LMO\in A}\sum_{\alpha,\beta}^{\{x,y,z\}}(\tilde{p}^{A}_{n,\alpha})\left(\sum_{\gamma}^{\{x,y,z\}}\frac{\partial D_{nm,\alpha\beta}}{\partial\langle n\,|\,\gamma\,|\,n\rangle}\frac{\partial\langle n\,|\,\gamma\,|\,n\rangle}{\partial x_{K\in A}}\right)p^{B}_{m,\beta} \\
&+\frac{1}{2}\sum_{C\neq A}^{\text{fragments}}\sum_{m}^{LMO\in A}\sum_{n}^{LMO\in C}\sum_{\alpha,\beta}^{\{x,y,z\}}(\tilde{p}^{C}_{n,\alpha})\left(\sum_{\gamma}^{\{x,y,z\}}\frac{\partial D_{nm,\alpha\beta}}{\partial\langle m\,|\,\gamma\,|\,m\rangle}\frac{\partial\langle m\,|\,\gamma\,|\,m\rangle}{\partial x_{K\in A}}\right)p^{A}_{m,\beta} \\
&= \frac{1}{2}\sum_{n}^{LMO\in A}\sum_{\beta,\gamma}^{\{x,y,z\}}(\tilde{p}^{A}_{n,\beta})\left(\frac{\partial\left(\alpha^{-1}_{n,\beta\gamma}\right)}{\partial x_{K\in A}}\right)p^{A}_{n,\gamma} \\
&+\frac{1}{2}\sum_{n}^{LMO\in A}\sum_{\gamma}^{\{x,y,z\}}\frac{\partial\langle n\,|\,\gamma\,|\,n\rangle}{\partial x_{K\in A}}\sum_{B\neq A}^{\text{fragments}}\sum_{m}^{LMO\in B}\sum_{\alpha,\beta}^{\{x,y,z\}}\left[(\tilde{p}^{A}_{n,\alpha})\left(\frac{\partial D_{nm,\alpha\beta}}{\partial\langle n\,|\,\gamma\,|\,n\rangle}\right)p^{B}_{m,\beta} + (\tilde{p}^{B}_{m,\alpha})\left(\frac{\partial D_{mn,\alpha\beta}}{\partial\langle n\,|\,\gamma\,|\,n\rangle}\right)p^{A}_{n,\beta}\right]
\end{aligned}
\tag{D.6}
$$

D2: Details of the expansion of the three terms in Eq. (4.15)

The LMO transform derivative can be written as

$$
\begin{aligned}
&\sum_{n}^{LMO\in A}\sum_{\beta,\gamma}^{\{x,y,z\}}\tilde{E}^{tot,A}_{n,\beta}\left(\sum_{jk}^{occ}\sum_{a}^{vir\in A}\frac{\partial L_{nj}}{\partial x_{K\in A}}L_{nk}U^{\gamma A}_{aj}\langle a\,|\,\beta\,|\,k\rangle\right)E^{tot,A}_{n,\gamma} + \sum_{n}^{LMO\in A}\sum_{\beta,\gamma}^{\{x,y,z\}}\tilde{E}^{tot,A}_{n,\beta}\left(\sum_{jk}^{occ}\sum_{a}^{vir\in A}L_{nj}\frac{\partial L_{nk}}{\partial x_{K\in A}}U^{\gamma A}_{aj}\langle a\,|\,\beta\,|\,k\rangle\right)E^{tot,A}_{n,\gamma} \\
&= \sum_{n}^{LMO\in A}\sum_{j}^{occ\,CMO\in A}\frac{\partial L_{nj}}{\partial x_{K\in A}}\sum_{\beta,\gamma}^{\{x,y,z\}}\tilde{E}^{tot,A}_{n,\beta}\sum_{k}^{occ\,CMO\in A}\sum_{a}^{vir\in A}L_{nk}\left(U^{\gamma A}_{aj}\langle a\,|\,\beta\,|\,k\rangle + U^{\gamma A}_{ak}\langle a\,|\,\beta\,|\,k\rangle\right)E^{tot,A}_{n,\gamma} \\
&= \sum_{n}^{LMO\in A}\sum_{j}^{occ\,CMO\in A}\sum_{l}^{LMO\in A}L_{lj}v^{x_K A}_{ln}\sum_{\beta,\gamma}^{\{x,y,z\}}\tilde{E}^{tot,A}_{n,\beta}\sum_{k}^{occ\,CMO\in A}\sum_{a}^{vir\in A}L_{nk}\left(U^{\gamma A}_{aj}\langle a\,|\,\beta\,|\,k\rangle + U^{\gamma A}_{ak}\langle a\,|\,\beta\,|\,k\rangle\right)E^{tot,A}_{n,\gamma} \\
&= \sum_{n,l}^{LMO\in A}v^{x_K A}_{ln}\left(\sum_{\beta,\gamma}^{\{x,y,z\}}\tilde{E}^{tot,A}_{n,\beta}\sum_{jk}^{occ\,CMO\in A}\sum_{a}^{vir\in A}L_{lj}L_{nk}\left(U^{\gamma A}_{aj}\langle a\,|\,\beta\,|\,k\rangle + U^{\gamma A}_{ak}\langle a\,|\,\beta\,|\,k\rangle\right)E^{tot,A}_{n,\gamma}\right) \\
&= \sum_{l,n}^{LMO\in A}v^{x_K A}_{ln}D_{ln}
\end{aligned}
\tag{D.7}
$$

where D is a term containing the coefficient of v.

The MO field response term can be written as

$$
\sum_{\gamma}^{\{x,y,z\}}\sum_{j}^{occ\,CMO\in A}\sum_{a}^{vir\in A}\frac{\partial U^{\gamma A}_{aj}}{\partial x_{K\in A}}\left[2\sum_{n}^{LMO\in A}\sum_{\beta}^{\{x,y,z\}}\tilde{E}^{tot,A}_{n,\beta}\sum_{k}^{occ\,CMO\in A}L_{nj}L_{nk}\langle a\,|\,\beta\,|\,k\rangle E^{tot,A}_{n,\gamma}\right]
\tag{D.8}
$$

The dipole derivative term can be written as

$$\sum_{\beta}^{\{x,y,z\}}\sum_{k}^{occ}\sum_{a}^{CMO\in A}\sum^{vir\in A}\frac{\partial\langle a\,|\,\beta\,|\,k\rangle}{\partial x_{K\in A}}\left[\sum_{n}^{LMO\in A}\sum_{\gamma}^{\{x,y,z\}}\tilde{E}_{n,\beta}^{tot,A}\left(2\sum_{j}^{occ}{}^{CMO\in A}L_{nj}L_{nk}U_{aj}^{\gamma}\right)E_{n,\gamma}^{tot,A}\right]$$

$$=\sum_{\beta}^{\{x,y,z\}}\sum_{k}^{occ}\sum_{a}^{CMO\in A}\sum^{vir\in A}\frac{\partial\langle a\,|\,\beta\,|\,k\rangle}{\partial x_{K\in A}}\left[W_{\beta,a,k}^{dip}\right] \tag{D.9}$$

where $W_{\beta,a,k}^{dip}$ contains the coefficients of the dipole derivative. Using the definition of the derivative of a CMO, Eq. (D.9) can be written as:

$$\sum_{\beta}^{\{x,y,z\}}\sum_{k}^{occ}\sum_{a}^{CMO\in A}\sum^{vir\in A}\frac{\partial\langle a\,|\,\beta\,|\,k\rangle}{\partial x_{K\in A}}\left[W_{\beta,a,k}^{dip}\right]=\sum_{ki}^{occ}{}^{CMO\in A}U_{ik}^{x_KA}\sum_{a}^{vir\in A}\sum_{\beta}^{\{x,y,z\}}<a\,|\,\beta\,|\,i>\left[W_{\beta,a,k}^{dip}\right]$$

$$+\sum_{j}^{occ}{}^{CMO\in A}\sum_{b}^{vir\in A}U_{bj}^{x_KA}\left(\begin{array}{l}\displaystyle\sum_{a}^{vir\in A}\sum_{\beta}^{\{x,y,z\}}<a\,|\,\beta\,|\,b>\left[W_{\beta,a,j}^{dip}\right]\\ \displaystyle-\sum_{k}^{occ}{}^{CMO\in A}\sum_{\beta}^{\{x,y,z\}}<k\,|\,\beta\,|\,j>\left[W_{\beta,b,k}^{dip}\right]\end{array}\right)$$

$$-\sum_{ab}^{vir\in A}U_{ab}^{x_KA}\sum_{k}^{occ}{}^{CMO\in A}\sum_{\beta}^{\{x,y,z\}}<k\,|\,\beta\,|\,b>\left[W_{\beta,a,k}^{dip}\right]$$

$$+\sum_{a}^{vir\in A}\sum_{p}^{MO\in A}\left(-S_{ap}^{(x_K)}\right)\sum_{k}^{occ}{}^{CMO\in A}\sum_{\beta}^{\{x,y,z\}}<k\,|\,\beta\,|\,p>\left[W_{\beta,a,k}^{dip}\right]$$

$$+\sum_{\beta}^{\{x,y,z\}}\sum_{\mu\nu}^{AO\in A}\frac{\partial\langle\mu\,|\,\beta\,|\,\nu\rangle}{\partial x_{K\in A}}\sum_{k}^{occ}{}^{CMO\in A}\sum_{a}^{vir\in A}\left[c_{\mu a}c_{\nu k}W_{\beta,a,k}^{dip}\right] \tag{D.10}$$

Combining Eq. (D.7), (D.8), and (D.10), the last term in Eq. (4.22) can be expanded. The polarization energy gradient can then be rewritten as in Eq. (4.16).

D3: Z-vector method applied to second-order CPHF

The Z-vector method can be used to replace the term involving the derivative of the canonical MO response. This method replaces the second order canonical response with first order canonical response terms. The first order canonical response terms can be collected with the other canonical response terms.

Following the Z-vector method technique in Section A7, and using Section A4, the second-order response term in Eq. (4.23) is written as

$$\sum_{\beta}^{\{x,y,z\}}\sum_{i}^{occ}\sum_{a}^{CMO\in A}\sum^{vir\in A}\frac{\partial U_{ai}^{\beta A}}{\partial x_K}N_{ai,tot}^{\beta,A}$$
$$=\sum_{\beta}^{\{x,y,z\}}\sum_{i}^{occ}\sum_{a}^{CMO\in A}\sum^{vir\in A}Z_{ai,\beta}^{scphf,A}\left(\frac{\partial}{\partial x_K}\left(\langle a\,|\,\beta\,|\,i\rangle\right)+\sum_{b}^{vir\in A}\left(U_{bi}^{\beta A}\frac{\partial F_{ba}}{\partial x_K}\right)+\sum_{j}^{occ}\sum^{CMO\in A}\left(U_{ja}^{\beta A}\frac{\partial F_{ji}}{\partial x_K}\right)+\sum_{b}^{vir\in A}\sum_{j}^{occ}\sum^{CMO\in A}\left(U_{bj}^{\beta A}\frac{\partial A'_{ai,bj}}{\partial x_K}\right)\right)$$

(D.11)

where $Z^{scphf,A}$ is the solution of the Z-vector equation $\sum_{bj}\mathrm{A}_{ai,bj}\;Z_{ai,\beta}^{scphf,A}=N_{bj,tot}^{\beta,A}$.

The right hand side of Eq. (D.11) can then be re-written as:

$$\sum_{\beta}^{\{x,y,z\}}\sum_{i}^{occ}\sum_{a}^{CMO\in A}\sum^{vir\in A}\frac{\partial U_{ai}^{\beta,A}}{\partial x_K}N_{ai,tot}^{\beta,A}=\sum_{\beta}^{\{x,y,z\}}\sum_{i}^{occ}\sum_{a}^{CMO\in A}\sum^{vir\in A}\frac{\partial}{\partial x_K}\left(\langle a\,|\,\beta\,|\,i\rangle\right)Z_{ai,\beta}^{scphf,A}+\sum_{ab}^{vir\in A}\sum_{ij}^{occ}\sum^{CMO\in A}\frac{\partial A'_{ai,bj}}{\partial x_K}\left(\sum_{\beta}^{\{x,y,z\}}Z_{ai,\beta}^{scphf,A}U_{bj}^{\beta A}\right)$$
$$+\sum_{a}^{vir\in A}\sum_{b}^{vir\in A}\frac{\partial F_{ba}}{\partial x_K}\left(\sum_{\beta}^{\{x,y,z\}}\sum_{i}^{occ}\sum^{CMO\in A}Z_{ai,\beta}^{scphf,A}U_{bi}^{\beta A}\right)+\sum_{i}^{occ}\sum_{j}^{CMO\in A}\sum^{occ}\sum^{CMO\in A}\frac{\partial F_{ji}}{\partial x_K}\left(\sum_{\beta}^{\{x,y,z\}}\sum_{a}^{vir\in A}Z_{ai,\beta}^{scphf,A}\left(-U_{aj}^{\beta A}\right)\right)$$

(D.12)

where $U_{ja}^{\beta} = -U_{aj}^{\beta}$ [9]is used to put the known response matrices in the form (vir, occ). There are three derivatives in Eq. (D.12): A dipole integral derivative, A' (defined in Appendix A1) integral derivative, and a Fock matrix derivative. Using algebra and standard quantum chemistry techniques, Eq. (D.12) can be written as:

$$\sum_{\beta}\sum_{\{x,y,z\}}\sum_{i}^{occ}\sum_{CMO\in A}\sum_{a}^{vir\in A}\frac{\partial U_{ai}^{\beta,A}}{\partial x_K}N_{ai,tot}^{\beta,A} = \mathrm{NR}_{A,tot,x_K}^{pol,2} + \sum_{ab}^{vir\in A}U_{ab}^{x_K A}L_{ab,tot}^{scphf} + \sum_{a}^{vir\in A}\sum_{k}^{occ}\sum_{CMO\in A}U_{ak}^{x_K A}L_{ak,tot}^{scphf} + \sum_{ki}^{occ}\sum_{CMO\in A}U_{ki}^{x_K A}L_{ki,tot}^{scphf} \tag{D.13}$$

where $\mathrm{NR}_{A,tot,x_K}^{pol,2}$ is the sum of the non-response contributions, L_{tot}^{scphf} is the coefficient of the CMO responses, separated into occupied-occupied, virtual-virtual, and occupied-virtual blocks. See the Supporting Information for more details.

Appendix Section E: Dispersion gradient derivation details

E1: Using the Z-vector method to replace second-order response term

The Z-vector method can be used to remove the derivative of the time-dependent response term, and replace it with terms involving the canonical MO response. This is similar to how the second-order canonical MO response was replaced in Appendix D (with further details in the Supporting Information).

Following the Z-vector method,

$$\sum_{b}^{vir\in A}\sum_{j}^{occ}\sum_{CMO\in A}\sum_{c}^{vir\in A}\sum_{k}^{occ}\sum_{CMO\in A}\left(H_{ai,bj}^{(1)}H_{bj,ck}^{(2)}Z_{ck,\omega,\beta}^{stdcphf,A}\right) - (i\omega)^2 Z_{ai,\omega,\beta}^{stdcphf,A} = N_{ai,tot}^{\beta,\omega,A} \tag{E.1}$$

Eq. (E.1) is solved for $Z_{\omega,\beta}^{stdcphf,A}$.

Then, using Section A5, the fourth term in Eq. (4.23) is replaced with

$$\sum_{f}^{12}\sum_{\beta}^{\{x,y,z\}}\sum_{a}^{vir\in A}\sum_{i}^{occ\,CMO\in A}\frac{\partial Z_{ai}^{\beta A}(i\omega_f)}{\partial x_{K\in A}}N_{ai,tot}^{\beta,\omega_f,A}=$$

$$\sum_{f}^{12}\sum_{\beta}^{\{x,y,z\}}\sum_{a}^{vir\in A}\sum_{i}^{occ\,CMO\in A}Z_{ai,\omega_f,\beta}^{stdcphf,A}\left(\begin{array}{l}
-2\sum_{b}^{vir\in A}\sum_{j}^{occ\,CMO\in A}H_{ai,bj}^{(2)}\frac{\partial\langle b|\beta|j\rangle}{\partial x_K}-\sum_{bc}^{vir\in A}\sum_{jk}^{occ\,CMO\in A}H_{ai,bj}^{(2)}Z_{ck}^{\beta A}(i\omega_f)\frac{\partial A'_{bj,ck}}{\partial x_K}\\
-\sum_{bc}^{vir\in A}\sum_{j}^{occ\,CMO\in A}H_{ai,cj}^{(2)}Z_{bj}^{\beta A}(i\omega_f)\frac{\partial F_{bc}}{\partial x_K}+\sum_{b}^{vir\in A}\sum_{jk}^{occ\,CMO\in A}H_{ai,bj}^{(2)}Z_{bk}^{\beta A}(i\omega_f)\frac{\partial F_{jk}}{\partial x_K}\\
-\sum_{b}^{vir\in A}\sum_{j}^{occ\,CMO\in A}\left[2\langle b|\beta|j\rangle+\sum_{c}^{vir\in A}\sum_{k}^{occ\,CMO\in A}H_{bj,ck}^{(1)}Z_{ck}^{\beta A}(i\omega_f)\right]\frac{\partial}{\partial x_K}((aj|bi)-(ab|ij))\\
-\sum_{b}^{vir\in A}\left[2\langle b|\beta|i\rangle+\sum_{c}^{vir\in A}\sum_{k}^{occ\,CMO\in A}H_{bi,ck}^{(1)}Z_{ck}^{\beta A}(i\omega_f)\right]\frac{\partial F_{ab}}{\partial x_K}\\
+\sum_{j}^{occ\,CMO\in A}\left[2\langle a|\beta|j\rangle+\sum_{c}^{vir\in A}\sum_{k}^{occ\,CMO\in A}H_{aj,ck}^{(1)}Z_{ck}^{\beta A}(i\omega_f)\right]\frac{\partial F_{ij}}{\partial x_K}
\end{array}\right)$$

(E.2)

Then, the integrals are separated out, as shown below:

$$\sum_{f}^{12}\sum_{\beta}^{\{x,y,z\}}\sum_{a}^{vir\in A}\sum_{i}^{occ}\sum^{CMO\in A}\frac{\partial Z_{ai}^{\beta A}(i\omega_f)}{\partial x_{K\in A}}N_{ai,tot}^{\beta,\omega_f,A}=\sum_{\beta}^{\{x,y,z\}}\sum_{i}^{occ}\sum^{CMO\in A}\sum_{a}^{\text{vir}\in\text{A}}\frac{\partial}{\partial x_K}(\langle a|\beta|i\rangle)2\left(-\sum_{f}^{12}\sum_{b}^{vir\in A}\sum_{j}^{occ}\sum^{CMO\in A}H_{bj,ai}^{(2)}Z_{bj,\omega_f,\beta}^{stdcphf,A}\right)$$
$$+\sum_{ab}^{vir\in A}\sum_{ij}^{occ}\sum^{CMO\in A}\frac{\partial A'_{ai,bj}}{\partial x_K}\left(\sum_{f}^{12}\sum_{\beta}^{\{x,y,z\}}\left(-\sum_{c}^{vir}\sum_{k}^{occ}\sum^{CMO\in A}H_{ck,ai}^{(2)}Z_{ck,\omega_f,\beta}^{stdcphf,A}\right)Z_{bj}^{\beta A}(i\omega_f)\right)$$
$$+\sum_{a}^{vir\in A}\sum_{b}^{vir\in A}\frac{\partial F_{ba}}{\partial x_K}\left(\sum_{f}^{12}\sum_{\beta}^{\{x,y,z\}}\sum_{i}^{occ}\sum^{CMO\in A}\left(-\sum_{c}^{vir\in A}\sum_{j}^{occ}\sum^{CMO\in A}H_{cj,ai}^{(2)}Z_{cj,\omega_f,\beta}^{stdcphf,A}\right)Z_{bi}^{\beta A}(i\omega_f)\right)$$
$$+\sum_{i}^{occ}\sum_{j}^{occ}\sum^{CMO\in A}\frac{\partial F_{ji}}{\partial x_K}\left(\sum_{f}^{12}\sum_{\beta}^{\{x,y,z\}}\sum_{a}^{vir\in A}\left(-\sum_{b}^{vir\in A}\sum_{k}^{occ}\sum^{CMO\in A}H_{bk,ai}^{(2)}Z_{bk,\omega_f,\beta}^{stdcphf,A}\right)\left(-Z_{aj}^{\beta A}(i\omega_f)\right)\right)$$
$$+\sum_{ab}^{vir\in A}\sum_{ij}^{occ}\sum^{CMO\in A}\frac{\partial}{\partial x_K}((aj|bi)-(ab|ij))\left(\sum_{f}^{12}\sum_{\beta}^{\{x,y,z\}}\left(-\left[2\langle b|\beta|j\rangle+\sum_{c}^{vir\in A}\sum_{k}^{occ}\sum^{CMO\in A}H_{bj,ck}^{(1)}Z_{ck}^{\beta A}(i\omega_f)\right]\right)Z_{ai,\omega_f,\beta}^{stdcphf,A}\right)$$
$$+\sum_{a}^{vir\in A}\sum_{b}^{vir\in A}\frac{\partial F_{ba}}{\partial x_K}\left(\sum_{f}^{12}\sum_{\beta}^{\{x,y,z\}}\sum_{i}^{occ}\sum^{CMO\in A}\left(-\left[2\langle a|\beta|i\rangle+\sum_{c}^{vir\in A}\sum_{k}^{occ}\sum^{CMO\in A}H_{ai,ck}^{(1)}Z_{ck}^{\beta A}(i\omega_f)\right]\right)Z_{bi,\omega_f,\beta}^{stdcphf,A}\right)$$
$$+\sum_{i}^{occ}\sum_{j}^{occ}\sum^{CMO\in A}\frac{\partial F_{ji}}{\partial x_K}\left(\sum_{f}^{12}\sum_{\beta}^{\{x,y,z\}}\sum_{a}^{vir\in A}\left(-\left[2\langle a|\beta|i\rangle+\sum_{c}^{vir\in A}\sum_{k}^{occ}\sum^{CMO\in A}H_{ai,ck}^{(1)}Z_{ck}^{\beta A}(i\omega_f)\right]\right)\left(-Z_{aj,\omega_f,\beta}^{stdcphf,A}\right)\right)$$

(E.3)

where $Z_{bj}^{\beta}(i\omega)=-Z_{jb}^{\beta}(i\omega)$[28] has been used to put the response matrix in (vir, occ) order.

There are four derivatives in Eq. (E.3): A dipole integral derivative similar to the one in the polarization gradient, an A' integral derivative similar to the one in the polarization gradient, a Fock matrix derivative similar to the one in the polarization gradient, and a second two-electron derivative. These can be expanded using similar techniques as in the polarization gradient. Then, Eq. (E.3) can be written as:

$$\sum_{f}^{12}\sum_{\beta}^{\{x,y,z\}}\sum_{a}^{vir\in A}\sum_{i}^{occ}\sum^{CMO\in A}\frac{\partial Z_{ai}^{\beta}(i\omega_f)}{\partial x_{K\in A}}N_{ai,tot}^{\beta,\omega_f,A}=\text{NR}_{A,tot,x_K}^{disp,2}+\sum_{ab}^{vir\in A}U_{ab}^{x_K A}L_{ab,tot}^{stdcphf}+\sum_{a}^{vir\in A}\sum_{k}^{occ}\sum^{CMO\in A}U_{ak}^{x_K A}L_{ak,tot}^{stdcphf}+\sum_{ki}^{occ}\sum^{CMO\in A}U_{ki}^{x_K A}L_{ki,tot}^{stdcphf}$$

(E.4)

where $\mathrm{NR}^{disp,2}_{A,tot,x_K}$ is the sum of the non-response contributions, $L^{stdcphf}_{tot}$ is the coefficient of the CMO responses, separated into occupied-occupied, virtual-virtual, and occupied-virtual blocks.

E2: Dynamic polarizability derivative term

The second term in Eq. (4.19) is expanded using Eq. (3.16) and Eq. (3.18):

$$\sum_{l}^{LMO\in A}\sum_{f}^{12}\frac{\partial\bar{\alpha}^{l}(i\omega_f)}{\partial x_{K\in A}}\left(-\frac{4}{\pi}\left(w_f\frac{2v_0}{(1-t_f)^2}\right)\sum_{m}^{LMO\in B}\frac{1}{R_{lm}^6}\bar{\alpha}^{m}(i\omega_f)\right)$$
$$=\sum_{l}^{LMO\in A}\sum_{f}^{12}\sum_{\beta}^{\{x,y,z\}}\frac{\partial}{\partial x_{K\in A}}\left[\sum_{b}^{vir\in A}\sum_{ij}^{occ\,CMO\in A}L_{li}L_{lj}\langle b|\beta|i\rangle Z_{bj}^{\beta A}(i\omega_f)\right]\left(\frac{8}{3\pi}\left(w_f\frac{2v_0}{(1-t_f)^2}\right)\sum_{m}^{LMO\in B}\frac{1}{R_{lm}^6}\bar{\alpha}^{m}(i\omega_f)\right) \tag{E.5}$$

Eq. (E.5) has the same form as Eq. (4.15), and can be calculated in an analogous manner, with $Z^{\beta}(i\omega)$ in place of U^{γ}. (Appendix D2 presents a more detailed expansion for the polarization gradient, which is very similar.)

Supporting Information

Supporting Information Section 1: Information about the Distributed Multipole Analysis

In the EFP method, the molecular charge density of the fragment is written in terms of a sum of a density times the product of two Gaussian functions, which is itself a Gaussian. The new Gaussian is centered at a point referred to here as the Gaussian function overlap center. Each product function can be considered to be one piece of the charge density. For EFP fragment *A*, the charge density can thus be written as:

$$\rho(\mathbf{r}) = \sum_{\mu\nu}^{AO\in A} P_{\mu\nu} \sum_{u}^{PG\in\mu} \sum_{t}^{PG\in\nu} P'_{ut} g_u(\mathbf{r}-\mathbf{r}_I,\alpha_u) g_t(\mathbf{r}-\mathbf{r}_J,\alpha_t)$$
$$= \sum_{\mu\nu}^{AO\in A} \sum_{u}^{PG\in\mu} \sum_{t}^{PG\in\nu} \left[P_{\mu\nu} P'_{ut} g_{ut}(\mathbf{r}-\mathbf{r}_K,(\alpha_u+\alpha_t)) \right]$$

(S1.1)

In Eq. (S1.1) $g_u(\mathbf{r}-\mathbf{r}_I,\alpha_u)$is a primitive Gaussian (PG) centered on atom *I* with contraction exponent α_u, P'_{ut} is the primitive Gaussian cross term that contains the product of the contraction coefficients for PG *u* and *t*, and $\mathbf{r}_K = \frac{\alpha_u \mathbf{r}_I + \alpha_t \mathbf{r}_J}{\alpha_u + \alpha_t}$.

Each piece of charge density (the quantity in square brackets in Eq. (S.1)) can be expressed in terms of a series of multipole moment integrals. The multipole moment integrals are then shifted to the nearest expansion point (that is, a nearest-site allocation algorithm is used). Shifting the multipole moment integrals to the selected expansion point is accomplished by calculating the multipole moment integrals for each piece of charge density around the nearest expansion point. In this work, the expansion sites are only on the nuclei.

Supporting Information Section 2: Details about the polarization derivative

Fock matrix derivatives:

Let

$$\mathrm{FF}(\beta,\{Z^{scphf,A}_{ai,\beta}\},\{U^{\beta A}_{bi}\}) \equiv \sum_{a}^{vir\in A}\sum_{b}^{vir\in A} \frac{\partial F_{ba}}{\partial x_K} \left(\sum_{\beta}^{\{x,y,z\}} \sum_{i}^{occ\,CMO\in A} Z^{scphf,A}_{ai,\beta} U^{\beta A}_{bi} \right) + \sum_{i}^{occ\,CMO\in A} \sum_{j}^{occ\,CMO\in A} \frac{\partial F_{ji}}{\partial x_K} \left(\sum_{\beta}^{\{x,y,z\}} \sum_{a}^{vir\in A} Z^{scphf,A}_{ai,\beta} \left(-U^{\beta A}_{aj}\right) \right)$$

(S2.2)

After rearranging, using the definition of the Fock matrix, and that the unperturbed orbitals are canonical, Eq. (S2.2) can be written as

$$\mathrm{FF}(\beta,\{Z_{ai,\beta}^{scphf,A}\},\{U_{bi}^{\beta A}\})=\sum_{a}^{vir\in A}\sum_{b}^{vir\in A}\left(U_{ab}^{x_K A}F_{aa}+U_{ba}^{x_K A}F_{bb}\right)\left(\sum_{\beta}^{\{x,y,z\}}\sum_{i}^{occ}Z_{ai,\beta}^{scphf,A}U_{bi}^{\beta A}\right)$$
$$+\sum_{\mu\nu}^{AO\in A}\left(F_{\mu\nu}^{x_K}+\sum_{p}^{MO\in A}\sum_{k}^{occ}U_{pk}^{x_K A}A'_{\mu\nu,pk}\right)\left(\sum_{ab}^{vir\in A}c_{\mu b}c_{\nu a}\sum_{\beta}^{\{x,y,z\}}\sum_{i}^{occ}Z_{ai,\beta}^{scphf,A}U_{bi}^{\beta A}+\sum_{ij}^{occ}c_{\mu j}c_{\nu i}\sum_{\beta}^{\{x,y,z\}}\sum_{a}^{vir\in A}Z_{ai,\beta}^{scphf,A}\left(-U_{aj}^{\beta A}\right)\right)$$
$$+\sum_{i}^{occ}\sum_{j}^{occ}\left(U_{ij}^{x_K A}F_{ii}+U_{ji}^{x_K A}F_{jj}\right)\left(\sum_{\beta}^{\{x,y,z\}}\sum_{a}^{vir\in A}Z_{ai,\beta}^{scphf,A}\left(-U_{aj}^{\beta A}\right)\right) \tag{S2.3}$$

After rearranging and using Section A2, Eq. (S2.3) can be written as

$$\mathrm{FF}(\beta,\{Z_{ai,\beta}^{scphf,A}\},\{U_{bi}^{\beta A}\})=$$
$$\sum_{a}^{vir\in A}\sum_{b}^{vir\in A}\left(U_{ab}^{x_K A}\left(F_{aa}-F_{bb}\right)\right)\left(\sum_{\beta}^{\{x,y,z\}}\sum_{i}^{occ}Z_{ai,\beta}^{scphf,A}U_{bi}^{\beta A}\right)$$
$$+\sum_{\mu\nu}^{AO\in A}F_{\mu\nu}^{x_K}\left(\sum_{ab}^{vir\in A}c_{\mu b}c_{\nu a}\sum_{\beta}^{\{x,y,z\}}\sum_{i}^{occ}Z_{ai,\beta}^{scphf,A}U_{bi}^{\beta A}+\sum_{ij}^{occ}c_{\mu j}c_{\nu i}\sum_{\beta}^{\{x,y,z\}}\sum_{a}^{vir\in A}Z_{ai,\beta}^{scphf,A}\left(-U_{aj}^{\beta A}\right)\right)$$
$$+\sum_{pk}^{occ}\left(-\frac{1}{2}S_{pk}^{(x_K)}\right)\left(\sum_{\mu\nu}^{AO\in A}A'_{\mu\nu,pk}\left(\sum_{ab}^{vir\in A}c_{\mu b}c_{\nu a}\sum_{\beta}^{\{x,y,z\}}\sum_{i}^{occ}Z_{ai,\beta}^{scphf,A}U_{bi}^{\beta A}+\sum_{ij}^{occ}c_{\mu j}c_{\nu i}\sum_{\beta}^{\{x,y,z\}}\sum_{a}^{vir\in A}Z_{ai,\beta}^{scphf,A}\left(-U_{aj}^{\beta A}\right)\right)\right)$$
$$+\sum_{p}^{vir\in A}\sum_{k}^{occ}U_{pk}^{x_K A}\left(\sum_{\mu\nu}^{AO\in A}A'_{\mu\nu,pk}\left(\sum_{ab}^{vir\in A}c_{\mu b}c_{\nu a}\sum_{\beta}^{\{x,y,z\}}\sum_{i}^{occ}Z_{ai,\beta}^{scphf,A}U_{bi}^{\beta A}+\sum_{ij}^{occ}c_{\mu j}c_{\nu i}\sum_{\beta}^{\{x,y,z\}}\sum_{a}^{vir\in A}Z_{ai,\beta}^{scphf,A}\left(-U_{aj}^{\beta A}\right)\right)\right)$$
$$+\sum_{i}^{occ}\sum_{j}^{occ}\left(U_{ij}^{x_K A}\left(F_{ii}-F_{jj}\right)\right)\left(\sum_{\beta}^{\{x,y,z\}}\sum_{a}^{vir\in A}Z_{ai,\beta}^{scphf,A}\left(-U_{aj}^{\beta A}\right)\right)$$
$$-\sum_{\mu\nu}^{AO\in A}S_{\mu\nu}^{x_K}\left(\sum_{a}^{vir\in A}\sum_{b}^{vir\in A}\left(c_{\mu a}c_{\nu b}F_{bb}\right)\left(\sum_{\beta}^{\{x,y,z\}}\sum_{i}^{occ}Z_{ai,\beta}^{scphf,A}U_{bi}^{\beta A}\right)+\sum_{i}^{occ}\sum_{j}^{occ}c_{\mu i}c_{\nu j}F_{jj}\left(\sum_{\beta}^{\{x,y,z\}}\sum_{a}^{vir\in A}Z_{ai,\beta}^{scphf,A}\left(-U_{aj}^{\beta A}\right)\right)\right) \tag{S2.4}$$

Eq. (S2.4) can be simplified, as shown below:

$$\mathrm{FF}(\beta,\{Z_{ai,\beta}^{scphf,A}\},\{U_{bi}^{\beta A}\})=\mathrm{NR}_{A,x_K}^{pol,F}+\sum_{ab}^{vir\in A}U_{ab}^{x_K A}L_{ab}^{F}+\sum_{p}^{vir\in A}\sum_{k}^{occ\,CMO\in A}U_{pk}^{x_K A}L_{pk}^{F}+\sum_{ij}^{occ\,CMO\in A}U_{ij}^{x_K A}L_{ij}^{F} \tag{S2.5}$$

where $\mathrm{NR}_{A,x_K}^{pol,F}$ holds all the non-response terms and L^F holds the coefficients of the response matrices.

A' derivative:

Let $AD(\beta,\{Z_{ai,\beta}^{scphf,A}\},\{U_{bj}^{\beta A}\})\equiv$

$$\begin{aligned}
&\sum_{ab}^{vir\in A}\sum_{ij}^{occ\,CMO\in A}\frac{\partial A'_{ai,bj}}{\partial x_K}\left(\sum_{\beta}^{\{x,y,z\}}Z_{ai,\beta}^{scphf,A}U_{bj}^{\beta A}\right)=\sum_{ab}^{vir\in A}\sum_{ij}^{occ\,CMO\in A}\left(\begin{array}{l}A'^{(x_K)}_{ai,bj}+\sum_{p}^{MO\in A}U_{pa}^{x_K A}A'_{pi,bj}+\sum_{p}^{MO\in A}U_{pi}^{x_K A}A'_{ap,bj}\\+\sum_{p}^{MO\in A}U_{pb}^{x_K A}A'_{ai,pj}+\sum_{p}^{MO\in A}U_{pj}^{x_K A}A'_{ai,bp}\end{array}\right)\left(\sum_{\beta}^{\{x,y,z\}}Z_{ai,\beta}^{scphf,A}U_{bj}^{\beta A}\right)\\
&=\sum_{ab}^{vir\in A}\sum_{ij}^{occ\,CMO\in A}\left(A'^{(x_K)}_{ai,bj}\right)\left(\sum_{\beta}^{\{x,y,z\}}Z_{ai,\beta}^{scphf,A}U_{bj}^{\beta A}\right)+\sum_{ab}^{vir\in A}\sum_{ij}^{occ\,CMO\in A}\left(\sum_{p}^{MO\in A}U_{pa}^{x_K A}A'_{pi,bj}+\sum_{p}^{MO\in A}U_{pi}^{x_K A}A'_{ap,bj}\right)\left(\sum_{\beta}^{\{x,y,z\}}Z_{ai,\beta}^{scphf,A}U_{bj}^{\beta A}\right)\\
&+\sum_{ab}^{vir\in A}\sum_{ij}^{occ\,CMO\in A}\left(\sum_{p}^{MO\in A}U_{pa}^{x_K A}A'_{pi,bj}+\sum_{p}^{MO\in A}U_{pi}^{x_K A}A'_{ap,bj}\right)\left(\sum_{\beta}^{\{x,y,z\}}Z_{bj,\beta}^{scphf,A}U_{ai}^{\beta A}\right)
\end{aligned} \tag{S2.6}$$

The second term on the RHS of Eq. (S2.6) can be rearranged using Section A2 as:

$$\sum_{ab}^{\text{virt MOs}}\sum_{ij}^{occ\,CMO\in A}\left(\sum_{p}^{MO\in A}U_{pa}^{x_K A}A'_{pi,bj}+\sum_{p}^{MO\in A}U_{pi}^{x_K A}A'_{ap,bj}\right)\left(\sum_{\beta}^{\{x,y,z\}}Z_{ai,\beta}^{scphf,A}U_{bj}^{\beta A}\right)$$

$$=\sum_{a}^{vir\in A}\sum_{i}^{CMO\in A}\sum_{p}^{MO\in A}\left(-S_{ap}^{(x_K)}\right)\sum_{b}^{vir\in A}\sum_{j}^{occ\,CMO\in A}A'_{pi,bj}\left(\sum_{\beta}^{\{x,y,z\}}Z_{ai,\beta}^{scphf,A}U_{bj}^{\beta A}\right)+\sum_{a}^{vir\in A}\sum_{c}^{vir\in A}U_{ac}^{x_K A}\left(-\sum_{b}^{vir\in A}\sum_{ij}^{occ\,CMO\in A}A'_{ci,bj}\left(\sum_{\beta}^{\{x,y,z\}}Z_{ai,\beta}^{scphf,A}U_{bj}^{\beta A}\right)\right)$$

$$+\sum_{i}^{CMO\in A}\sum_{k}^{occ\,CMO\in A}U_{ki}^{x_K A}\left(\sum_{ab}^{vir\in A}\sum_{j}^{occ\,CMO\in A}A'_{ak,bj}\left(\sum_{\beta}^{\{x,y,z\}}Z_{ai,\beta}^{scphf,A}U_{bj}^{\beta A}\right)\right)+\sum_{a}^{vir\in A}\sum_{k}^{occ\,CMO\in A}U_{ak}^{x_K A}\left(\begin{array}{l}-\sum_{b}^{vir\in A}\sum_{ij}^{occ\,CMO\in A}\left(A'_{ki,bj}\right)\left(\sum_{\beta}^{\{x,y,z\}}Z_{ai,\beta}^{scphf,A}U_{bj}^{\beta A}\right)\\+\sum_{b}^{vir\in A}\sum_{kj}^{occ\,CMO\in A}\left(A'_{ca,bj}\right)\left(\sum_{\beta}^{\{x,y,z\}}Z_{ck,\beta}^{scphf,A}U_{bj}^{\beta A}\right)\end{array}\right) \tag{S2.7}$$

This can be written in the AO basis. First, consider $\sum_{b}^{vir\in A}\sum_{j}^{occ\,CMO\in A}A'_{pi,bj}\left(\sum_{\beta}^{\{x,y,z\}}Z_{ai,\beta}^{scphf,A}U_{bj}^{\beta A}\right)$ in Eq. (S2.7) since it shows up in multiple terms:

$$\sum_{b}^{vir\in A}\sum_{j}^{occ\,CMO\in A}A'_{pi,bj}\left(\sum_{\beta}^{\{x,y,z\}}Z_{ai,\beta}^{scphf,A}U_{bj}^{\beta A}\right)=$$

$$=\sum_{\beta}^{\{x,y,z\}}Z_{ai,\beta}^{scphf,A}\sum_{\mu\nu}^{AO\in A}\left(4(pi|\mu\nu)-(p\mu|i\nu)-(p\nu|i\mu)\right)\left(\sum_{b}^{vir\in A}\sum_{j}^{occ\,CMO\in A}c_{\mu b}c_{\nu j}U_{bj}^{\beta A}\right)$$

$$=\sum_{\beta}^{\{x,y,z\}}Z_{ai,\beta}^{scphf,A}\sum_{\mu\nu}^{AO\in A}4\left(\frac{1}{2}\sum_{b}^{vir\in A}\sum_{j}^{occ\,CMO\in A}c_{\mu b}c_{\nu j}U_{bj}^{\beta A}+\frac{1}{2}\sum_{b}^{vir\in A}\sum_{j}^{occ\,CMO\in A}c_{\nu b}c_{\mu j}U_{bj}^{\beta A}\right)\left((pi|\mu\nu)-\frac{1}{2}(p\mu|i\nu)\right)$$

$$=\sum_{\beta}^{\{x,y,z\}}Z_{ai,\beta}^{scphf,A}\sum_{\mu\nu}^{AO\in A}4N_{\mu\nu}^{\beta}\left((pi|\mu\nu)-\frac{1}{2}(p\mu|i\nu)\right) \tag{S2.8}$$

where $N_{\mu\nu}^{\beta}\equiv\left(\frac{1}{2}\sum_{b}^{vir\in A}\sum_{j}^{occ\,CMO\in A}c_{\mu b}c_{\nu j}U_{bj}^{\beta A}+\frac{1}{2}\sum_{b}^{vir\in A}\sum_{j}^{occ\,CMO\in A}c_{\nu b}c_{\mu j}U_{bj}^{\beta A}\right)$. Simplifying more, this can be written as shown below.

$$\sum_{b}^{vir\in A}\sum_{j}^{occ}\sum_{CMO\in A} A'_{pi,bj}\left(\sum_{\beta}^{\{x,y,z\}} Z_{ai,\beta}^{scphf,A}U_{bj}^{\beta A}\right)=\sum_{\beta}^{\{x,y,z\}} Z_{ai,\beta}^{scphf,A}C_{pi}^{N,\beta}$$

(S2.9)

where $C_{pi}^{N,\beta}\equiv\sum_{\mu\nu}^{AO\in A}4N_{\mu\nu}^{\beta}\left((pi\,|\,\mu\nu)-\frac{1}{2}(p\mu\,|\,i\nu)\right)$

Eq. (S2.9) can be substituted into Eq. (S2.7), so the second term in Eq. (S2.6) can be written as:

$$\begin{aligned}
&\sum_{ab}^{\text{virt MOs}}\sum_{ij}^{occ}\sum_{CMO\in A}\left(\sum_{p}^{MO\in A}U_{pa}^{x_K A}A'_{pi,bj}+\sum_{p}^{MO\in A}U_{pi}^{x_K A}A'_{ap,bj}\right)\left(\sum_{\beta}^{\{x,y,z\}}Z_{ai,\beta}^{scphf,A}U_{bj}^{\beta A}\right)=\\
&\sum_{a}^{vir\in A}\sum_{p}^{MO\in A}S_{ap}^{(x_K)}\left(-\sum_{i}^{occ}\sum_{CMO\in A}\sum_{\beta}^{\{x,y,z\}}Z_{ai,\beta}^{scphf,A}C_{pi}^{N,\beta}\right)+\sum_{a}^{vir\in A}\sum_{c}^{vir\in A}U_{ac}^{x_K A}\left(-\sum_{i}^{occ}\sum_{CMO\in A}\sum_{\beta}^{\{x,y,z\}}Z_{ai,\beta}^{scphf,A}C_{ci}^{N,\beta}\right)\\
&+\sum_{i}^{occ}\sum_{CMO\in A}\sum_{k}^{occ}\sum_{CMO\in A}U_{ki}^{x_K A}\left(\sum_{a}^{vir\in A}\sum_{\beta}^{\{x,y,z\}}Z_{ai,\beta}^{scphf,A}C_{ak}^{N,\beta}\right)\\
&+\sum_{a}^{vir\in A}\sum_{k}^{occ}\sum_{CMO\in A}U_{ak}^{x_K A}\left(-\sum_{i}^{occ}\sum_{CMO\in A}\sum_{\beta}^{\{x,y,z\}}Z_{ai,\beta}^{scphf,A}C_{ki}^{N,\beta}+\sum_{k}^{occ}\sum_{CMO\in A}\sum_{\beta}^{\{x,y,z\}}Z_{ck,\beta}^{scphf,A}C_{ca}^{N,\beta}\right)
\end{aligned}$$

(S2.10)

Then, note that the third term in Eq. (S2.6) can be expanded in a similar way to the second term. The result is shown below.

$$\sum_{ab}^{vir\in A}\sum_{ij}^{occ\,CMO\in A}\left(\sum_{p}^{MO\in A}U_{pa}^{x_K A}A'_{pi,bj}+\sum_{p}^{MO\in A}U_{pi}^{x_K A}A'_{ap,bj}\right)\left(\sum_{\beta}^{\{x,y,z\}}Z_{bj,\beta}^{scphf,A}U_{ai}^{\beta A}\right)=$$

$$=\sum_{a}^{vir\in A}\sum_{p}^{MO\in A}S_{ap}^{(x_K)}\left(-\sum_{i}^{occ\,CMO\in A}\sum_{\beta}^{\{x,y,z\}}U_{ai}^{\beta A}C_{pi}^{M,\beta}\right)+\sum_{a}^{vir\in A}\sum_{c}^{vir\in A}U_{ac}^{x_K A}\left(-\sum_{i}^{occ\,CMO\in A}\sum_{\beta}^{\{x,y,z\}}U_{ai}^{\beta A}C_{ci}^{M,\beta}\right)$$

$$+\sum_{i}^{occ\,CMO\in A}\sum_{k}^{occ\,CMO\in A}U_{ki}^{x_K A}\left(\sum_{a}^{vir\in A}\sum_{\beta}^{\{x,y,z\}}U_{ai}^{\beta A}C_{ak}^{M,\beta}\right)$$

$$+\sum_{a}^{vir\in A}\sum_{k}^{occ\,CMO\in A}U_{ak}^{x_K A}\left(-\sum_{i}^{occ\,CMO\in A}\sum_{\beta}^{\{x,y,z\}}U_{ai}^{\beta A}C_{ki}^{M,\beta}+\sum_{k}^{occ\,CMO\in A}\sum_{\beta}^{\{x,y,z\}}U_{ck}^{\beta A}C_{ca}^{M,\beta}\right)$$

(S2.11)

where $C_{pi}^{M,\beta}\equiv\sum_{\mu\nu}^{AO\in A}4M_{\mu\nu}^{\beta}\left((pi|\mu\nu)-\frac{1}{2}(p\mu|i\nu)\right)$

and $M_{\mu\nu}^{\beta}\equiv\left(\frac{1}{2}\sum_{b}^{vir\in A}\sum_{j}^{occ\,CMO\in A}c_{\mu b}c_{\nu j}Z_{bj,\beta}^{scphf,A}+\frac{1}{2}\sum_{b}^{vir\in A}\sum_{j}^{occ\,CMO\in A}c_{\nu b}c_{\mu j}Z_{bj,\beta}^{scphf,A}\right)$

Then, Eq. (S2.11) and Eq. (S2.10) can be substituted into Eq. (S2.6):

$$\sum_{ab}^{vir\in A}\sum_{ij}^{occ\,CMO\in A}\frac{\partial A'_{ai,bj}}{\partial x_K}\left(\sum_{\beta}^{\{x,y,z\}}Z_{ai,\beta}^{scphf,A}U_{bj}^{\beta A}\right)=\sum_{ab}^{vir\in A}\sum_{ij}^{occ\,CMO\in A}\left(A'^{(x_K)}_{ai,bj}\right)\left(\sum_{\beta}^{\{x,y,z\}}Z_{ai,\beta}^{scphf,A}U_{bj}^{\beta A}\right)$$

$$+\sum_{a}^{vir\in A}\sum_{p}^{MO\in A}S_{ap}^{(x_K)}\left(-\sum_{i}^{occ\,CMO\in A}\sum_{\beta}^{\{x,y,z\}}U_{ai}^{\beta A}C_{pi}^{M,\beta}+-\sum_{i}^{occ\,CMO\in A}\sum_{\beta}^{\{x,y,z\}}Z_{ai,\beta}^{scphf,A}C_{pi}^{N,\beta}\right)$$

$$+\sum_{a}^{vir\in A}\sum_{c}^{vir\in A}U_{ac}^{x_K A}\left(-\sum_{i}^{occ\,CMO\in A}\sum_{\beta}^{\{x,y,z\}}U_{ai}^{\beta A}C_{ci}^{M,\beta}-\sum_{i}^{occ\,CMO\in A}\sum_{\beta}^{\{x,y,z\}}Z_{ai,\beta}^{scphf,A}C_{ci}^{N,\beta}\right)$$

$$+\sum_{i}^{occ\,CMO\in A}\sum_{k}^{occ\,CMO\in A}U_{ki}^{x_K A}\left(\sum_{a}^{vir\in A}\sum_{\beta}^{\{x,y,z\}}U_{ai}^{\beta A}C_{ak}^{M,\beta}+\sum_{a}^{vir\in A}\sum_{\beta}^{\{x,y,z\}}Z_{ai,\beta}^{scphf,A}C_{ak}^{N,\beta}\right)$$

$$+\sum_{a}^{vir\in A}\sum_{k}^{occ\,CMO\in A}U_{ak}^{x_K A}\left(-\sum_{i}^{occ\,CMO\in A}\sum_{\beta}^{\{x,y,z\}}U_{ai}^{\beta A}C_{ki}^{M,\beta}+\sum_{k}^{occ\,CMO\in A}\sum_{\beta}^{\{x,y,z\}}U_{ck}^{\beta A}C_{ca}^{M,\beta}-\sum_{i}^{occ\,CMO\in A}\sum_{\beta}^{\{x,y,z\}}Z_{ai,\beta}^{scphf,A}C_{ki}^{N,\beta}+\sum_{k}^{occ\,CMO\in A}\sum_{\beta}^{\{x,y,z\}}Z_{ck,\beta}^{scphf,A}C_{ca}^{N,\beta}\right)$$

(S2.12)

The non-response terms can be combined, and the coefficients of the response matrices can be combined as shown below:

$$\sum_{ab}^{vir\in A}\sum_{ij}^{occ\,CMO\in A}\frac{\partial A'_{ai,bj}}{\partial x_K}\left(\sum_{\beta}^{\{x,y,z\}}Z_{ai,\beta}^{scphf,A}U_{bj}^{\beta A}\right)$$
$$=\mathrm{NR}_{A,x_K}^{pol,A'}+\sum_{ab}^{vir\in A}U_{ab}^{x_K A}L_{ab}^{A'}+\sum_{a}^{vir\in A}\sum_{k}^{occ\,CMO\in A}U_{ak}^{x_K A}L_{ak}^{A'}+\sum_{ki}^{occ\,CMO\in A}U_{ki}^{x_K A}L_{ki}^{A'}$$

(S2.13)

where $\mathrm{NR}_{A,x_K}^{pol,A'}$ is the collection of all non-response terms, and $L^{A'}$ is the coefficient of the response matrices.

Dipole derivative:

$$\sum_{\beta}^{\{x,y,z\}}\sum_{i}^{occ\,CMO\in A}\sum_{a}^{vir\in A}Z_{ai,\beta}^{scphf,A}\frac{\partial}{\partial x_K}\left(\langle a|\beta|i\rangle\right)$$
$$=\sum_{i}^{occ\,CMO\in A}\sum_{a}^{vir\in A}\sum_{\beta}^{\{x,y,z\}}Z_{ai,\beta}^{scphf,A}\left(\sum_{p}^{MO\in A}U_{pa}^{x_K A}\langle p|\beta|i\rangle+\sum_{p}^{MO\in A}U_{pi}^{x_K A}\langle p|\beta|a\rangle\right)$$
$$+\sum_{\nu\mu}^{AO\in A}\sum_{\beta}^{\{x,y,z\}}\frac{\partial}{\partial x_K}\langle\mu|\beta|\nu\rangle\sum_{i}^{occ\,CMO\in A}\sum_{a}^{vir\in A}c_{\mu a}c_{\nu i}Z_{ai,\beta}^{scphf,A}$$
$$=\sum_{a}^{vir\in A}\sum_{b}^{vir\in A}U_{ba}^{x_K A}\left(-\sum_{i}^{occ\,CMO\in A}\sum_{\beta}^{\{x,y,z\}}Z_{bi,\beta}^{scphf,A}\langle a|\beta|i\rangle\right)+\sum_{a}^{vir\in A}\sum_{p}^{MO\in A}S_{pa}^{(x_K)}\left(-\sum_{i}^{occ\,CMO\in A}\sum_{\beta}^{\{x,y,z\}}Z_{ai,\beta}^{scphf,A}\langle p|\beta|i\rangle\right)$$
$$+\sum_{i}^{occ\,CMO\in A}\sum_{b}^{vir\in A}U_{bi}^{x_K A}\left(\sum_{a}^{vir\in A\{x,y,z\}}\sum_{\beta}^{}Z_{ai,\beta}^{scphf,A}\langle b|\beta|a\rangle-\sum_{j}^{occ\,CMO\in A}\sum_{\beta}^{\{x,y,z\}}Z_{bj,\beta}^{scphf,A}\langle i|\beta|j\rangle\right)$$
$$+\sum_{ij}^{occ\,CMO\in A}U_{ji}^{x_K A}\left(\sum_{a}^{vir\in A\{x,y,z\}}\sum_{\beta}^{}Z_{ai,\beta}^{scphf,A}\langle j|\beta|a\rangle\right)+\sum_{\nu\mu}^{AO\in A}\sum_{\beta}^{\{x,y,z\}}\frac{\partial}{\partial x_K}\langle\mu|\beta|\nu\rangle\sum_{i}^{occ\,CMO\in A}\sum_{a}^{vir\in A}c_{\mu a}c_{\nu i}Z_{ai,\beta}^{scphf,A}$$

(S2.14)

The coefficients of the response matrices can be combined, and the non-response terms can be combined to simplify the term, as shown below.

$$\sum_{\beta}^{\{x,y,z\}} \sum_{i}^{occ} \sum_{a}^{vir\in A} Z_{ai,\beta}^{scphf,A} \frac{\partial}{\partial x_K}\left(\langle a|\beta|i\rangle\right)$$
$$= \mathrm{NR}_{A,x_K}^{pol,dipole} + \sum_{ab}^{vir\in A} U_{ab}^{x_K A} L_{ab}^{dipole} + \sum_{a}^{vir\in A} \sum_{k}^{occ\,CMO\in A} U_{ak}^{x_K A} L_{ak}^{dipole} + \sum_{ki}^{occ\,CMO\in A} U_{ki}^{x_K A} L_{ki}^{dipole}$$

(S2.15)

where $\mathrm{NR}_{A,x_K}^{pol,dipole}$ contains all the non-response terms and L^{dipole} holds the coefficients of the response matrices.

Supporting Information Section 3: Details of the dispersion derivative

Fock derivatives:

The terms involving the Fock derivatives in the dispersion derivative are the same as the terms involving the Fock derivatives for the polarization derivative in Appendix D3, with different coefficients. The term in the polarization derivative was written as $\mathrm{FF}(\beta, \{Z_{ai,\beta}^{scphf,A}\}, \{U_{bi}^{\beta A}\})$. Then, the terms in the dispersion derivative can be written as

$$\mathrm{FF}(f*\beta, \{-\begin{bmatrix} 2\langle a|\beta|i\rangle \\ +\sum_{c}^{vir\in A} \sum_{k}^{occ\,CMO\in A} H_{ai,ck}^{(1)} Z_{ck}^{\beta A}(i\omega_f) \end{bmatrix}\}, \{Z_{bi,\omega_f,\beta}^{stdcphf,A}\})$$
$$+\mathrm{FF}(f*\beta, \{-\sum_{c}^{vir\in A} \sum_{k}^{occ\,CMO\in A} H_{ck,ai}^{(2)} Z_{ck,\omega_f,\beta}^{stdcphf,A}\}, \{Z_{bi}^{\beta A}(i\omega_f)\})$$
$$= \mathrm{NR}_{A,x_K}^{disp,F} + \sum_{ab}^{vir\in A} U_{ab}^{x_K A} L_{ab}^{disp,F} + \sum_{p}^{vir\in A} \sum_{k}^{occ\,CMO\in A} U_{pk}^{x_K A} L_{pk}^{disp,F} + \sum_{ij}^{occ\,CMO\in A} U_{ij}^{x_K A} L_{ij}^{disp,F}$$

(S3.1)

A' derivative:

These are the same as the derivatives in Section D3, with different coefficients. The term in the polarization derivative was written as $AD(\beta, \{Z_{ai,\beta}^{scphf,A}\}, \{U_{bj}^{\beta A}\})$. Then, the terms in the dispersion derivative can be written as:

$$AD(f*\beta, \{-\sum_{c}^{vir\in A}\sum_{k}^{occ\ CMO\in A} H_{ck,ai}^{(2)} Z_{ck,\omega_f,\beta}^{stdcphf,A}\}, \{Z_{bj}^{\beta A}(i\omega_f)\})$$
$$= \mathrm{NR}_{A,x_K}^{disp,A'} + \sum_{ab}^{vir\in A} U_{ab}^{x_K A} L_{ab}^{disp,A'} + \sum_{a}^{vir\in A}\sum_{k}^{occ\ CMO\in A} U_{ak}^{x_K A} L_{ak}^{disp,A'} + \sum_{ki}^{occ\ CMO\in A} U_{ki}^{x_K A} L_{ki}^{disp,A'} \tag{S3.2}$$

Dipole integral derivative:

These are the same as the derivatives in Appendix D Section 3, with different coefficients.

$$\sum_{\beta}^{\{x,y,z\}}\sum_{i}^{occ\ CMO\in A}\sum_{a}^{\mathrm{vir}\in \mathrm{A}} \frac{\partial}{\partial x_K}(\langle a|\beta|i\rangle) 2\left(-\sum_{f}^{12}\sum_{b}^{vir}\sum_{j}^{occ\ CMO\in A} H_{bj,ai}^{(2)} Z_{bj,\omega_f,\beta}^{stdcphf,A}\right)$$
$$= \mathrm{NR}_{A,x_K}^{disp,dipole} + \sum_{ab}^{vir\in A} U_{ab}^{x_K A} L_{ab}^{disp,dipole} + \sum_{a}^{vir\in A}\sum_{k}^{occ\ CMO\in A} U_{ak}^{x_K A} L_{ak}^{disp,dipole} + \sum_{ki}^{occ\ CMO\in A} U_{ki}^{x_K A} L_{ki}^{disp,dipole} \tag{S3.3}$$

where $\mathrm{NR}_{A,x_K}^{disp,dipole}$ contains all the non-response terms and $L^{disp,dipole}$ holds the coefficients of the response matrices.

(aj|bi)-(ab|ij) derivative:

This is similar to the A' derivative.

$$\sum_{ab}^{virA}\sum_{ij}^{occCMOA}\frac{\partial}{\partial x_K}((aj\,|\,bi)-(ab\,|\,ij))\left(\sum_{f}^{12}\sum_{\beta}^{\{x,y,z\}}\left(-\left[2\langle b\,|\,\beta\,|\,j\rangle+\sum_{c}^{virA}\sum_{k}^{occCMOA}H^{(1)}_{bj,ck}Z^{\beta A}_{ck}(i\omega_f)\right]\right)Z^{stdcphf,A}_{ai,\omega_f,\beta}\right)$$

$$=\sum_{ab}^{virA}\sum_{ij}^{occCMOA}\begin{pmatrix}((aj\,|\,bi)-(ab\,|\,ij))^{(x_K)}+\sum_{p}^{MOA}U^{x_K}_{pa}\left((pj\,|\,bi)-(pb\,|\,ij)\right)\\+\sum_{p}^{MOA}U^{x_K A}_{pi}\left((aj\,|\,bp)-(ab\,|\,pj)\right)\\+\sum_{p}^{MOA}U^{x_K A}_{pb}\left((aj\,|\,pi)-(ap\,|\,ij)\right)+\sum_{p}^{MOA}U^{x_K A}_{pj}\left((ap\,|\,bi)-(ab\,|\,ip)\right)\end{pmatrix}\left(\sum_{f}^{12}\sum_{\beta}^{\{x,y,z\}}D^{stdcphf,A}_{bj,f\beta}Z^{stdcphf,A}_{ai,\omega_f,\beta}\right)$$

(S3.4)

where the integral derivative has been expanded, and the coefficient of $Z^{stdcphf,A}$ defined as

$$D^{stdcphf,A}_{bj,f\beta}\equiv-\left[2\langle b\,|\,\beta\,|\,j\rangle+\sum_{c}^{virA}\sum_{k}^{occCMOA}H^{(1)}_{bj,ck}Z^{\beta A}_{ck}(i\omega_f)\right]$$

The relationships in Section A2 can be used to manipulate the response matrices, and the terms can be expanded in the AO basis, in a similar manner to how the *A'* derivative was expanded. Eq. (S3.4) can then be written as shown below.

$$\sum_{ab}^{vir\in A}\sum_{ij}^{occ\,CMO\in A}\frac{\partial}{\partial x_K}((aj\,|\,bi)-(ab\,|\,ij))\left(\sum_{f}^{12}\sum_{\beta}^{\{x,y,z\}}\left(-\left[2\langle b\,|\,\beta\,|\,j\rangle+\sum_{c}^{vir\in A}\sum_{k}^{occ\,CMO\in A}H^{(1)}_{bj,ck}Z^{\beta A}_{ck}(i\omega_f)\right]\right)Z^{stdcphf,A}_{ai,\omega_f,\beta}\right)=$$

$$=\sum_{ab}^{vir\in A}\sum_{ij}^{occ\,CMO\in A}\left(((aj\,|\,bi)-(ab\,|\,ij))^{(x_K)}\right)\left(\sum_{f}^{12}\sum_{\beta}^{\{x,y,z\}}D^{stdcphf,A}_{bj,f\beta}Z^{stdcphf,A}_{ai,\omega_f,\beta}\right)$$

$$+\sum_{a}^{vir\in A}\sum_{c}^{vir\in A}U^{x_K A}_{ac}\left(-\sum_{i}^{occ\,CMO\in A}\sum_{f}^{12}\sum_{\beta}^{\{x,y,z\}}D^{stdcphf,A}_{ai,f\beta}C^{M,Z,\beta f}_{ci}-\sum_{i}^{occ\,CMO\in A}\sum_{f}^{12}\sum_{\beta}^{\{x,y,z\}}Z^{stdcphf,A}_{ai,\omega_f,\beta}C^{N,D,\beta f}_{ci}\right)$$

$$+\sum_{a}^{vir\in A}\sum_{k}^{occ\,CMO\in A}U^{x_K A}_{ak}\left(\begin{array}{l}-\sum_{i}^{occ\,CMO\in A}\sum_{f}^{12}\sum_{\beta}^{\{x,y,z\}}D^{stdcphf,A}_{ai,f\beta}C^{M,Z,\beta f}_{ki}+\sum_{c}^{vir\in A}\sum_{f}^{12}\sum_{\beta}^{\{x,y,z\}}D^{stdcphf,A}_{ck,f\beta}C^{M,Z,\beta f}_{ca}-\sum_{i}^{occ\,CMO\in A}\sum_{f}^{12}\sum_{\beta}^{\{x,y,z\}}Z^{stdcphf,A}_{ai,\omega_f,\beta}C^{N,D,\beta f}_{ki}\\+\sum_{c}^{vir\in A}\sum_{f}^{12}\sum_{\beta}^{\{x,y,z\}}Z^{stdcphf,A}_{ck,\omega_f,\beta}C^{N,D,\beta f}_{ca}\end{array}\right)$$

$$+\sum_{a}^{vir\in A}\sum_{p}^{MO\in A}S^{(x_K)}_{ap}\left(-\sum_{i}^{occ\,CMO\in A}\sum_{f}^{12}\sum_{\beta}^{\{x,y,z\}}D^{stdcphf,A}_{ai,f\beta}C^{M,Z,\beta f}_{pi}-\sum_{i}^{occ\,CMO\in A}\sum_{f}^{12}\sum_{\beta}^{\{x,y,z\}}Z^{stdcphf,A}_{ai,\omega_f,\beta}C^{N,D,\beta f}_{pi}\right)$$

$$+\sum_{i}^{occ\,CMO\in A}\sum_{k}^{occ\,CMO\in A}U^{x_K A}_{ki}\left(\sum_{a}^{vir\in A}\sum_{f}^{12}\sum_{\beta}^{\{x,y,z\}}D^{stdcphf,A}_{ai,f\beta}C^{M,Z,\beta f}_{ak}+\sum_{a}^{vir\in A}\sum_{f}^{12}\sum_{\beta}^{\{x,y,z\}}Z^{stdcphf,A}_{ai,\omega_f,\beta}C^{N,D,\beta f}_{ak}\right)$$

(S3.5)

$$C^{M,Z,\beta f}_{ci}\equiv\sum_{\xi\sigma}^{AO\in A}c_{\xi c}c_{\sigma i}\sum_{\mu\nu}^{AO\in A}(\xi\nu\,|\,\mu\sigma)M^{Z,\beta f}_{\mu\nu}$$

where

$$C^{N,D,\beta f}_{ci}\equiv\sum_{\xi\sigma}^{AO\in A}c_{\xi c}c_{\sigma i}\sum_{\mu\nu}^{AO\in A}(\xi\nu\,|\,\mu\sigma)N^{D,\beta f}_{\mu\nu}$$

$$M^{Z,\beta f}_{\mu\nu}\equiv\left(\sum_{b}^{vir\in A}\sum_{j}^{occ\,CMO\in A}c_{\mu b}c_{\nu j}Z^{stdcphf,A}_{bj,\omega_f,\beta}-\sum_{b}^{vir\in A}\sum_{j}^{occ\,CMO\in A}c_{\nu b}c_{\mu j}Z^{stdcphf,A}_{bj,\omega_f,\beta}\right)$$

and

$$N^{D,\beta f}_{\mu\nu}\equiv\left(\sum_{b}^{vir\in A}\sum_{j}^{occ\,CMO\in A}c_{\mu b}c_{\nu j}D^{stdcphf,A}_{bj,f,\beta}-\sum_{b}^{vir\in A}\sum_{j}^{occ\,CMO\in A}c_{\nu b}c_{\mu j}D^{stdcphf,A}_{bj,f,\beta}\right)$$

To simplify Eq. (S3.5), the non-response terms are combined, and the coefficients of the response matrices are combined, as shown below:

$$\sum_{ab}^{vir\in A}\sum_{ij}^{occ CMO\in A}\frac{\partial}{\partial x_K}((aj\,|\,bi)-(ab\,|\,ij))\left(\sum_{f}^{12}\sum_{\beta}^{\{x,y,z\}}\left(-\left[2\langle b\,|\,\beta\,|\,j\rangle+\sum_{c}^{vir\in A}\sum_{k}^{occ CMO\in A}H^{(1)}_{bj,ck}Z^{\beta A}_{ck}(i\omega_f)\right]\right)Z^{stdcphf,A}_{ai,\omega_f,\beta}\right)=$$

$$=NR^{disp,H^{(2)}}_{A,x_K}+\sum_{ab}^{vir\in A}U^{x_KA}_{ab}L^{H^{(2)}}_{ab}+\sum_{a}^{vir\in A}\sum_{k}^{occ CMO\in A}U^{x_KA}_{ak}L^{H^{(2)}}_{ak}+\sum_{ki}^{occ CMO\in A}U^{x_KA}_{ki}L^{H^{(2)}}_{ki}$$

(S3.6)

where $NR^{disp,H^{(2)}}_{A,x_K}$ is the collection of all non-response terms, and $L^{H(2)}$ is the collection of the coefficients of the response matrices.

Supporting Information Section 4: Details about the product rule used in the Coulomb derivative

In the Coulomb gradient, the product rule can be expressed as:

$$\frac{\partial\left(m^I T^{IJ}_{\alpha\beta\ldots\gamma}\right)}{\partial x_{K\in A}}=\left(m^I\frac{\partial T^{IJ}_{\alpha\beta\ldots\gamma}}{\partial x_{K\in A}}+T^{IJ}_{\alpha\beta\ldots\gamma}\frac{\partial m^I}{\partial x_{K\in A}}\right)$$

(S4.1)

where m^I is an arbitrary multipole moment and $T^{IJ}_{\alpha\beta\ldots\gamma}$ is a multipole moment interaction tensor of the appropriate rank. After substituting Eq. (S4.1) into Eq. (4.6):

$$\frac{\partial E^{Coul}_{AB}}{\partial x_{K\in A}}=\sum_{I}^{A}\sum_{J}^{B}\left[q^J\frac{\partial\left(q^I\right)}{\partial x_{K\in A}}T^{IJ}+q^Jq^I\frac{\partial\left(T^{IJ}\right)}{\partial x_{K\in A}}-\sum_{\alpha}^{x,y,z}q^J\frac{\partial\left(\mu^I_\alpha\right)}{\partial x_{K\in A}}T^{IJ}_\alpha-\sum_{\alpha}^{x,y,z}q^J\mu^I_\alpha\frac{\partial\left(T^{IJ}_\alpha\right)}{\partial x_{K\in A}}+\ldots\right]$$

(S4.2)

References

1. Gordon, M. S.; Fedorov, D. G.; Pruitt, S. R.; Slipchenko, L. V., Fragmentation Methods: A Route to Accurate Calculations on Large Systems. *Chem. Rev.* **2012,** *112*, 632-672.

2. Day, P. N.; Jensen, J. H.; Gordon, M. S.; Webb, S. P.; Stevens, W. J.; Krauss, M.; Garmer, D.; Basch, H.; Cohen, D., An effective fragment method for modeling solvent effects in quantum mechanical calculations. *J. Chem. Phys.* **1996,** *105*, 1968-1986.

3. Kitaura, K.; Ikeo, E.; Asada, T.; Nakano, T.; Uebayasi, M., Fragment molecular orbital method: an approximate computational method for large molecules. *Chem. Phys. Lett.* **1999,** *313*, 701-706.

4. Steinmann, C.; Fedorov, D. G.; Jensen, J. H., Effective Fragment Molecular Orbital Method: A Merger of the Effective Fragment Potential and Fragment Molecular Orbital Methods. *J. Phys. Chem. A* **2010,** *114*, 8705-8712.

5. Fedorov, D. G.; Kitaura, K., Extending the Power of Quantum Chemistry to Large Systems with the Fragment Molecular Orbital Method. *J. Phys. Chem. A* **2007,** *111*, 6904-6914.

6. Gordon, M. S.; Freitag, M. A.; Bandyopadhyay, P.; Jensen, J. H.; Kairys, V.; Stevens, W. J., The Effective Fragment Potential Method: A QM-Based MM Approach to Modeling Environmental Effects in Chemistry. *J. Phys. Chem. A* **2001,** *105*, 293-307.

7. Pruitt, S. R.; Steinmann, C.; Jensen, J. H.; Gordon, M. S., Fully Integrated Effective Fragment Molecular Orbital Method. *J. Chem. Theory Comput.* **2013,** *9*, 2235-2249.

8. Brorsen, K. R.; Minezawa, N.; Xu, F.; Windus, T. L.; Gordon, M. S., Fragment Molecular Orbital Molecular Dynamics with the Fully Analytic Energy Gradient. *J. Chem. Theory Comput.* **2012,** *8*, 5008-5012.

9. Yamaguchi, Y.; Schaefer, H. F.; Osamura, Y.; Goddard, J., *A New Dimension to Quantum Chemistry: Analytical Derivative Methods in Ab Initio Molecular Electronic Structure Theory*. Oxford University Press: New York, 1994.

10. Boys, S. F., Construction of Some Molecular Orbitals to Be Approximately Invariant for Changes from One Molecule to Another. *Rev. Mod. Phys.* **1960,** *32*, 296-299.

11. Edmiston, C.; Ruedenberg, K., Localized Atomic and Molecular Orbitals. *Rev. Mod. Phys.* **1963,** *35*, 457-464.

12. Subotnik, J. E.; Dutoi, A. D.; Head-Gordon, M., Fast localized orthonormal virtual orbitals which depend smoothly on nuclear coordinates. *J. Chem. Phys.* **2005,** *123*, 114108.

13. El Azhary, A.; Rauhut, G.; Pulay, P.; Werner, H.-J., Analytical energy gradients for local second-order Mo/ller–Plesset perturbation theory. *J. Chem. Phys.* **1998,** *108*, 5185-5193.

14. Rauhut, G.; Werner, H.-J., Analytical energy gradients for local coupled-cluster methods. *Phys. Chem. Chem. Phys.* **2001,** *3*, 4853-4862.

15. Autschbach, J.; King, H. F., Analyzing molecular static linear response properties with perturbed localized orbitals. *J. Chem. Phys.* **2010,** *133*, 044109.

16. Maestro, M.; Moccia, R., Localized molecular second-order properties. *Mol. Phys.* **1975,** *29*, 81-96.

17. Fedorov, D. G.; Olson, R. M.; Kitaura, K.; Gordon, M. S.; Koseki, S., A new hierarchical parallelization scheme: Generalized distributed data interface (GDDI), and an application to the fragment molecular orbital method (FMO). *J. Comput. Chem.* **2004,** *25*, 872-880.

18. Stone, A. J., *The Theory of Intermolecular Forces*. Oxford University Press: New York, 1997.

19. Boys, S. F., Electronic Wave Functions. I. A General Method of Calculation for the Stationary States of Any Molecular System. *Proc. Roy. Soc. A* **1950,** *200*, 542-554.

20. Jensen, H. J.; M. S. G., An approximate formula for the intermolecular Pauli repulsion between closed shell molecules. *Mol. Phys.* **1996,** *89*, 1313-1325.

21. Li, H.; Netzloff, H. M.; Gordon, M. S., Gradients of the polarization energy in the effective fragment potential method *J. Chem. Phys.* **2006,** *125*, 194103.

22. Webb, S. P. Derivatives, dimers, and solutions. Ph.D. Thesis, Iowa State University, 1997.

23. Garmer, D. R.; Stevens, W. J., Transferability of molecular distributed polarizabilities from a simple localized orbital based method. *J. Phys. Chem.* **1989,** *93*, 8263-8270.

24. Slipchenko, L. V.; Gordon, M. S., Damping functions in the effective fragment potential method. *Mol. Phys.* **2009,** *107*, 999-1016.

25. Adamovic, I.; Gordon, M. S., Dynamic polarizability, dispersion coefficient C6 and dispersion energy in the effective fragment potential method. *Mol. Phys.* **2005,** *103*, 379-387.

26. Xu, P.; Zahariev, F.; Gordon, M. S., The R–7 Dispersion Interaction in the General Effective Fragment Potential Method. *J. Chem. Theory Comput.* **2014,** *10*, 1576-1587.

27. Guidez, E. B.; Xu, P.; Gordon, M. S., Derivation and Implementation of the Gradient of the R–7 Dispersion Interaction in the Effective Fragment Potential Method. *J. Phys. Chem. A* **2016,** *120*, 639-647.

28. Rice, J. E.; Amos, R. D.; Colwell, S. M.; Handy, N. C.; Sanz, J., Frequency dependent hyperpolarizabilities with application to formaldehyde and methyl fluoride. *J. Chem. Phys.* **1990,** *93*, 8828-8839.

29. Guidez, E. B.; Gordon, M. S., Dispersion Correction Derived from First Principles for Density Functional Theory and Hartree–Fock Theory. *J. Phys. Chem. A* **2015,** *119*, 2161-2168.

30. Pulay, P., Ab initio calculation of force constants and equilibrium geometries in polyatomic molecules. *Mol. Phys.* **1969,** *17*, 197-204.

31. Nagata, T.; Brorsen, K.; Fedorov, D. G.; Kitaura, K.; Gordon, M. S., Fully analytic energy gradient in the fragment molecular orbital method. *J. Chem. Phys.* **2011,** *134*, 124115.

32. Li, H.; Gordon, M., Gradients of the Exchange-repulsion Energy in the General Effective Fragment Potential Method. *Theor. Chem. Acc.* **2006,** *115*, 385-390.

33. Schmidt, M. W.; Baldridge, K. K.; Boatz, J. A.; Elbert, S. T.; Gordon, M. S.; Jensen, J. H.; Koseki, S.; Matsunaga, N.; Nguyen, K. A.; Su, S.; Windus, T. L.; Dupuis, M.; Montgomery, J. A., General atomic and molecular electronic structure system. *J. Comput. Chem.* **1993,** *14*, 1347-1363.

34. Nakata, H.; Schmidt, M. W.; Fedorov, D. G.; Kitaura, K.; Nakamura, S.; Gordon, M. S., Efficient Molecular Dynamics Simulations of Multiple Radical Center Systems Based on the Fragment Molecular Orbital Method. *J. Phys. Chem. A* **2014,** *118*, 9762-9771.

35. Jayatilaka, D.; Handy, N. C., Implications of unitary invariance for gradient theory. *Int. J. Quantum Chem.* **1992,** *42*, 445-458.

36. Handy, N. C.; Amos, R. D.; Gaw, J. F.; Rice, J. E.; Simandiras, E. D., The elimination of singularities in derivative calculations. *Chem. Phys. Lett.* **1985,** *120*, 151-158.

37. Schütz, M.; Werner, H.-J.; Lindh, R.; Manby, F. R., Analytical energy gradients for local second-order Møller–Plesset perturbation theory using density fitting approximations. *J. Chem. Phys.* **2004,** *121*, 737-750.

38. Karna, S. P.; Dupuis, M., Frequency dependent nonlinear optical properties of molecules: Formulation and implementation in the HONDO program. *J. Comput. Chem.* **1991,** *12*, 487-504.

39. Quinet, O.; Champagne, B., Time-dependent Hartree–Fock schemes for analytical evaluation of the Raman intensities. *J. Chem. Phys.* **2001,** *115*, 6293-6299.

40. Aikens, C. M.; Webb, S. P.; Bell, R. L.; Fletcher, G. D.; Schmidt, M. W.; Gordon, M. S., A derivation of the frozen-orbital unrestricted open-shell and restricted closed-shell second- order perturbation theory analytic gradient expressions. *Theor. Chem. Acc* **2003,** *110*, 233-253.

41. England, W., Continuous degeneracy and energy-localization of molecular orbitals. *Int. J. Quantum Chem.* **1971,** *5*, 683-697.

42. Helgaker, T.; Jørgensen, P., Calculation of Geometrical Derivatives in Molecular Electronic Structure Theory. In *Methods in Computational Molecular Physics*, Wilson, S.; Diercksen, G. H. F., Eds. Springer US: Boston, MA, 1992; pp 353-421.

43. Pruitt, S.R.; Leang, S.S.; Xu, P.; Fedorov, D.G.; Gordon, M.S., Hexamers and Whichamers: Which Hex do you Choose?, *Comput. Theor. Chem.*, **2013,** *1021, 70*.

CHAPTER 3. MULTIPOLE MOMENTS IN THE EFFECTIVE FRAGMENT POTENTIAL METHOD

A paper to be submitted for publication at a later date

Colleen Bertoni, Alston J. Misquitta, Lyudmila V. Slipchenko, Mark S. Gordon

Abstract

In the effective fragment potential (EFP) the Coulomb potential is represented using a set of multipole moments generated by the distributed multipole analysis (DMA) method. Misquitta and Stone recently developed the basis space-iterated stockholder atom (BS-ISA+DF) method to generate multipole moments. This study benchmarks the accuracy of the EFP interaction energies using sets of multipole moments generated from the BS-ISA+DF method, and several versions of the DMA method (such as analytic and numeric grid-based), and with varying basis sets. Both methods lead to reasonable results, although using certain implementations of the DMA method can result in large errors. With respect to the CCSD(T)/CBS interaction energies, the mean unsigned error (MUE) of the EFP method for the S22 data set using BS-ISA+DF –generated multipole moments and DMA-generated multipole moments (using a small basis set and the analytic DMA procedure) is 0.78 and 0.72 kcal/mol, respectively. The MUE accuracy is on the same order as MP2 and SCS-MP2. The MUEs are lower than in a previous study benchmarking the EFP method without the EFP charge transfer term, demonstrating that the charge transfer term increases the accuracy of the EFP method. Regardless of the multipole moment method used, it is likely that much of the error is due to an insufficient

short-range electrostatic term (i.e. charge penetration term), as shown by comparisons with symmetry-adapted perturbation theory.

1. Introduction

A main goal of quantum chemistry is to perform fast and accurate calculations on challenging systems, such as solvated proteins or reactions occurring in solution, and to provide insight into the interactions between molecules. Although there are methods that give highly accurate results for small molecules, it is difficult to extend these methods to larger species and still retain their accuracy. Thus, there has been considerable effort to develop more computationally efficient methods. In particular, interaction energy methods have had success in describing non-covalent interactions of large systems in a computationally efficient manner. Interaction energy methods have their roots in the splitting of a system into non-interacting fragments (usually molecules), and then using perturbation theory to calculate the interaction energy between the fragments. For long-range interactions, like Coulomb, polarization, and dispersion, the perturbation between the fragments is the Coulomb operator. The first order perturbation energy is the Coulomb energy, while polarization and dispersion are each part of the second order energy. The Coulomb field is typically used in calculating the Coulomb energy, and can also be used in other terms, like the polarization term. Since the Coulomb field can be used in multiple terms, it is essential to represent it accurately and in a computationally inexpensive manner.

To represent the Coulomb field, many interaction energy methods use a multipole moment expansion, which arises from a Taylor expansion of the classical Coulomb energy expression. However, using a multipole moment expansion in which each

fragment has a single monopole, dipole, quadrupole, etc., has poor convergence properties. That is, if the fragments are too close together, the expansion no longer converges. Additionally, if the fragments are close, there is an attractive charge penetration energy that is not accounted for in the multipole moment expansion. To solve the convergence problem, a distributed multipole moment expansion can be used, where there is a monopole, dipole, quadrupole, etc., for an arbitrary number of sites distributed throughout each fragment. Then, the issue is how to calculate the distributed multipole moments themselves. Calculating the distributed multipoles typically depends on partitioning the molecular charge density among atom centers, bond midpoints, or other sites in the fragment. There has been much work on how to assign electronic charge densities to atoms. Several examples are: Mulliken charges[1], the Stone distributed multipole moment analysis (DMA) [2], the atoms-in-molecules method by Bader[3], the Hirschfeld-Stockholder method[4], the iterated Hirschfeld method[5], the atoms-in-molecules method by Popelier[6], the iterated Stockholder atom method by Lillestonen and Wheately[7], and the recently developed basis-space Iterated Stockholder Atoms with density fitting [8] (BS-ISA+DF) method by Misquitta and Stone.

The Effective Fragment Potential (EFP) method is an interaction energy method that has been extensively developed. [9] [10] Several terms in the EFP method (Coulomb energy, polarization energy, charge transfer energy) use a set of multipole moments to represent the Coulomb field. Thus, an accurate set of multipole moments is important to ensure that the total interaction energy is accurate. Currently, the multipole moments are calculated with the Stone DMA. As discussed later, the DMA method can be unstable depending on the basis set, although a numerical version has been developed to overcome

this problem. [11] The BS-ISA+DF method has been shown to be accurate and have promising convergence properties, and it is worthwhile to explore how the EFP method performs if the multipole moments generated by the BS-ISA+DF method are used.

In this work, the EFP energy with BS-ISA+DF-generated multipole moments (referred to here as EFP/ISA) and the EFP energy with DMA-generated multipole moments (referred to here as EFP/DMA) are compared. The structure of this paper is: Section 2 discusses the theory behind EFP, DMA, and BS-ISA+DF; Section 3 discusses the computational details used in the comparisons; and Section 4 discusses the comparison and results.

2. Theoretical Background

This section summarizes the EFP method, with a particular emphasis on the terms that use multipole moments, and background on the DMA and the BS-ISA+DF methods.

2.1 The Effective Fragment Potential method

The EFP method calculates the intermolecular interaction energy between molecules. In the EFP method, molecules are modeled with potentials with functional forms derived from first principles, and parameters that are generated from an *ab initio* calculation.

There are five terms in the Effective Fragment Potential: Coulomb, polarization, exchange repulsion, dispersion, and charge transfer. As shown in the equation below, polarization is a many-body term, while the other four terms are pairwise additive.

$$E_{AB}^{EFP} = E_{AB}^{\text{Coul}} + E_{AB}^{\text{exchange-repulsion}} + E_{AB}^{\text{dispersion}} + E_{AB}^{\text{charge-transfer}}$$
$$E_{\text{total}}^{EFP} = \sum_{A>B} E_{AB}^{EFP} + E_{\text{total}}^{\text{polarization}} \quad (1)$$

Each of the five terms depends on parameters generated from an *ab initio* calculation. The Coulomb, polarization, and charge transfer energy terms depend on a set of multipole moments to describe the electrostatic potential of the molecule. The polarization energy also depends on a set of distributed polarizability tensors generated from the Coupled Perturbed Hartree-Fock (CPHF) equation, which are distributed throughout the molecule using a set of localized molecular orbitals (LMOs). In addition to the multipole moments, the charge transfer energy depends on the basis set, the Fock matrix and a set of canonical virtual orbitals or valence virtual orbitals (VVOs).[12 13] The exchange-repulsion energy depends on the set of LMOs, the basis set, and the Fock matrix. The dispersion energy depends on a set of distributed dynamic polarizability tensors generated from the dynamic analog of the CPHF equation and are distributed throughout the molecule using a set of LMOs.

An EFP energy calculation requires two steps. The first is an *ab initio* calculation on an isolated molecule performed to generate the parameters for the molecule of interest. Then, these parameters are used in the EFP energy terms.

The next three sections consider the three EFP terms that depend explicitly on the set of multipole moments (Coulomb, polarization, and charge transfer).

2.1.1 Coulomb energy term

The Coulomb interaction energy term between two molecules A and B can be calculated by a distributed multipole moment expansion, as shown below.

$$E_{AB}^{Coul} = \sum_{I}^{A}\sum_{J}^{B}\left[\begin{array}{l} q^J q^I T^{IJ} - \sum_{\alpha}^{x,y,z} q^J \mu_\alpha^I T_\alpha^{IJ} + \frac{1}{3}\sum_{\alpha,\beta}^{x,y,z} q^J \Theta_{\alpha\beta}^I T_{\alpha\beta}^{IJ} - \frac{1}{15}\sum_{\alpha,\beta,\gamma}^{x,y,z} q^J \Omega_{\alpha\beta\gamma}^I T_{\alpha\beta\gamma}^{IJ} \\ + \sum_{\alpha}^{x,y,z} \mu_\alpha^J q^I T_\alpha^{IJ} - \sum_{\alpha,\beta}^{x,y,z} \mu_\alpha^J \mu_\beta^I T_{\alpha\beta}^{IJ} + \frac{1}{3}\sum_{\alpha,\beta,\gamma}^{x,y,z} \mu_\alpha^J \Theta_{\beta\gamma}^I T_{\alpha\beta\gamma}^{IJ} \\ + \frac{1}{3}\sum_{\alpha,\beta}^{x,y,z} \Theta_{\alpha\beta}^J q^I T_{\alpha\beta}^{IJ} - \frac{1}{3}\sum_{\alpha,\beta,\gamma}^{x,y,z} \Theta_{\alpha\beta}^J \mu_\gamma^I T_{\alpha\beta\gamma}^{IJ} + \frac{1}{9}\sum_{\alpha,\beta,\gamma,\delta}^{x,y,z} \Theta_{\alpha\beta}^J \Theta_{\gamma\delta}^I T_{\alpha\beta\gamma\delta}^{IJ} \\ + \frac{1}{15}\sum_{\alpha,\beta,\gamma}^{x,y,z} \Omega_{\alpha\beta\gamma}^J q^I T_{\alpha\beta\gamma}^{IJ} \end{array}\right] \quad (2)$$

I (*J*) runs over all multipole moment expansion points in *A* (*B*), q^I is the monopole on site *I*, μ^I is the dipole on site *I*, Θ^I is the quadrupole on site *I*, Ω^I is the octopole on site *I* and $T_{\alpha\beta\ldots\nu}^{IJ} = \nabla_\alpha \nabla_\beta \ldots \nabla_\nu \frac{1}{R_{IJ}}$ is the multipole interaction tensor for sites *I* and *J*. R_{IJ} is the distance between sites *I* and *J*, where $\boldsymbol{R_{IJ}=R_J-R_I}$ in vector notation.

Charge penetration for the Coulomb energy term

Since the multipole moment expansion does not take into account the energy lowering when the charge densities of fragments overlap, a charge penetration term or a damping term is added. There are two types of damping for the Coulomb energy in the EFP method.[14] One is an exponential damping term, which is not used here, so is not considered further. The second is based on the overlap of LMOs on the two fragments, and is used to calculate an approximation to the charge-penetration energy. The charge-penetration energy for fragments *A* and *B* is calculated as shown below.

$$E_{AB}^{chgpen} = \sum_{l}^{LMO\in A} \sum_{m}^{LMO\in B} \frac{-2S_{lm}^2}{R_{lm}} \sqrt{\left(\frac{1}{-2\ln|S_{lm}|} \right)} \tag{3}$$

where S_{lm} is the overlap integral between l and m, and R_{lm} is the distance between the LMO centroid of l ($\langle l|x|l\rangle$ for the x-position) and the LMO centroid of m ($\langle m|x|m\rangle$ for the x-position).

2.1.2 Polarization energy term

The polarization energy is a many-body energy term that is due to the generation of induced dipoles on all of the fragments in the total electric field (static and induced fields) of all the other fragments. The polarization interaction energy term is modeled by placing dipole polarizability tensors on LMO centroids. Then, in the presence of the static and induced electric field on the other fragments, the dipole polarizability tensors generate induced dipoles. The induced dipoles are iterated to self-consistency, and then used in the calculation of the polarization energy. The static electrostatic field is modeled by the same distributed multipole moment expansion as in the Coulomb term.

The induced dipole on fragment A on LMO centroid l in the β direction can be written as:

$$p_{l,\beta}^{A} = \sum_{\gamma}^{\{x,y,z\}} \alpha_{l,\beta\gamma} \left(E_{l,\gamma}^{0,A} + \sum_{B\neq A}^{\text{fragments}} \sum_{m}^{LMO\in B} \sum_{\kappa}^{\{x,y,z\}} T_{\gamma\kappa}^{lm} p_{m,\kappa}^{B} \right) \tag{4}$$

where

$T_{\gamma\kappa}^{lm}$ is the dipole-dipole interaction tensor for sites l and m

$\alpha_{l,\beta\gamma}$ is the dipole polarizability tensor on LMO l

$E_{l,\gamma}^{0,A}$ is the static electric field on fragment A on LMO centroid l in the γ direction

The static electric field is expressed using the same distributed multipole moments as in the Coulomb energy term:

$$E_{l,\gamma}^{0,A} = \sum_{B\neq A}^{\text{fragments}} \sum_{I}^{B} E_{lI,\gamma}^{0} = \sum_{B\neq A}^{\text{fragments}} \sum_{I}^{B} \left(q^{I} T_{\gamma}^{lI} + \sum_{\alpha}^{\{x,y,z\}} \mu_{\alpha}^{I} T_{\gamma\alpha}^{lI} + \frac{1}{3} \sum_{\alpha\beta}^{\{x,y,z\}} \Theta_{\alpha\beta}^{I} T_{\gamma\alpha\beta}^{lI} \right) \tag{5}$$

where I runs over the multipole moment expansion points in fragment B.

The polarization interaction energy term is shown below:

$$E^{pol} = \sum_{A}^{\text{fragments}} \left[-\frac{1}{2} \sum_{n}^{LMO\in A} \sum_{\alpha}^{\{x,y,z\}} E_{n,\alpha}^{0,A} p_{n,\alpha}^{A} \right] \tag{6}$$

Damping for the polarization energy term

The polarization energy is damped by a Tang-Toennies style Gaussian formula[14] [15]. The damping is accomplished by multiplying the multipole interaction tensors by a damping function, and then rewriting the induced dipoles in terms of the damped multipole interaction tensors. The damping function is $F_{damp,lI}^{pol} = 1 - \exp\left(-R_{lI}^{2}\sqrt{fg}\right)\left(1 + R_{lI}^{2}\sqrt{fg}\right)$, where the terms f and g are constants usually set to 0.6. The damped polarization energy equations are similar to the non-damped version but with damped multipole moment interaction tensors replacing regular multipole moment interaction tensors. Defining $T_{\alpha\beta\ldots\nu}^{lI,damped} \equiv F_{damp,lI}^{pol} T_{\alpha\beta\ldots\nu}^{lI}$, the damped static electric field can be written as:

$$E_{l,\gamma}^{0,A,damped} = \sum_{B\neq A}^{\text{fragments}} \sum_{I}^{B} E_{lI,\gamma}^{0,damped} = \sum_{B\neq A}^{\text{fragments}} \sum_{I}^{B} \left(q^{I} T_{\gamma}^{lI,damped} + \sum_{\alpha}^{\{x,y,z\}} \mu_{\alpha}^{I} T_{\gamma\alpha}^{lI,damped} + \frac{1}{3} \sum_{\alpha\beta}^{\{x,y,z\}} \Theta_{\alpha\beta}^{I} T_{\gamma\alpha\beta}^{lI,damped} \right) \tag{7}$$

Following the same substitution, the damped induced dipoles, $p_{l,\beta}^{A,damped}$, can then be written as: $p_{l,\beta}^{A,damped} = \sum_{\gamma}^{\{x,y,z\}} \alpha_{l,\beta\gamma} \left(E_{l,\gamma}^{0,A,damped} + \sum_{B \neq A}^{\text{fragments}} \sum_{m}^{LMO \in B} \sum_{\kappa}^{\{x,y,z\}} T_{\gamma\kappa}^{lm,damped} p_{m,\kappa}^{B,damped} \right)$

2.1.3 Charge transfer energy term

The charge transfer energy can be thought of as a stabilizing energy due to the interaction of the occupied orbitals on one molecule with the virtual orbitals on another molecule.[13 16] The EFP charge transfer term was derived using a second-order perturbative approach beginning with an antisymmetrized wavefunction at the Hartee-Fock level of theory.

In the derivation, approximations are used to simplify the second-order energy expression. One approximation is to represent the electrostatic potential as a multipole moment expansion, using the same mulitpole moments as in the Coulomb and polarization terms. The EFP charge transfer energy of molecule A induced by molecule B is:

$$CT^{A(B)} = 2 \sum_{i}^{\substack{\text{occ} \\ \text{CMO} \in \text{A}}} \sum_{n}^{\text{vir} \in \text{B}} \frac{1}{1 - \sum_{m}^{\substack{\text{all} \\ \text{MOs} \in \text{A}}} S_{nm}^2} \frac{V_{in}^{\text{EFB}} - \sum_{m}^{\substack{\text{all} \\ \text{MOs} \in \text{A}}} S_{nm} V_{im}^{\text{EFB}}}{\left(F_{ii}^{A} - T_{nn} \right)} \times \left[V_{in}^{\text{EFB}} - \sum_{m}^{\substack{\text{all} \\ \text{MOs} \in \text{A}}} S_{nm} V_{im}^{\text{EFB}} + \sum_{j}^{\substack{\text{occ} \\ \text{CMO} \in \text{B}}} S_{ij} \left(T_{nj} - \sum_{m}^{\substack{\text{all} \\ \text{MOs} \in \text{A}}} S_{nm} T_{mj} \right) \right] \tag{8}$$

where T_{nj} is the kinetic energy integral between orbitals *n* and *j*, F_{ii}^{A} is the diagonal Fock matrix element at orbital *i* in the canonical MO basis for fragment *A*, and V_{in}^{EFPB} is the

matrix element of the molecular electrostatic potential of fragment *B* between orbitals *i* and *n*. This can written as:

$$V_{in}^{EFPB} = \sum_{I}^{B} \langle i | \left(q^I \hat{T}^I - \sum_{\beta}^{\{x,y,z\}} \mu_\beta^I \hat{T}_\beta^I + \frac{1}{3} \sum_{\beta\gamma}^{\{x,y,z\}} \Theta_{\beta\gamma}^I \hat{T}_{\beta\gamma}^I \right) | n \rangle$$
$$= \sum_{I}^{B} \int dr_1 \chi_i^*(r_1) \left(q^I T^{Ir_1} - \sum_{\beta}^{\{x,y,z\}} \mu_\beta^I T_\beta^{Ir_1} + \frac{1}{3} \sum_{\beta\gamma}^{\{x,y,z\}} \Theta_{\beta\gamma}^I T_{\beta\gamma}^{Ir_1} \right) \chi_n(r_1) \quad (9)$$

where *I* runs over the multipole moment expansion points in fragment *B*, $r_I (= x_I, y_I, z_I)$ is the position of the electron, $\chi_i(r_i)$ is molecular orbital *i* written out explicitly. The right hand side of Eq. (9) is evaluated in a similar manner to the standard nuclear attraction integral.

While there is not unanimous agreement regarding the importance of the charge transfer interaction energy [10 17], the EFP method predicts relatively large charge transfer contributions for polar and ionic complexes, and systems with hydrogen bonds[13]. [18]

2.2 Multipole moment methods

2.2.1 Distributed Multipole Analysis

In the DMA method, the molecular charge density is partitioned, and each piece of charge density is represented by its own multipole moment expansion. The partitioning can be done in basis function space or real space. Basis function space DMA is denoted here as DMA0 or analytical DMA.

For restricted Hartee-Fock (RHF), the molecular charge density can be written in terms of primitive Gaussians:

$$\begin{aligned}\rho(\mathbf{r}) &= \sum_{\mu,\nu}^{\mathrm{AOs}} P_{\mu\nu}\chi_\mu(\mathbf{r}-\mathbf{r}_I)\chi_\nu(\mathbf{r}-\mathbf{r}_J) \\ &= \sum_{\mu,\nu}^{\mathrm{AOs}} P_{\mu\nu} \sum_{u}^{PG\in\nu} \sum_{t}^{PG\in\mu} P'_{ut} g_u(\mathbf{r}-\mathbf{r}_I,\alpha_u) g_t(\mathbf{r}-\mathbf{r}_J,\alpha_t) \\ &= \sum_{\mu,\nu}^{\mathrm{AOs}} \sum_{u}^{PG\in\nu} \sum_{t}^{PG\in\mu} \left[P_{\mu\nu} P'_{ut} g_{ut}(\mathbf{r}-\mathbf{r}_K,(\alpha_u+\alpha_t)) \right]\end{aligned} \tag{10}$$

where $\chi_\mu(\mathbf{r}-\mathbf{r}_I)$ is a basis function composed of a sum of primitive Gaussians (PGs) centered on atom *I*, $g_u(\mathbf{r}-\mathbf{r}_I,\alpha_u)$ is a primitive Gaussian centered on atom *I* with contraction exponent α_u, P'_{ut} is the primitive Gaussian cross term that contains the product of the contraction coefficients for PGs *u* and *t*, $P_{\mu\nu}$ is the RHF density matrix element for AOs μ and ν, and $\mathbf{r}_K = \dfrac{\alpha_u\mathbf{r}_I + \alpha_t\mathbf{r}_J}{\alpha_u+\alpha_t}$.

As shown in the last equality in Eq. (10), the charge density is a sum over pieces of charge density (the term in the brackets) centered at the Gaussian overlap point r_k. Each piece of charge density can be described by a set of multipole moment integrals at the overlap point associated with the piece of charge density. A certain number of expansion sites are chosen in the molecule, such as all atom centers or all atom centers and bond midpoints. Then, the origins of the multipole moment integrals are shifted to the nearest expansion site.

It is well known that the DMA0 multipole moments are unstable with respect to expanding the basis set[11]. Although the multipole moments from different basis sets should produce similar electrostatic potentials, the values for the multipole moments themselves can be basis set dependent. Consequently, the appropriate termination of the multipole expansion (e.g., at quadrupoles or octopoles) may depend on the basis set used. Thus, even though the electrostatic potential should be the same, the error due to the

multipole truncation can vary. This is especially the case for basis sets with diffuse functions or with high angular momenta, since these functions tend to make a larger contribution to the higher moments and therefore the truncation point is important.[19 2] Because of the instability with respect to basis set size, real space DMA was developed.

Real space DMA involves modifying the DMA0 algorithm such that if the exponent of a product of primitives (e.g., $\alpha_u + \alpha_t$) is smaller than a chosen cutoff, a grid-based numerical integration scheme is used to partition the contribution to the multipole moments. If the exponent is greater than the cutoff, DMA0 is used to partition the contribution to the multipole moments. Ref. [11] recommends a cutoff value of 4, and so the method is referred to here as DMA4.

It is also important to note that when the molecules are too close to each other, the multipole moment expansion of the Coulomb energy between them can diverge. How close the molecules can get to each other before the expansion diverges depends on the allocation algorithm mentioned above, and on the expansion points chosen. The greater the number of expansion points, the more accurately the multipole expansion mimics the correct quantum density. So, the fewer the number of expansions points used, the more likely it is that the expansion will diverge at a given distance.

2.2.2 BS-ISA+DF

In the implementation of the BS-ISA+DF method used in this work, the molecular charge density is partitioned among the atoms, and a set of multipole moments is calculated for each atom. Instead of directly partitioning the density as in Eq. (10), the

BS-ISA+DF approach is to first define atoms so that the atoms are as spherical as possible.

The BS-ISA+DF method has its origins in the Hirschfeld stockholder method for calculating atomic densities. In the Hirschfeld stockholder method, the charge density for each atom *a* is given as:

$$\rho^a(\mathbf{r}) = \rho(\mathbf{r}) \frac{w^a(\mathbf{r})}{\sum_{b}^{atoms} w^b(\mathbf{r})} \tag{11}$$

where $\rho(\mathbf{r})$ is the total molecular density and $w^a(\mathbf{r})$ is a function that describes the shape of the atom *a*. The form of the shape function $w^a(\mathbf{r})$ varies by method. An insight by Lillestolen and Wheately was to use the spherical average of the atomic density as the shape function, which avoids creating a shape function for each atom, and results in an equation that must be solved iteratively.[7] The BS-ISA+DF method follows an analogous iteration scheme, but in basis space. That is, in the BS-ISA+DF method, the terms in Eq. (11) are expanded in a basis, as shown below.

$$\begin{aligned} \rho^a(\mathbf{r}) &= \sum_k c_k^a \zeta_k^a(\mathbf{r}) \\ w^a(\mathbf{r}) &= \sum_{k \in s-\text{func}} c_k^a \zeta_{k,s}^a(\mathbf{r}) \end{aligned} \tag{12}$$

where c_k^a is a coefficient associated with atom *a* and is determined in the iterative procedure, $\zeta_k^a(\mathbf{r})$ is a basis function centered on atom *a*, *k* runs over all basis functions, $\zeta_{k,s}^a(\mathbf{r})$ is an s-type function on atom *a*, and $k \in s$ runs over all s-functions in the basis.

To determine the atomic density, the coefficients are calculated using an iterative procedure that minimizes a BS-ISA+DF functional. The functional and minimization algorithm have been developed to make the procedure stable, accurate, and reliably

convergent. Additionally, to ensure that the tail regions of the atomic densities are well-described, the shape functions are modified so that they decay exponentially.

Once the atomic densities are obtained, multipole moment integrals can be computed. BS-ISA+DF has many appealing properties, such as having a more systematic convergence with respect to multipole moment rank than DMA0 or DMA4. However, the DMA methods are more computationally efficient and algorithmically simpler. [8]

3. Computational Details

As mentioned in the Background section, the EFP method has several parameters determined from an *ab initio* MAKEFP calculation. For the EFP/ISA and EFP/DMA calculations, all parameters except for the multipole moments are the same. That is, the static polarizability tensors, dynamic polarizability tensors, basis set, localized molecular orbitals, Fock matrix elements, and virtual molecular orbital coefficients are the same for the EFP/ISA and EFP/DMA calculations. All parameters except the multipole moments were generated using the 6-311++G(3df,2p) basis set. The EFP calculations, and MAKEFP calculations were done with the GAMESS[20 21] package. Several integral cutoffs were changed from the default values (ITOL was set to 24, ICUT to 12), and the SCF density convergence was tightened to 10^{-7}. Overlap-based damping was used to account for charge-penetration effects in the Coulomb energy. The localization method used was Boys[22, 23] and the set of all canonical virtual orbitals was used for the charge transfer term.

The ISA multipole moments were generated with CamCASP 5.8.[24] The main basis set was aug-cc-pVTZ[25 26], the aux/ISA basis set was RI-MP2 aug-cc-pVTZ with

ISA-set2[8] for s-functions (except for ethyne, which used RI-MP2 aug-cc-pVQZ with ISA-set2 for s-functions), and the ISA algorithm used was A+DF with ζ=0.1. Densities were from the PBE0 functional/AC. The asymptotic correction (AC) is the Casida-Salahub version of AC present in NWChem[27] with default (un-optimized) shift. NWChem was used for these calculations.

To consider the effects of basis set and the different DMA algorithms, the DMA multipole moments were generated in four different ways:

1. Following a previous paper that measured the accuracy of EFP against other force field methods[28], the DMA multipole moments were generated using HF/6-31+(d) for non-aromatic molecules (ammonia, ethene, ethyne, formamide, formic acid, hcn, methane, water), and HF/6-31(d) for aromatic molecules (2-aminopyridine, 2-pyridoxine, adenine, benzene, indole, phenol, pyrazine, thymine, uracil). The original analytic DMA procedure (DMA0) was used. This method is referred to as EFP/DMA0-small, since it uses a smaller basis set to generate the multipole moments.
2. DMA0 multiple moments were computed using HF/6-311++G(3df,2p). This method is referred to as EFP/DMA0.
3. DMA4 multiple moments were computed using the HF/6-311++G(3df,2p). This method is referred to as EFP/DMA4.
4. The DMA multipole moments were computed using HF/6-311++G(3df,2p), with DMA0 for non-aromatic molecules and DMA4 for aromatic molecules. This method is referred to as EFP/DMA-mixed.

The geometries at which ISA multipole moments and EFP potentials were generated are from the S22 dataset complexes. The geometry for ammonia, ethene, formic acid, phenol, pyrazine, water, and formamide is the geometry of the first monomer in the S22 dataset dimer for that molecule. The geometry of uracil is the geometry of the first monomer in the uracil H-bonded dimer. The geometry of benzene is the geometry of the first monomer in the benzene dimer T-shaped complex. The geometry of indole is the geometry of the indole in the benzene-indole T-shaped complex. The geometry of methane is the geometry of the methane in the benzene-methane dimer. The other molecules show up only once in the S22 dataset, and the S22 geometries are used for those molecules. Since the geometry of adenine and thymine in the Watson-Crick complex and the stacked complex differ significantly, the ISA multipole moments and EFP potentials were generated at both geometries, and used in the corresponding EFP calculations.

The DMA method can use the set of all atom centers or the set of all atoms centers and bond midpoints as expansion points for the multipole moments. For EFP/DMA0-small, calculations were done with the set of all atom centers (denoted as EFP/DMA0-small-atoms) and with the set of all atom centers and bond midpoints as expansion points (denoted as EFP/DMA0-small). For all other EFP calculations using DMA, the expansion points are the set of all atom centers and bond midpoints. That is, six types of calculations are compared: EFP/ISA, EFP/DMA0-small, EFP/DMA0-small-atoms, EFP/DMA0, EFP/DMA4, and EFP/DMA-mixed.

4. Results

To test the accuracy of and compare the methods, several comparisons are presented here. To compare predicted geometries, the S22 complexes were geometry-optimized using all methods. The resulting geometries are compared to the corresponding S22 geometries to assess the quality of geometry prediction. Since the EFP fragments are internally frozen, the geometry optimization changes only the angles and the distances between fragments. Next, the total interaction energy at each optimized geometry is compared to the CCSD(T)/CBS binding energy at the standard S22 geometry to assess the quality of the interaction energy calculation for each method. In addition, the EFP energy components that depend on the multipole moments (Coulomb energy, polarization energy, and charge transfer energy) are compared to the corresponding SAPT2+(3)/aug-cc-pVTZ (referred to as "SAPT" in this work) energy components. For this comparison, the EFP and SAPT calculations were done at the S22 geometries. The SAPT values are from the Addition/Correction to Ref. [28].

The equivalent SAPT terms used in the comparison are [See Ref. [29] and [30] for the notation]:

$$\begin{aligned} E_{SAPT}^{\text{Coulomb}} &= E_{\text{elst, resp}}^{(10)} + E_{\text{elst, resp}}^{(12)} + E_{\text{elst, resp}}^{(13)} \\ E_{SAPT}^{\text{exchange-repulsion}} &= E_{\text{exch}}^{(10)} + E_{\text{exch}}^{(11)} + E_{\text{exch}}^{(12)} \\ E_{SAPT}^{\text{induction}} &= E_{\text{ind, resp}}^{(20)} + E_{\text{exch-ind, resp}}^{(20)} + {}^{t}E_{\text{ind}}^{(22)} + {}^{t}E_{\text{exch-ind}}^{(22)} + \delta E_{\text{HF}}^{(2)} \\ E_{SAPT}^{\text{dispersion}} &= E_{\text{disp}}^{(20)} + E_{\text{disp}}^{(30)} + E_{\text{disp}}^{(21)} + E_{\text{disp}}^{(22)} + E_{\text{exch-disp}}^{(20)} \end{aligned} \tag{13}$$

The sum of the EFP polarization and charge transfer energy is compared to the SAPT induction energy.

To help gain insight into the differences in the dimers in the S22 dataset, the dimers are split into hydrogen bonding, dispersion dominated, and mixed types, following a previous EFP study. [28]

Predicted Geometries of the S22 Complexes

In the S22 dataset, the T-shaped benzene dimer is constrained to C_{2V} symmetry, so this prescription is followed for the EFP methods. Table 1 shows the differences relative to the S22 values for specific atom-atom distances. The mean unsigned error (MUE) is also given in the table. In Table 1, X···RD denotes the distance between the atom X and the center of the plane made by the benzene ring. (The plane is calculated using the first three atoms of the benzene in the dimer.) R1 and R2 are the vertical and horizontal distances between the planes of the rings, respectively. (See Figure 1.) The notation in Table 1 is similar to that in Ref. [28].

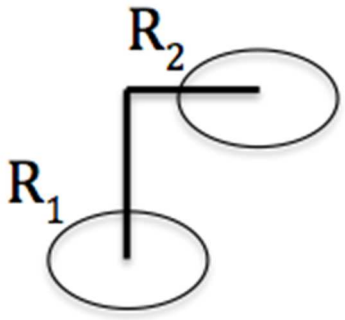

Figure 1. A definition of the R_1 and R_2 values.

Table 1: Differences (Å) in distance between the *ab initio* S22 geometry and the EFP geometries after optimization

	distance[a]	ΔEFP/ISA	ΔEFP/DMA0-small	ΔEFP/DMA0-small-atoms	ΔEFP/DMA0	ΔEFP/DMA4	ΔEFP/DMA-mixed
Hydrogen-Bonded Complexes							
ammonia dimer	N1···N5	-0.02	-0.1	-0.17	0	0.16	0
water dimer	O1···O4	0	-0.07	-0.12	0.05	0.04	0.05
formic acid dimer	O2···O8	0.11	0.05	-0.04	0.09	0.2	0.09
formamide dimer	O2···N9	0.1	-0.03	-0.03	0.04	0.2	0.04
uracil H-bonded dimer	N1···O23	0.08	0.04	0.01	0.02	0.18	0.18
2-pyridoxine 2-aminopyridine	N1···N15	0.04	-0.18	-[b]	-0.06	0.22	0.22
adenine–thymine WC	N1···N20	0	-0.18	-[b]	-0.06	0.23	0.23
MUE for Hydrogen-Bonded Complexes		0.05	0.09	0.07[e]	0.05	0.18	0.12
Dispersion-Dominated Complexes							
methane dimer	C1···C6	-0.12	-0.08	-0.12	-0.12	0.04	-0.12
ethene dimer	C1···C7	-0.07	-0.09	-0.16	-0.1	0.1	-0.1
benzene–methane	C1···RD[c]	0.21	0.23	0.21	-0.11	0.21	0.28
benzene stack	R1/R2[d]	0.43/-0.42	0.44/-0.3	0.41/-0.15	0.44/0.11	0.48/-0.59	0.48/-0.59
pyrazine dimer	R1/R2 [d]	0.28/-0.11	0.3/-0.23	0.27/-0.12	0.35/-0.32	0.33/-1.04	0.33/-1.04
uracil stack	R1/R2 [d]	0.18/-0.02	0.14/-0.02	0.13/-0.01	0.06/0.92	0.19/0.03	0.19/0.03
indole–benzene stack	R1/R2 [d]	0.38/0	0.35/0.28	0.33/0.26	-[b]	0.44/-0.36	0.44/-0.36
adenine–thymine stack	R1/R2 [d]	0.24/-0.2	0.22/-0.07	0.2/0	0.02/0.18	0.22/-0.22	0.22/-0.22
MUE for Dispersion-Dominated Complexes		0.20	0.21	0.18	0.25[e]	0.33	0.34

Table 1 continued

Mixed Complexes							
ethene–ethyne	C8···C2	0.16	0.07	0.08	0.06	0.19	0.06
benzene–water	O1···RD[c]	0.1	0.07	-0.04	-0.02	0.16	0.19
benzene–ammonia	N···RD[c]	0.15	0.17	0.11	-0.02	0.16	0.01
benzene–HCN	C14···RD[c]	0.24	0.15	0.09	0.17	0.21	0.25
benzene dimer T-shaped	C1···RD[c]	0.30	0.30	0.30	0.25	0.30	0.30
indole–benzene T-shaped	N21···RD[c]	0.23	0.21	0.15	-0.05	0.26	0.26
phenol dimer	O7···O20	0.07	0.03	-0.01	0.07	0	0
MUE for Mixed Complexes		0.18	0.14	0.11	0.06	0.14	0.11
Overall MUE		0.16	0.16	0.14[e]	0.15[e]	0.25	0.23

[a]Atoms are numbered as in Ref. 28. [b]The geometry optimization did not complete, since the induced dipole procedure failed to converge. [c] The distance between the atom X and the center of the plane made by the benzene ring, where the plane is calculated using the first three atoms of the benzene.[d] R1 and R2 are the vertical and horizontal distances between the planes of the rings, respectively. [e] The MUE is computed without the cases where the induced dipole procedure does not converge.

ΔX is the difference between method X and the *ab initio* result. The values of the distances are in Section 1 of the Supporting Information.

Among the hydrogen-bonding complexes, the error for all methods is less than 0.25 Å, which is in good agreement with the S22 geometries. The EFP/ISA, EFP/DMA4, and EFP/DMA-mixed methods have mostly positive differences, meaning that they overestimate the intermolecular separation. The methods that used a smaller basis set to calculation the multipole moments, the EFP/DMA0-small and EFP/DMA0-small-atoms methods, mostly have negative differences, meaning that they underestimate the

intermolecular distance. A previous study used EFP/DMA0-small without charge transfer to optimize the S22 set, and found that the intermolecular separations were overestimated. Thus the effect of including the EFP charge transfer is to decrease the distances, which is expected, since charge transfer is typically an attractive interaction. Use of the smaller basis set might make the interaction too attractive, since the distance is underestimated. The induced dipole procedure did not converge when using the EFP/DMA0-small-atoms method for two aromatic complexes, possibly because there are not enough expansion points.

In the dispersion-dominated complexes, the distances in the methane and ethene dimers are underestimated by all methods except for EFP/DMA4, which overestimates the distance. All of these errors are less than 0.3 A, which is in good agreement with the S22 geometries. In the aromatic ring complexes, all methods overestimate the distance between the ring planes, which implies that at least the sign of this distance is not dependent on the multipole moments used. For the EFP/ISA method and the methods that used a smaller basis set for the DMA multipole moments, the parallel shift of the ring planes (R2) is underestimated for all complexes except for indole-benzene. The induced dipole procedure did not converge when using the EFP/DMA0 method for the indole-benzene stack complex. Although overall the error is low, the methods using DMA multipole moments generated from large basis sets performed the worst for the aromatic complexes. The EFP/DMA4 and EFP/DMA-mixed methods (which are the same in this case), predict the R2 value for pyrazine dimer to be about 1 Å different from the S22 geometry, and the EFP/DMA0 method predicts the R2 value for the uracil dimer 0.9 Å different from the S22 geometry.

In the mixed complexes, the EFP/ISA, EFP/DMA0-small, EFP/DMA4, and EFP/DMA4-mixed methods slightly overestimate the distance for all complexes. The EFP/DMA0 and EFP/DMA0-small-atoms methods underestimate the distance for certain complexes and underestimate the distance for others. Overall, all methods are in good agreement with the S22 dataset, with the maximum error not exceeding 0.3 Å.

For all three interaction energy types and for all methods studied here, the overall mean unsigned error is under 0.35 Å. In two of the methods, EFP/DMA0-small-atoms and EFP/DMA0 the self-consistent induced-dipole procedure does not converge during one step of the geometry optimization for at least one complex. The possible causes for the divergence will be discussed in a later section. As can be seen in Section 1 of the SI, there were several geometries that differed from the S22 geometry by a small rotation, but the difference in the CCSD(T) energy between the different rotations are also very small.

Total interaction energies of the S22 Complexes

The total interaction energies of the methods at the optimized geometries are compared to CCSD(T)/CBS values [31,28] to test the accuracy of the energy calculations. The total EFP energy values are provided in Section 2 of the Supporting Information.

Figures 2, 3, and 4 show the differences in interaction energies between each method and CCSD(T)/CBS for each category of interaction energy. Note that if geometry optimization failed due to non-convergence of the induced dipole procedure, the corresponding interaction energies are not shown in the figures. To summarize the results, the MUE for each method is shown in Table 2.

Table 2: MUE for all methods with respect to CCSD(T)/CBS (kcal/mol)

	EFP/ISA	**EFP/DMA-mixed**	**EFP/DMA0-small-atoms**	**EFP/DMA0**	**EFP/DMA4**	**EFP/DMA0-small**
MUE(HB)	1.297	2.771	2.854*	0.715	3.741	1.672
MUE(DISP)	0.429	0.666	0.279	0.957*	0.555	0.331
MUE(MIXED)	0.668	0.282	0.413	0.752	0.195	0.199
MUE(overall)	0.781	1.214	0.970*	0.808*	1.454	0.716

* The cases for which the induced dipole procedure does not converge are omitted

For the hydrogen-bonding complexes, the EFP/DMA0 method has the smallest MUE, while the EFP/DMA0-small-atoms has the lowest MUE for the dispersion-dominated species. The smallest MUE for the mixed system is obtained with both the EFP/DMA0-small and the EFP/DMA4 methods. For the dispersion-dominated species and the mixed species, all of the MUEs are below 1 kcal/mol, so all methods work very well for these two types of dimers. The errors in interaction energies for the hydrogen bonded species range from 0.7 kcal/mol (DMA0) to 3.7 kcal/mol (DMA4). The EFP/ISA and EFP/DMA4 methods consistently overestimate the energy, while the EFP/DMA0-small and EFP/DMA0-small-atoms methods consistently underestimate the energy. The EFP/DMA0 method underestimates and overestimates the energy for various complexes. The EFP/DMA-mixed method also shows positive and negative differences. The EFP/DMA4 and EFP/DMA-mixed methods have the largest individual errors, overestimating the energy by up to 6.8 kcal/mol on the adenine-thymine Watson-Crick complex in particular. As noted above, the optimized geometries for the EFP/DMA4 and EFP/DMA-mixed methods also overestimate the distances between all the dimers.

Overall, the hydrogen bonding complexes are the major source of error for most methods. For the EFP/DMA0-small-atoms and EFP/DMA0 methods a small number of

the induced dipoles do not converge during the optimizations. The divergence is likely due to the multipole moment expansion being truncated too soon, which is easily remedied by adding additional multipole moments.

EFP energy components at S22 geometry

To gain insight into the interaction energy errors, the EFP energy decomposition at the initial S22 geometry for each method is compared to the SAPT energy decomposition at the S22 geometry. Tables 3, 4, and 5 present the MUEs for the Coulomb term, the sum of the polarization and charge transfer terms, and the total interaction energy term, respectively. Figures 5, 6, and 7 show the energy differences between each method and the SAPT energies. Section 2 of the Supporting Information contains the SAPT and EFP interaction energy components for the S22 complexes.

Table 3: MUE for the EFP Coulomb term (kcal/mol)

	EFP/ISA	EFP/DMA-mixed	EFP/DMA0-small-atoms	EFP/DMA0	EFP/DMA4	EFP/DMA0-small
MUE(HB)	2.485	3.596	1.806	0.863	5.453	1.631
MUE(DISP)	2.560	1.487	2.431	3.105	1.514	2.475
MUE(MIXED)	0.960	0.897	0.614	0.806	0.816	0.553
MUE(overall)	2.027	1.970	1.654	1.677	2.545	1.595

Overall, the three EFP/DMA0 methods have the smallest MUEs, all within 0.1 kcal/mol of each other and below 2 kcal/mol. The EFP/ISA and EFP/DMA-mixed methods have MUEs that are only slightly larger, and the MUE for the EFP/DMA4 method is about 0.5 kcal/mol larger than the others. The latter is still reasonable. For the hydrogen-bonded dimers, the general trend for all methods is to overestimate the Coulomb term. The EFP/DMA0 method has the lowest MUE, with a value less than 0.9 kcal/mol. The error in the Coulomb energy could be from the multipole moment expansion or the charge penetration term. The largest errors are likely due to the charge penetration term not accounting for all charge penetration, especially for particularly strong interactions. However, the EFP/DMA4 and EFP/DMA-mixed methods have very large positive errors. .

For the dispersion-dominated dimers, all methods have errors of less than 0.9 kcal/mol for the complexes without ring systems, agreeing well with SAPT. However, all methods have large positive errors for the ring systems. For most of the methods and complexes, the positive error can be explained by an insufficient charge penetration term. Although the multipole moment expansion part of the EFP Coulomb term is often positive, the SAPT Coulomb energy is negative, so the charge penetration term is necessary to change the sign of the EFP Coulomb energy. The largest individual error is that for the indole-benzene stacked structure, with the EFP/DMA0 method. As mentioned above, during the geometry optimization of the benzene-indole stacked structure using the EFP/DMA0 method, the induced dipole procedure did not converge. A reason for the non-convergence could be the large error in the Coulomb term seen here.

For the mixed complexes, the EFP Coulomb energy is similar to the SAPT Coulomb energy, with the MUE for all methods less than 1 kcal/mol. The Coulomb energies are relatively small for the mixed complexes.

There are several interesting comparisons to make. As may be seen by comparing the EFP/DMA0-small and EFP/DMA0-small-atoms methods, having expansion points on only atoms results in similar Coulomb energies to having expansion points on atoms and bond midpoints. The numeric EFP/DMA4 method has similar or smaller errors than the EFP/DMA0 method, except for the hydrogen-bonded complexes, for which the reverse is true. The EFP/ISA method consistently slightly overestimates the Coulomb energy, which points towards a consistent error due to a lack of charge penetration.

Table 4: MUE for the EFP Polarization and Charge transfer term (kcal/mol)

	EFP/ISA	EFP/DMA-mixed	EFP/DMA0-small-atoms	EFP/DMA0	EFP/DMA4	EFP/DMA0-small
MUE(HB)	2.098	2.416	0.871	1.641	3.366	0.705
MUE(DISP)	0.395	0.916	0.177	1.097	0.973	0.366
MUE(MIXED)	0.313	0.494	0.228	0.418	0.639	0.196
MUE(overall)	0.911	1.259	0.414	1.054	1.628	0.420

Now, consider the polarization + charge transfer (P+CT) term (Table 4). Overall, the MUEs for the EFP/ISA, EFP/DMA0-small-atoms and EFP/DMA0-small methods are all less than 1 kcal/mol, and the MUE for the EFP/DMA0 method is only slightly larger than 1 kcal/mol. For the hydrogen-bonded complexes, all the methods except EFP/DMA0-small and EFP/DMA0-small-atoms generally overestimate the P+CT interaction energy. This could be due to an underestimation of the charge penetration energy. Since the polarization term uses the static electric field generated by the multipole moments, and since the multipole moment expansion is not accurate at short distances, the error might be due to the multipole moment expansion not properly describing short-range interactions. While the EFP Coulomb term includes a charge penetration term to offset this problem, the EFP polarization term includes a multiplicative damping term, and the EFP charge transfer term does not include any damping. It is possible that the polarization damping term does not account for all of the effects of charge penetration and that the lack of CT damping results in an

underestimation of the energy. Almost all methods have large errors for the formic acid dimer, with EFP/DMA4 having the largest error. This might be due to the multipole expansion produced by DMA4 being truncated too soon. The potential could easily be improved by including higher-rank multipoles.

For the dispersion-dominated dimers, all methods are in good agreement with the SAPT induction term for the complexes without ring systems, with the error being less than 0.5 kcal/mol for all methods. The errors are larger for the ring-systems.

All methods agree very well with the SAPT induction energy for the mixed complexes. The errors are generally small, less than 1.2 kcal/mol for all methods and complexes.

Overall, all methods have relatively small errors when compared to the SAPT induction term, with the MUEs less than 1.7 kcal/mol for all methods. As in the previous section, there are several interesting comparisons to make. For example, the EFP/DMA0-small method gives consistently better results than EFP/DMA0, which might be due to a basis set effect, as mentioned above, or due to the multipole moment expansion for EFP/DMA0 being truncated too soon. The EFP/ISA method has consistent small overestimations, unlike any of the other methods.

Table 5: MUE for the total EFP energies (kcal/mol)

	EFP/ISA	EFP/DMA-mixed	EFP/DMA0-small-atoms	EFP/DMA0	EFP/DMA4	EFP/DMA0-small
MUE(HB)	1.939	3.773	2.105	0.612	6.215	1.315
MUE(DISP)	2.109	1.619	1.852	2.069	1.504	2.022
MUE(MIXED)	1.272	1.308	0.399	0.825	0.998	0.535
MUE(overall)	1.788	2.205	1.470	1.210	2.842	1.324

As described in Ref. [28], the exchange-repulsion term is generally underestimated, partially cancelling out the overestimation of the Coulomb and polarization term. The dispersion interaction energy is generally similar to the SAPT dispersion energy. The EFP/DMA4 method has the largest errors, mostly due to overestimating the interaction energy in the Coulomb and induction terms in the hydrogen-bonded dimers. The EFP/DMA0 method has the lowest overall MUE, partially due to error cancelation. Most methods have the largest errors in the hydrogen-bonded and dispersion-dominated complexes, suggesting problems with the electrostatic potential, either in the charge penetration term or in the multipole moment expansion.

5. Conclusion

An important strength of the EFP method is that, because there are no empirically fitted parameters, the method can systematically be improved. As demonstrated in this work, it is straightforward to use a different set of multipole moments in the calculation, and still get accurate and reasonable results. As long as a set of multipole moments is

provided that describes the electrostatic potential of a molecule reasonably well, the EFP method will provide reasonable results.

Of the methods considered here, the EFP/ISA and EFP/DMA0-small methods have the lowest overall error compared to the CCSD(T)/CBS results. The MUE for the S22 complexes is 0.78 and 0.72 kcal/mol for EFP/ISA and EFP/DMA0-small, respectively. The MUEs are similar to the MUEs for MP2 and SCS-MP2 when compared to CCSD(T)/CBS (0.88 and 0.8 kcal/mol, respectively). A similar study of the EFP/DMA0-small accuracy in which the charge transfer term was not included had a MUE of 0.9 kcal/mol, so including charge transfer increased the accuracy. [28]

Using a larger basis set to calculate the multipole moments with the DMA0 or DMA4 method results in a higher MUE than the DMA0-small method, but overall provides reasonable results, with MUEs of 0.808, 1.454, and 1.214 kcal/mol compared to the CCSD(T)/CBS results for the EFP/DMA0, EFP/DMA4, and EFP/DMA-mixed methods, respectively. In the case of the EFP/DMA0 method, the induced dipole procedure did not converge during the course of the indole-benzene stack geometry optimization. This is thought to be because the DMA0 multipole moment expansion is truncated too soon for indole or benzene with the basis set used. This is easy to remedy by including a higher multipole moment rank in the multipole moment expansion.

Computing the multipole moments using the smaller basis set and expansion points only on atom centers (EFP/DMA0-small-atoms) results in a similar MUE to using bond midpoints and atom centers as expansion points, but in two cases results in the induced dipole procedure not converging during the geometry optimization. Fewer expansion points leads can lead to divergence of the multipole moment expansion at short

ranges. Although the EFP/ISA method also only uses atom centers as expansion points, it does not have induced dipole procedure divergence. Thus, the convergence of the multipole moments in the ISA procedure seems to be more robust than in DMA, as noted in Ref. [8].

Overall, EFP/ISA method is a promising method. As noted in Ref. [8], the ISA multipole moments tend to systematically converge the multipole moment expansion at a lower term than DMA methods, which is likely why the EFP/ISA method has low errors, and consistently slightly overestimates the SAPT components. The main downside to using ISA multipole moments is that the procedure to generate them is much more computationally expensive than the procedure used to generate the DMA multipole moments.

Analyzing the energy components at the S22 geometry shows that many of the methods predict that the energies are too repulsive. Thus, it is clear that the short-range penetration effects (charge penetration term, the electric field damping) might be underestimated in the EFP method. Additionally, for certain molecules, the multipole moment expansion generated with DMA0 or DMA4 for the larger basis sets does not seem to be converged for the level of truncation used. Additional multipole moments can be straightforwardly included in the multipole moment expansion.

Acknowledgements. This work was supported by the U.S. Department of Energy, Office of Basic Energy Sciences, Division of Chemical Sciences, Geosciences, and Biosciences, through the Ames Laboratory Chemical Physics program. The Ames Laboratory is operated for the U.S. Department of Energy by Iowa State University under Contract No. DE-AC02-07CH11358.

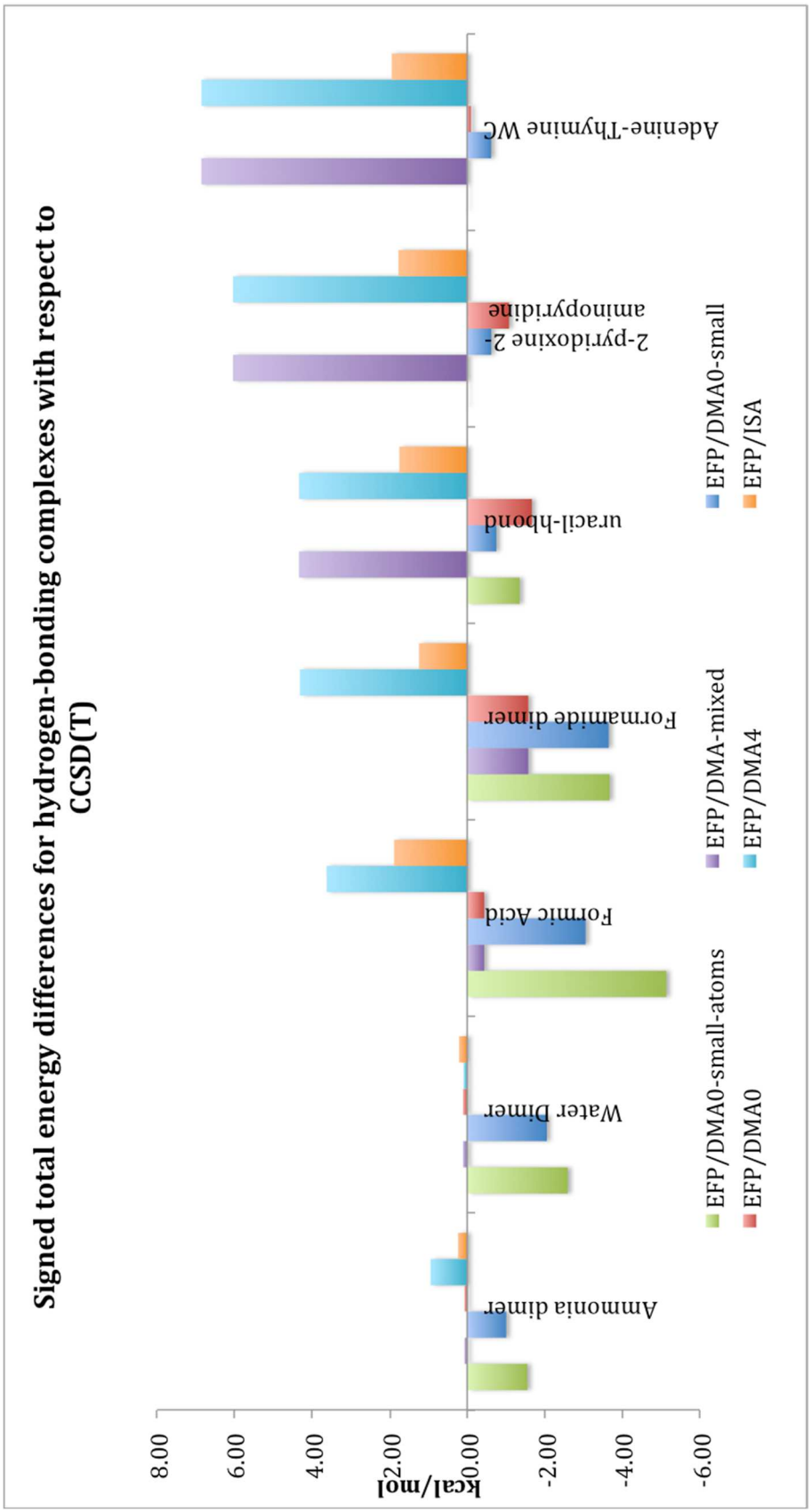

Figure 2: Comparison of the total energy differences for the hydrogen bonding complexes at the optimized geometry

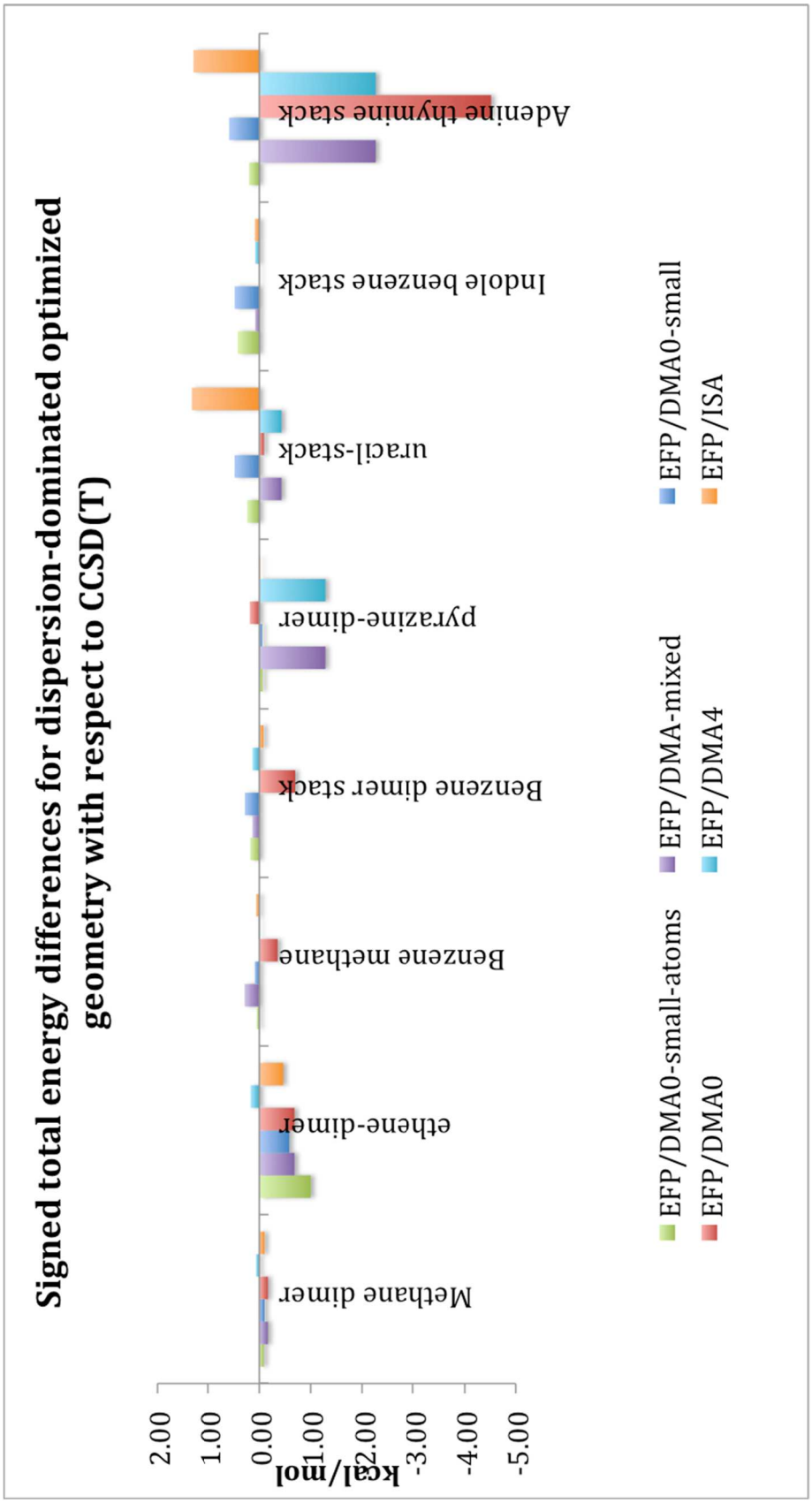

Figure 3: Comparison of the total energy differences for the dispersion-dominated complexes at the optimized geometry

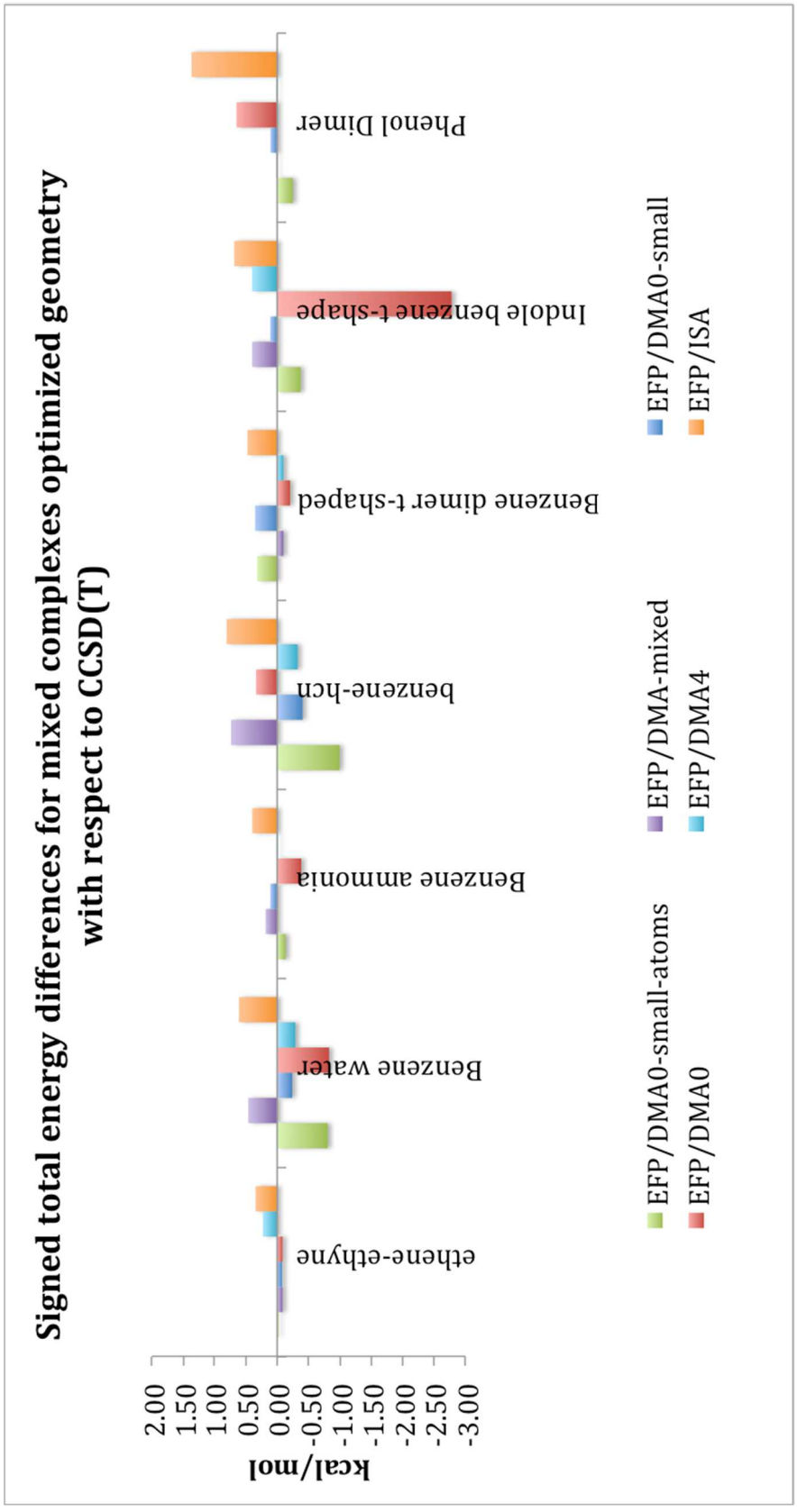

Figure 4: Comparison of the total energy differences for the mixed complexes at the optimized geometry

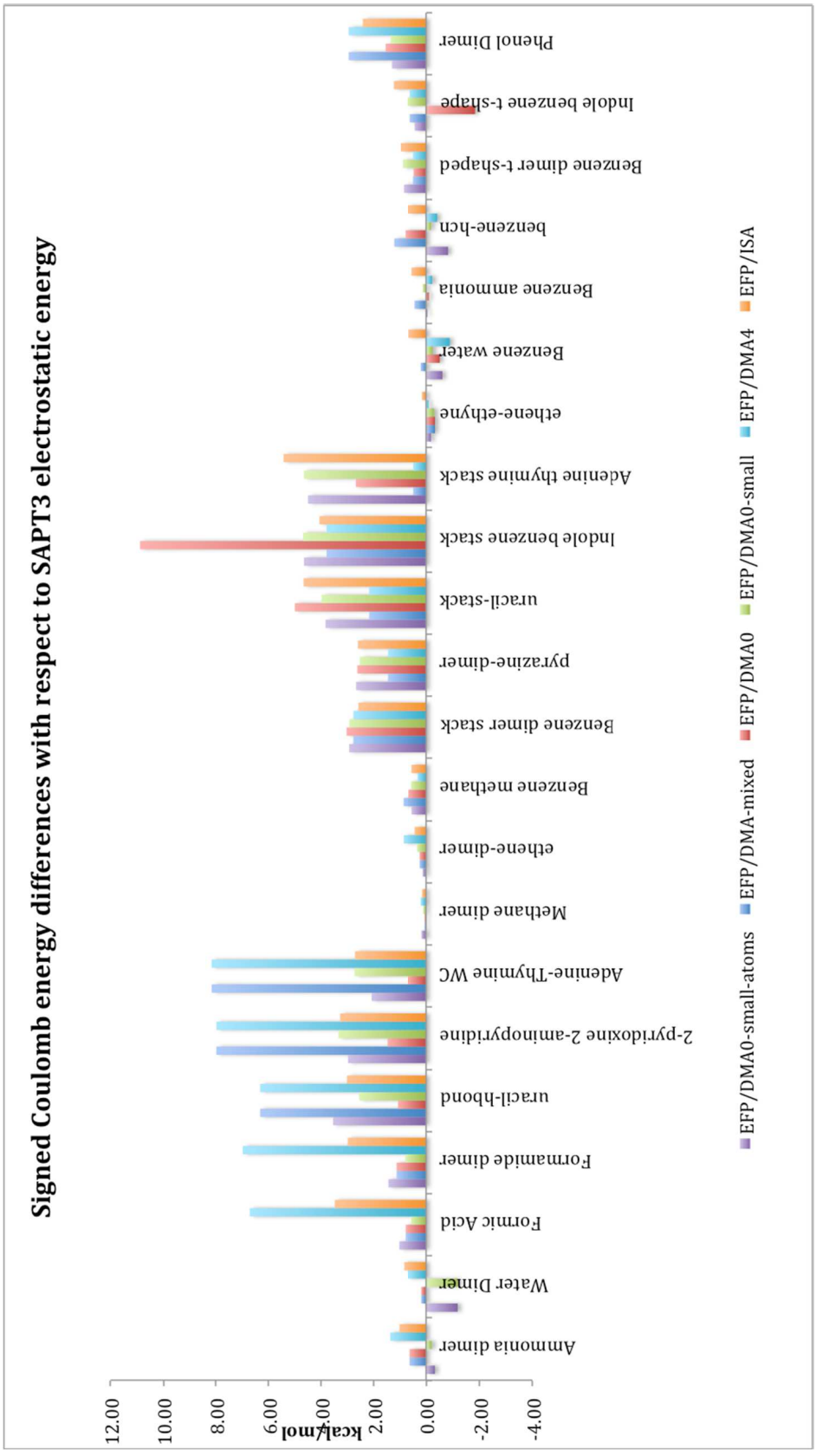

Figure 5: Comparison of the Coulomb energy differences for the S22 geometries

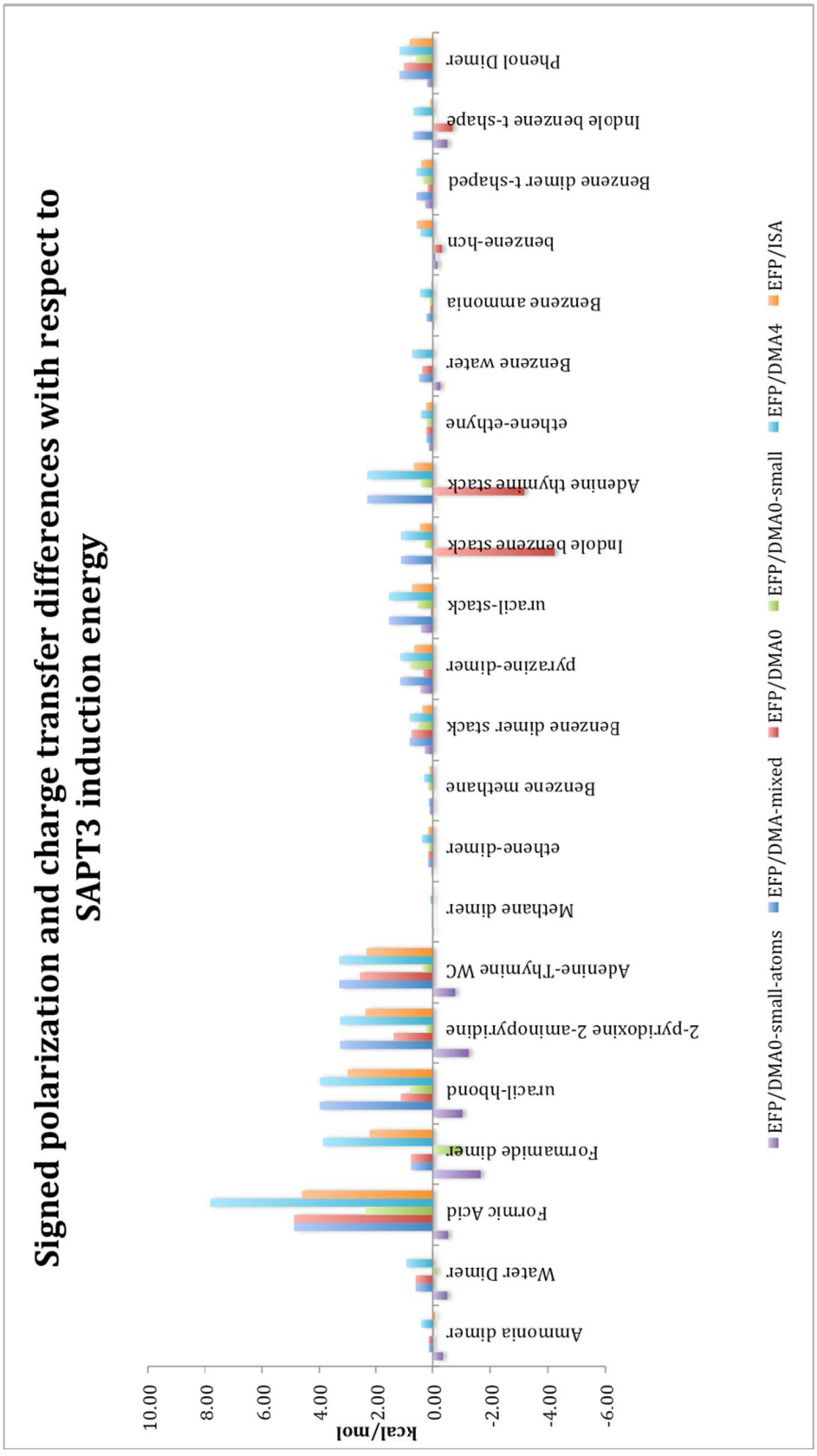

Figure 6: Comparison of the polarization and charge transfer energy differences for the S22 geometries

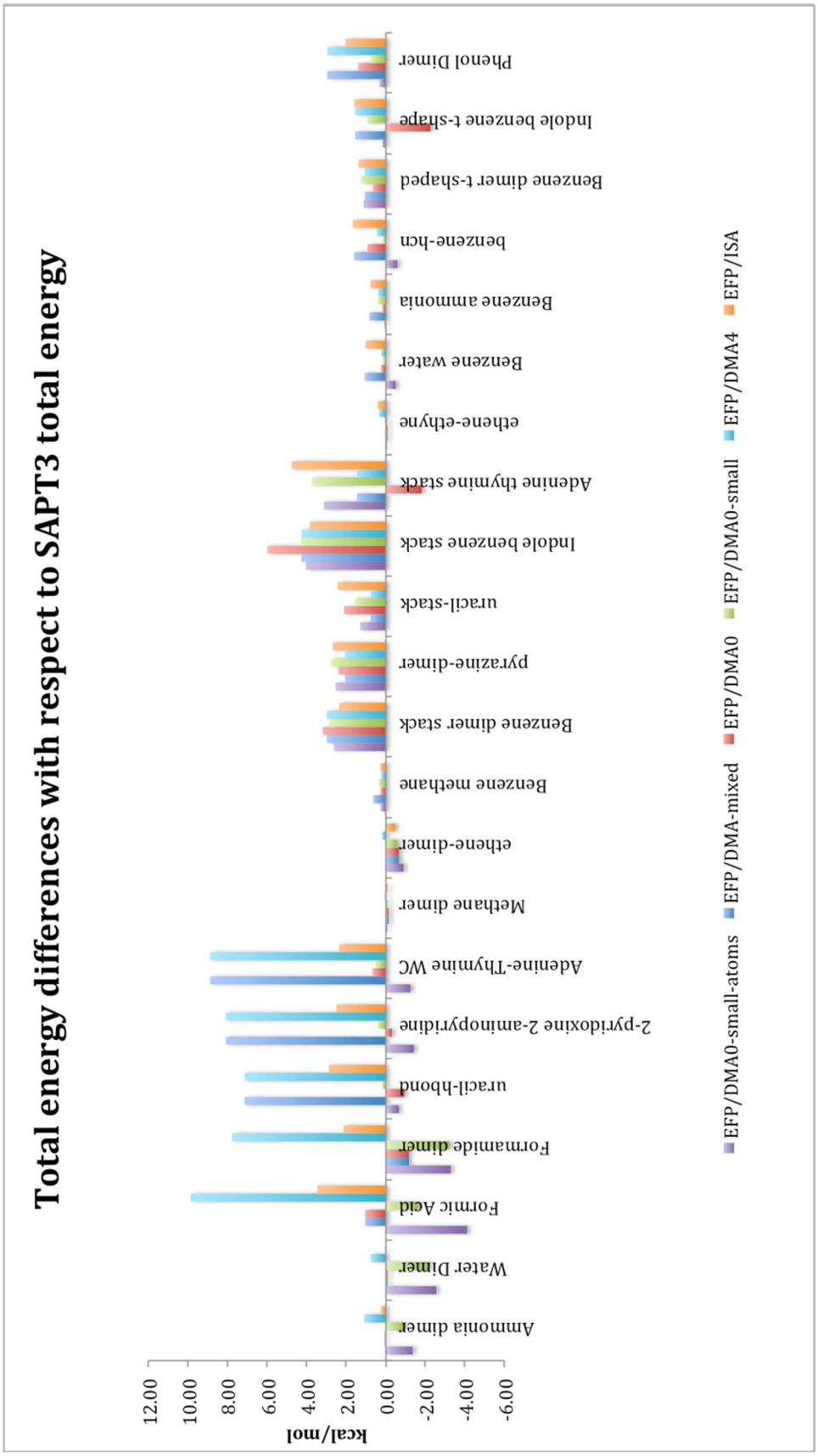

Figure 7: Comparison of the total energy differences for the S22 geometries

Supporting Information

Supporting Information Section 1: Distance information for optimized S22 geometries

As mentioned in the main text, some geometries differed from the S22 geometry by a small rotation. The minimum energy geometry found for the benzene-methane dimer using EFP/DMA0 has the three C-H bonds on the methane pointing at the center of the benzene ring ("tridentate" geometry), which is qualitatively different from the S22 geometry, which only has one C-H bond pointing at the center of the benzene ring ("monodentate").[32] The difference between tridentate and monodentate is a rotation of the methane. The minimum energy geometry for benzene-ammonia using EFP/DMA-mixed has two hydrogen atoms on the ammonia pointing at the center of the benzene ring, which is also different than the monodentate *ab initio* S22 geometry. The difference in the CCSD(T) energy at the basis set limit between the monodentate and bidentate geometries is 0.15 kcal/mol, which is very small.[33]

Table S1: Distances in *ab initio* and EFP-optimized S22 geometries, Å

	distance	**ab initio**	**EFP/ISA**	**EFP/DMA0-small**	**EFP/DMA0-small-atoms**	**EFP/DMA0**	**EFP/DMA4**	**EFP/DMA-mixed**
Hydrogen-Bonded Complexes								
ammonia dimer	N1···N5	3.16	3.14	3.06	2.99	3.16	3.32	3.16
water dimer	O1···O4	2.91	2.91	2.84	2.79	2.96	2.95	2.96

Table S1 continued

formic acid dimer	O2···O8	2.67	2.78	2.72	2.63	2.76	2.87	2.76
formamide dimer	O2···N9	2.86	2.96	2.83	2.83	2.9	3.06	2.9
uracil H-bonded dimer	N1···O23	2.8	2.88	2.84	2.81	2.82	2.98	2.98
2-pyridoxine 2-aminopyridine	N1···N15	2.9	2.94	2.72	--	2.84	3.12	3.12
adenine–thymine WC	N1···N20	2.86	2.86	2.68	--	2.8	3.09	3.09
Dispersion-Dominated Complexes								
methane dimer	C1···C6	3.72	3.6	3.64	3.6	3.6	3.76	3.6
ethene dimer	C1···C7	3.84	3.77	3.75	3.68	3.74	3.94	3.74
benzene–methane	C1···RD	3.72	3.93	3.95	3.93	3.61	3.93	4
benzene stack	R1/R2	3.36/1.7	3.79/1,28	3.8/1,4	3.77/1.55	3.8/1.81	3.84/1.11	3.84/1.11
pyrazine dimer	R1/R2	3.3/1.22	3.58/1.11	3.6/0.99	3.57/1.1	3.65/0.9	3.63/0.18	3.63/0.18
uracil stack	R1/R2	3.12/0.54	3.3/0.52	3.26/0.52	3.25/0.53	3.18/1.46	3.31/0.57	3.31/0.57
indole–benzene stack	R1/R2	3.26/1.27	3.64/1.27	3.61/1.55	3.59/1.53	--	3.7/0.91	3.7/0.91
adenine–thymine stack	R1/R2	3.15/0.34	3.39/0.14	3.37/0.27	3.35/0.34	3.17/0.52	3.37/0.12	3.37/0.12
Mixed Complexes								
ethene–ethyne	C8···C2	3.88	4.04	3.95	3.96	3.94	4.07	3.94
benzene–water	O1···RD	3.41	3.51	3.48	3.37	3.39	3.57	3.6
benzene–ammonia	N···RD	3.57	3.72	3.74	3.68	3.55	3.73	3.58
benzene–HCN	C14···RD	3.39	3.63	3.54	3.48	3.56	3.6	3.64

Table S1 continued

benzene dimer T-shaped	C1⋯ RD	3.51	3.81	3.81	3.81	3.76	3.81	3.81
indole–benzene T-shaped	N21⋯RD	3.24	3.47	3.45	3.39	3.19	3.5	3.5
phenol dimer	O7⋯O20	2.89	2.96	2.92	2.88	2.96	2.89	2.89

Supporting Information Section 2: Interaction energies for optimized geometries and S22 geometries

Table S2: Comparison of CCSD(T) energies and EFP energies for optimized geometries (kcal/mol)

	CCSD(T)	EFP/ISA	EFP/DMA0-small	EFP/DMA0-small-atom	EFP/DMA0	EFP/DMA4	EFP/DMA-mixed
Ammonia dimer	-3.15	-2.91	-4.15	-4.69	-3.08	-2.21	-3.08
Water Dimer	-5.07	-4.86	-7.11	-7.65	-4.96	-4.98	-4.96
Formic Acid	-18.81	-16.91	-21.85	-23.94	-19.24	-15.18	-19.24
Formamide dimer	-16.11	-14.87	-19.76	-19.78	-17.68	-11.80	-17.68
uracil-hbond	-20.69	-18.93	-21.44	-22.03	-22.35	-16.36	-16.36
2-pyridoxine 2-aminopyridine	-17	-15.21	-17.62	-	-18.07	-10.97	-10.97
Adenine-Thymine WC	-16.74	-14.78	-17.35	-	-16.83	-9.88	-9.88
Methane dimer	-0.53	-0.63	-0.63	-0.62	-0.70	-0.47	-0.70
ethene-dimer	-1.48	-1.94	-2.06	-2.48	-2.16	-1.31	-2.16
Benzene methane	-1.45	-1.39	-1.36	-1.40	-1.81	-1.43	-1.16
Benzene dimer stack	-2.62	-2.70	-2.34	-2.44	-3.32	-2.49	-2.49
pyrazine-dimer	-4.2	-4.21	-4.25	-4.26	-4.01	-5.48	-5.48

Table S2 continued

uracil-stack	-9.74	-8.41	-9.26	-9.51	-9.83	-10.17	-10.17
Indole benzene stack	-4.59	-4.50	-4.11	-4.17	-	-4.51	-4.51
Adenine thymine stack	-11.66	-10.37	-11.07	-11.46	-16.18	-13.92	-13.92
ethene-ethyne	-1.5	-1.16	-1.58	-1.52	-1.59	-1.27	-1.59
Benzene water	-3.29	-2.68	-3.53	-4.09	-4.12	-3.58	-2.83
Benzene ammonia	-2.32	-1.92	-2.21	-2.45	-2.70	-2.33	-2.14
benzene-hcn	-4.55	-3.75	-4.95	-5.54	-4.21	-4.88	-3.82
Benzene dimer t-shaped	-2.71	-2.24	-2.36	-2.39	-2.92	-2.81	-2.81
Indole benzene t-shape	-5.62	-4.94	-5.51	-5.99	-8.40	-5.22	-5.22
Phenol Dimer	-7.09	-5.72	-6.98	-7.34	-6.44	-7.07	-7.07

Table S3: Comparison of SAPT and EFP Coulomb energy (kcal/mol)

	SAPT	EFP/ISA	EFP/DMA0-small	EFP/DMA0-small-atom	EFP/DMA0	EFP/DMA4	EFP/DMA-mixed
Ammonia dimer	-4.89	-3.85	-5.10	-5.22	-4.27	-3.50	-4.27
Water Dimer	-8.1	-7.24	-9.29	-9.29	-7.91	-7.40	-7.91
Formic Acid	-32.22	-28.73	-31.66	-31.18	-31.42	-25.52	-31.42
Formamide dimer	-25.36	-22.37	-24.55	-23.90	-24.21	-18.39	-24.21
uracil-hbond	-29.79	-26.76	-27.23	-26.24	-28.70	-23.48	-23.48
2-pyridoxine 2-aminopyridine	-26.91	-23.63	-23.57	-23.93	-25.42	-18.94	-18.94

Table S3 continued

Adenine-Thymine WC	-26.58	-23.86	-23.84	-24.49	-25.88	-18.44	-18.44
Methane dimer	-0.15	0.00	-0.04	0.03	-0.10	0.05	-0.10
ethene-dimer	-1.13	-0.70	-0.79	-1.00	-0.89	-0.25	-0.89
Benzene methane	-0.96	-0.41	-0.39	-0.41	-0.29	-0.64	-0.08
Benzene dimer stack	-2.54	0.05	0.39	0.40	0.50	0.24	0.24
pyrazine-dimer	-4.27	-1.66	-1.73	-1.59	-1.64	-2.80	-2.80
uracil-stack	-8.52	-3.86	-4.54	-4.68	-3.52	-6.34	-6.34
Indole benzene stack	-4.31	-0.25	0.37	0.34	6.58	-0.51	-0.51
Adenine thymine stack	-10.66	-5.24	-6.01	-6.16	-7.97	-10.17	-10.17
ethene-ethyne	-1.77	-1.61	-2.08	-1.95	-2.10	-1.87	-2.10
Benzene water	-2.71	-2.04	-2.96	-3.32	-3.23	-3.60	-2.51
Benzene ammonia	-1.74	-1.19	-1.61	-1.80	-1.84	-1.97	-1.30
benzene-hcn	-3.84	-3.15	-4.03	-4.67	-3.03	-4.26	-2.60
Benzene dimer t-shaped	-2	-1.01	-1.09	-1.13	-1.53	-1.50	-1.50
Indole benzene t-shape	-4.25	-3.00	-3.52	-3.82	-6.10	-3.63	-3.63
Phenol Dimer	-8.57	-6.15	-7.21	-7.25	-7.01	-5.61	-5.61

Table S4: Comparison of SAPT induction energy and the sum of EFP polarization and charge transfer energy (kcal/mol)

	SAPT	EFP/ISA	EFP/DMA0-small	EFP/DMA0-small-atom	EFP/DMA0	EFP/DMA4	EFP/DMA-mixed
Ammonia dimer	-0.91	-0.99	-0.95	-1.26	-0.77	-0.50	-0.77
Water Dimer	-2.45	-2.41	-2.58	-2.95	-1.85	-1.49	-1.85
Formic Acid	-18.94	-14.34	-16.56	-19.47	-14.07	-11.14	-14.07
Formamide dimer	-11.26	-9.03	-12.23	-12.93	-10.50	-7.40	-10.50
uracil-hbond	-14.01	-11.01	-13.21	-15.04	-12.86	-10.04	-10.04
2-pyridoxine 2-aminopyridine	-12.65	-10.26	-12.41	-13.90	-11.25	-9.39	-9.39
Adenine-Thymine WC	-11.88	-9.54	-11.50	-12.66	-9.31	-8.58	-8.58
Methane dimer	-0.03	-0.04	0.00	-0.05	0.00	0.06	0.00
ethene-dimer	-0.23	-0.07	-0.07	-0.18	-0.06	0.16	-0.06
Benzene methane	-0.31	-0.19	-0.14	-0.20	-0.32	0.00	-0.17
Benzene dimer stack	-0.93	-0.56	-0.42	-0.64	-0.18	-0.12	-0.12
pyrazine-dimer	-1.02	-0.37	-0.23	-0.59	-0.69	0.15	0.15
uracil-stack	-1.75	-1.02	-1.20	-1.33	-1.67	-0.19	-0.19
Indole benzene stack	-1.48	-1.02	-1.18	-1.41	-5.71	-0.34	-0.34
Adenine thymine stack	-2.49	-1.82	-2.06	-2.52	-5.67	-0.17	-0.17
ethene-ethyne	-0.57	-0.33	-0.36	-0.42	-0.34	-0.15	-0.34
Benzene water	-1.00	-1.03	-0.99	-1.26	-0.62	-0.27	-0.52

Table S4 continued

Benzene ammonia	-0.53	-0.47	-0.42	-0.57	-0.42	-0.08	-0.31
benzene-hcn	-1.91	-1.35	-1.98	-2.07	-2.23	-1.47	-1.99
Benzene dimer t-shaped	-0.70	-0.30	-0.36	-0.43	-0.52	-0.13	-0.13
Indole benzene t-shape	-1.95	-1.85	-1.99	-2.45	-2.64	-1.27	-1.27
Phenol Dimer	-3.22	-2.41	-2.63	-3.01	-2.19	-2.03	-2.03

Table S5: Comparison of SAPT and EFP total interaction energy (kcal/mol)

	SAPT	EFP/ISA	EFP/DMA0-small	EFP/DMA0-small-atom	EFP/DMA0	EFP/DMA4	EFP/DMA-mixed
Ammonia dimer	-3.06	-2.81	-4.01	-4.44	-2.99	-1.97	-2.99
Water Dimer	-4.81	-4.80	-7.01	-7.38	-4.90	-4.03	-4.90
Formic Acid	-19.67	-16.21	-21.35	-23.78	-18.62	-9.79	-18.62
Formamide dimer	-16.44	-14.30	-19.68	-19.74	-17.62	-8.70	-17.62
uracil-hbond	-21.38	-18.51	-21.19	-22.03	-22.30	-14.26	-14.26
2-pyridoxine 2-aminopyridine	-17.34	-14.85	-16.93	-18.79	-17.64	-9.29	-9.29
Adenine-Thymine WC	-17.21	-14.85	-16.68	-18.48	-16.53	-8.36	-8.36
Methane dimer	-0.53	-0.62	-0.62	-0.60	-0.68	-0.46	-0.68
ethene-dimer	-1.46	-1.92	-2.02	-2.34	-2.11	-1.26	-2.11
Benzene methane	-1.46	-1.18	-1.11	-1.19	-1.19	-1.22	-0.83
Benzene dimer stack	-2.67	-0.31	0.17	-0.05	0.51	0.31	0.31
pyrazine-dimer	-4.47	-1.79	-1.71	-1.93	-2.08	-2.41	-2.41

Table S5 continued

uracil-stack	-10.72	-8.29	-9.15	-9.43	-8.61	-9.94	-9.94
Indole benzene stack	-4.83	-1.00	-0.54	-0.80	1.13	-0.58	-0.58
Adenine thymine stack	-13.12	-8.38	-9.39	-10.00	-14.96	-11.66	-11.66
ethene-ethyne	-1.48	-1.07	-1.56	-1.50	-1.57	-1.14	-1.57
Benzene water	-3.30	-2.27	-3.15	-3.79	-3.05	-3.08	-2.24
Benzene ammonia	-2.33	-1.55	-1.91	-2.25	-2.16	-1.94	-1.50
benzene-hcn	-4.86	-3.19	-4.69	-5.43	-3.92	-4.40	-3.26
Benzene dimer t-shaped	-2.90	-1.52	-1.66	-1.77	-2.25	-1.84	-1.84
Indole benzene t-shape	-5.79	-4.19	-4.85	-5.61	-8.07	-4.24	-4.24
Phenol Dimer	-7.20	-5.16	-6.44	-6.87	-5.80	-4.25	-4.25

References

1. Mulliken, R. S., Electronic Population Analysis on LCAO–MO Molecular Wave Functions. I. *The Journal of Chemical Physics* **1955,** *23* (10), 1833-1840.

2. Stone, A. J., *The Theory of Intermolecular Forces*. Oxford University Press: New York, 1997.

3. Bader, R. F. W., Atoms in Molecules. Clarendon Press: Oxford, 1990.

4. Hirshfeld, F. L., Bonded-atom fragments for describing molecular charge densities. *Theoretica chimica acta* **1977,** *44* (2), 129-138.

5. Bultinck, P.; Van Alsenoy, C.; Ayers, P. W.; Carbó-Dorca, R., Critical analysis and extension of the Hirshfeld atoms in molecules. *The Journal of Chemical Physics* **2007,** *126* (14), 144111.

6. Popelier, P. L., Atoms in Molecules: An Introduction. Prentice Hall: Harlow, 2000.

7. Lillestolen, T. C.; Wheatley, R. J., Redefining the atom: atomic charge densities produced by an iterative stockholder approach. *Chemical Communications* **2008,** (45), 5909-5911.

8. Misquitta, A. J.; Stone, A. J.; Fazeli, F., Distributed Multipoles from a Robust Basis-Space Implementation of the Iterated Stockholder Atoms Procedure. *Journal of Chemical Theory and Computation* **2014,** *10* (12), 5405-5418.

9. Day, P. N.; Jensen, J. H.; Gordon, M. S.; Webb, S. P.; Stevens, W. J.; Krauss, M.; Garmer, D.; Basch, H.; Cohen, D., An effective fragment method for modeling solvent effects in quantum mechanical calculations. *The Journal of Chemical Physics* **1996,** *105* (5), 1968-1986.

10. Gordon, M. S.; Smith, Q. A.; Xu, P.; Slipchenko, L. V., Accurate First Principles Model Potentials for Intermolecular Interactions. *Annual Review of Physical Chemistry* **2013,** *64* (1), 553-578.

11. Stone, A. J., Distributed Multipole Analysis: Stability for Large Basis Sets. *Journal of Chemical Theory and Computation* **2005,** *1* (6), 1128-1132.

12. Xu, P.; Gordon, M. S., Charge transfer interaction using quasiatomic minimal-basis orbitals in the effective fragment potential method. *The Journal of Chemical Physics* **2013,** *139* (19), 194104.

13. Li, H.; Gordon, M. S.; Jensen, J. H., Charge transfer interaction in the effective fragment potential method. *The Journal of Chemical Physics* **2006,** *124* (21), 214108.

14. Slipchenko†, L. V.; Gordon, M. S., Damping functions in the effective fragment potential method. *Molecular Physics* **2009,** *107* (8-12), 999-1016.

15. Tang, K. T.; Toennies, J. P., An improved simple model for the van der Waals potential based on universal damping functions for the dispersion coefficients. *The Journal of Chemical Physics* **1984,** *80* (8), 3726-3741.

16. Jensen, J. H., Intermolecular exchange-induction and charge transfer: Derivation of approximate formulas using nonorthogonal localized molecular orbitals. *The Journal of Chemical Physics* **2001,** *114* (20), 8775-8783.

17. Stone, A. J.; Misquitta, A. J., Charge-transfer in Symmetry-Adapted Perturbation Theory. *Chemical Physics Letters* **2009,** *473* (1–3), 201-205.

18. Gordon, M. S., *Fragmentation: Toward Accurate Calculations on Complex Molecular*

Systems. John Wiley and Sons: In Press.

19. Slipchenko, L. V.; Gordon, M. S., Electrostatic energy in the effective fragment potential method: Theory and application to benzene dimer. *Journal of Computational Chemistry* **2007,** *28* (1), 276-291.

20. Schmidt, M. W.; Baldridge, K. K.; Boatz, J. A.; Elbert, S. T.; Gordon, M. S.; Jensen, J. H.; Koseki, S.; Matsunaga, N.; Nguyen, K. A.; Su, S.; Windus, T. L.; Dupuis, M.; Montgomery, J. A., General atomic and molecular electronic structure system. *Journal of Computational Chemistry* **1993,** *14* (11), 1347-1363.

21. Gordon , M. S.; Schmidt , M. W., Advances in Electronic Structure Theory: GAMESS a Decade Later . In *Theory and Applications of Computational Chemistry: The First Forty Years*, Elsevier B.V.: Amsterdam, The Netherlands, 2005; pp 1167 – 1189.

22. Boys, S. F., Construction of Some Molecular Orbitals to Be Approximately Invariant for Changes from One Molecule to Another. *Reviews of Modern Physics* **1960,** *32* (2), 296-299.

23. Edmiston, C.; Ruedenberg, K., Localized Atomic and Molecular Orbitals. *Reviews of Modern Physics* **1963,** *35* (3), 457-464.

24. Misquitta, A. J.; Stone, A. J. *CamCASP: a program for studying intermolecular interactions and for the calculation of molecular properties in distributed form*, http://www-stone.ch.cam.ac.uk/programs.html - CamCASP.

25. Dunning, T. H., Gaussian basis sets for use in correlated molecular calculations. I. The atoms boron through neon and hydrogen. *Journal of Chemical Physics* **1989,** *90* (2), 1007.

26. Kendall, R. A.; Dunning, T. H.; Harrison, R. J., Electron affinities of the first-row atoms revisited. Systematic basis sets and wave functions. *The Journal of Chemical Physics* **1992,** *96* (9), 6796-6806.

27. Valiev, M.; Bylaska, E. J.; Govind, N.; Kowalski, K.; Straatsma, T. P.; Van Dam, H. J. J.; Wang, D.; Nieplocha, J.; Apra, E.; Windus, T. L.; de Jong, W. A., NWChem: A comprehensive and scalable open-source solution for large scale molecular simulations. *Computer Physics Communications* **2010,** *181* (9), 1477-1489.

28. Flick, J. C.; Kosenkov, D.; Hohenstein, E. G.; Sherrill, C. D.; Slipchenko, L. V., Accurate Prediction of Noncovalent Interaction Energies with the Effective Fragment Potential Method: Comparison of Energy Components to Symmetry-Adapted Perturbation Theory for the S22 Test Set. *Journal of Chemical Theory and Computation* **2012,** *8* (8), 2835-2843.

29. Jeziorski, B.; Moszynski, R.; Szalewicz, K., Perturbation Theory Approach to Intermolecular Potential Energy Surfaces of van der Waals Complexes. *Chemical Reviews* **1994,** *94* (7), 1887-1930.

30. Hohenstein, E. G.; Sherrill, C. D., Wavefunction methods for noncovalent interactions. *Wiley Interdisciplinary Reviews: Computational Molecular Science* **2012,** *2* (2), 304-326.

31. Takatani, T.; Hohenstein, E. G.; Malagoli, M.; Marshall, M. S.; Sherrill, C. D., Basis set consistent revision of the S22 test set of noncovalent interaction energies. *The Journal of Chemical Physics* **2010,** *132* (14), 144104.

32. Tsuzuki, S.; Honda, K.; Uchimaru, T.; Mikami, M.; Tanabe, K., The Magnitude of the CH/π Interaction between Benzene and Some Model Hydrocarbons. *Journal of the American Chemical Society* **2000,** *122* (15), 3746-3753.

33. Tsuzuki, S.; Honda, K.; Uchimaru, T.; Mikami, M.; Tanabe, K., Origin of the Attraction and Directionality of the NH/π Interaction: Comparison with OH/π and CH/π Interactions. *Journal of the American Chemical Society* **2000,** *122* (46), 11450-11458.

CHAPTER 4. THE MELTING TEMPERATURE OF WATER WITH THE EFFECTIVE FRAGMENT MOLECULAR ORBITAL METHOD

1. Introduction

Water is one of the most common solvents, both in nature and in experimental chemistry. Understanding water-water and water-solute interactions is vital to understanding the role water plays in chemical reactions. Because of this, water has been studied extensively theoretically, and much effort has been put into developing accurate and computationally efficient force fields for water. Since much of chemistry happens in water or a solvent, it is important to be able to model the solvents accurately in simulations.

An important benchmark of a force field is how well it predicts the phase diagram of water. For example, knowing the predicted melting temperature of ice enables one to run simulations using the proper phase of water. Many methods have been used to calculate the melting temperature of ice-I_h as a benchmark and to be sure that simulations are run in the right phase. Density functional theory (DFT) tends to predict melting temperatures (T_m) for ice-I_h that are too high. DFT with the PBE functional predicts a melting temperature of 417 ± 3 K, DFT/BLYP predicts a melting temperature of 411 ± 4 K, and DFT-BLYP with dispersion corrections predicts a melting temperature of 360 ± 2 K. [1 2]. Many classical force fields underestimate the melting temperature. For instance, the melting temperatures predicted by TIP3P[3], SPC/E[4], TIP4P [3], and TIP4P-Ew [5] are 145.6 K, 215.0 K, 245.5 K, respectively.[6] Other classical force fields predict a very accurate melting temperature, often because the method is explicitly parameterized to do so. The TIP4P/Ice method [7] predicts a melting temperature of 272.2 K.

There has been much effort to increase the accuracy of force fields by using parameters and functional forms generated from *ab initio* calculations. For instance, the TTM3-F [8], iAMEOBA [9], and Sum of Interactions Between Fragments Ab initio computed (SIBFA)[10] methods have been developed to include parameterization from *ab initio* calculations. The methods of interest in this study are the Effective Fragment Potential (EFP) and the Effective Fragment Molecular Orbital (EFMO) methods. The EFP method is a rigid-body model that is derived from first principles and employs no empirically fitted parameters. An EFP is generated from *ab initio* calculations. The EFP method provides interaction energies among fragments, based on five interaction energy terms: two-body Coulomb, dispersion, charge-transfer, and exchange-repulsion, and many-body polarization. The general expression for the EFP interaction energy can be written as follows:

$$E_{EFP} = \sum_{A<B}^{fragments} \left(E_{AB}^{\text{Coulomb}} + E_{AB}^{\text{dispersion}} + E_{AB}^{\text{charge-transfer}} + E_{AB}^{\text{exchange-repulsion}} \right) + E^{\text{polarization}} \tag{1}$$

The Coulomb term relies on multipole moments generated from the charge density of an *ab initio* calculation. The exchange-repulsion term relies on a set of localized molecular orbitals (LMOs), the Fock matrix, and the basis set used in the *ab initio* calculation. The charge transfer term relies on the Fock matrix, the basis set, and a set of canonical virtual orbitals or valence virtual orbitals (VVOs). The dispersion term relies on a set of dynamic polarizability tensors calculated from the time-dependent couple perturbed Hartree-Fock equation and distributed onto the centroids of the LMOs. The polarization term relies on a set of static polarizability tensors calculated from the coupled perturbed Hartree-Fock equations and distributed onto the centroids of the LMOs

and a set of multipole moments. More details can be found in Refs. 11 and 12. Importantly, an EFP can be generated easily and for any molecule since there are no fitted parameters.

The EFP method predicts the melting temperature of ice to be approximately 381 K.[13] Thus, the predicted temperature is about 100 K larger than the experimental value. There are at least two possible reasons why the melting temperature is too low. One is that the EFP method uses rigid fragments, and another is that it does not account for nuclear quantum effects.[14]

The EFMO method integrates the Fragment Molecular Orbital (FMO) [15] and EFP methods. The EFMO method can be thought of as an extension of the FMO method, in which fragment-fragment interactions are accounted for by the EFP method when the two fragments are sufficiently far apart. Therefore, the EFMO method allows for flexible EFP fragments.[16] [17] The flexible fragment EFMO energy can be written as

$$E^{EFMO} = \sum_{A}^{fragments} E_A^0 + \sum_{A>B}^{fragments} (E_{AB}^{\text{Coulomb}} + E_{AB}^{\text{dispersion}} + E_{AB}^{\text{charge-transfer}} + E_{AB}^{\text{exchange-repulsion}}) + E_{tot}^{\text{polarization}} \quad (2)$$

where E_A^0 is the gas phase *ab initio* energy of a fragment. Note that typically the EFMO energy equation contains a term in which close dimers are computed with an *ab initio* method. However, for the purpose of this paper, Eq. (2) can be used.

In the EFMO method, the parameters needed in the EFP method are re-generated on every time step, so that the method is fully flexible. The analytic gradient for the Coulomb, polarization, dispersion, and exchange-repulsion terms in EFMO has been derived and implemented. [18] The goal of the present study is to ascertain the effect of flexibility on the predicted melting temperature by comparing the melting temperatures

of ice-I_h predicted by the EFP and EFMO methods. Since the gradient for the EFMO charge transfer term has not been derived, the EFP and EFMO simulations are run without charge transfer.

Computer simulations can be used to calculate the predicted melting temperature of a material in multiple ways.[19] One commonly employed method uses Gibbs-Duhem integration and the fact that at the melting temperature, T_m, the Gibbs free energy of the solid and liquid are equal ($G_{liquid}(P,T)_{T=T_m} = G_{solid}(P,T)_{T=T_m}$). The procedure used in the present work is the method of direct coexistence. In the direct coexistence method, the liquid-solid interface is directly simulated by molecular dynamics (MD) calculations. That is, one uses a box in which half of the box is occupied by an equilibrated solid and half is occupied by an equilibrated liquid, and the total system is allowed to equilibrate. The direct coexistence method can be implemented in various ensembles, such as NVE, NVT, NPT, and NPH. Each type of ensemble has particular advantages and disadvantages. This study uses the NPH ensemble, since it has the advantage (with respect to NVT and NVE) that the volume of the box can change, allowing the solid and liquid halves of the system to relax, and that the temperature can spontaneously adjust until the Gibbs free energy of the liquid and solid phases are equal.

2. Computational Methods

All simulations were done using the GAMESS software package.[20 21] For the EFP calculations, the basis set used to generate the potential was 6-31++G(d,p). Since the gradient for the EFMO method does not contain terms needed for the use of bond midpoints in the EFP Coulomb term, only atom centers are used in generating the

multipole moments for the EFP potential. The gradient for the EFMO method also only contains terms in the multipole moment expansion through quadrupole-quadrupole. As mentioned above, charge transfer was not included. Thus, the EFP used here differs from the standard EFP used in Ref. [13], and will be referred to here as EFP-small-noct. Likewise, the EFMO used here will be referred to as EFMO-small-noct. Unless otherwise noted, all simulations in this study used a 0.35 fs time step and the Velocity-Verlet algorithm.

Since the phase diagram of EFP-noct and EFMO-noct is not known, first an appropriate pressure is calculated by performing NVT MD simulations with 192 water molecules at T=250 K and a density of 1 g/ml. A 4 ps NVT simulation was performed, where the average pressure of the last 2 ps was ~3167 bar for the EFP-small-noct method and ~5149 bar for the EFMO-small-noct method. Thus, the use of 4000 bar and 6000 bar should be reasonable choices for calculating the melting temperature for the EFP-small-noct and EFMO-small-noct, respectively. The pressure value is chosen so that it is at a higher value than the pressure at the triple point, with the rough assumption that the temperature at the triple point is near 250 K. As long as an ice-liquid coexistence is stable at the pressure, the melting temperature can be computed.

For reference, the pressure used for calculating the melting temperature with DFT-BLYP and DFT-PBE was 9869.23 bar and 2467.31 bar, respectively.[1] In Ref. 13, a pressure of 1.01 bar was used.

To perform the direct coexistence simulation, a box was prepared with 192 waters, 96 in the liquid state and 96 in the solid state. The 96 liquid state water molecules were prepared by equilibrating 96 waters in a 13.52 × 15.61 × 14.72 Å box using an NVT

simulation for 100 ps. The 96 solid state waters were prepared according to Bernal–Fowler rules.[22] The system is prepared to match the previous EFP study that determined the melting temperature of ice-I_h. [13]

To ensure that the ice-liquid interface has relaxed, and to prepare initial conditions for the NPH simulations, three 500 fs anisotropic NPT simulations were performed at T=250K, T=300K, and T=400K. The resulting geometries and velocities were then used as starting conditions for three NPH simulations. For the EFP-small-noct method, the three NPH simulations were run for ~30 ps, and for the EFMO-small-noct method, the three NPH simulations were run for ~10 ps.

3. Results and Discussion

For the EFP-small-noct method, the temperature change during the three NPH simulations is shown in Figure 1. All simulations were assumed to converge after 15 ps, and the last ~15 ps were used to calculate the average and standard deviation of the temperature. The averaged temperatures are 311 ± 11 K, 337 ± 13 K, 424 ± 15 K for simulation with initial conditions from the 250K, 300K, and 400K NPT ensembles, respectively. None of the temperatures agree within a standard deviation. The causes for the disagreement could be that the initial NPT simulations did not equilibrate, resulting in stress that causes the ice to melt too quickly, that the basis set differs enough from that used in Ref. [13] that there is no liquid-ice coexistence between 250K and 400K and a pressure of 4000 bar, or that it is necessary to include the charge transfer term for the melting temperature to be in the 250K to 400K range.

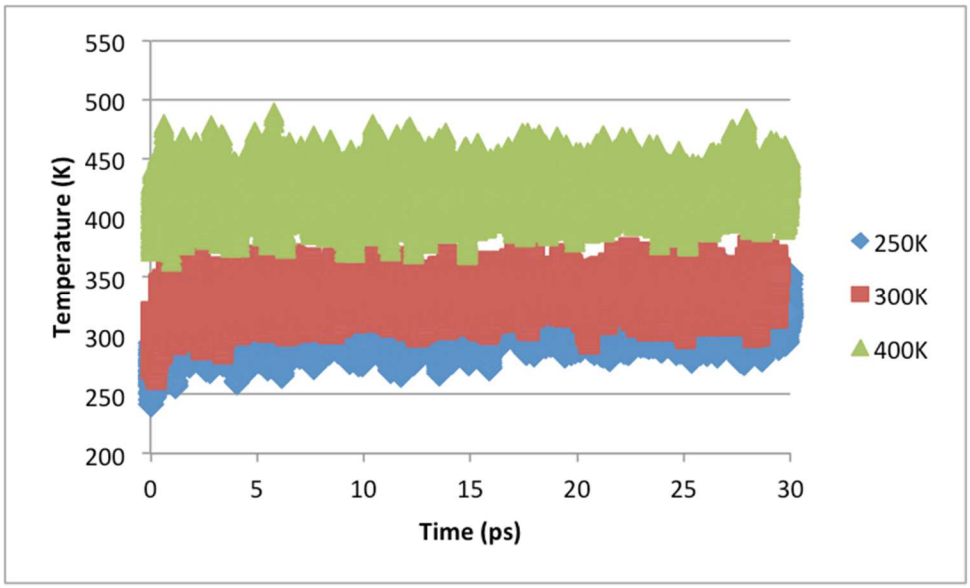

Figure 1: Temperature change as the EFP NPH simulations evolve, starting from initial conditions generated from a 250K, 300K, and 400K NPT ensembles.

The temperature change during the three NPH simulations using the EFMO-small-noct method is shown in Figure 2. As in the EFP-small-noct method, the simulations run at different initial temperatures did not equilibrate to the same temperature.

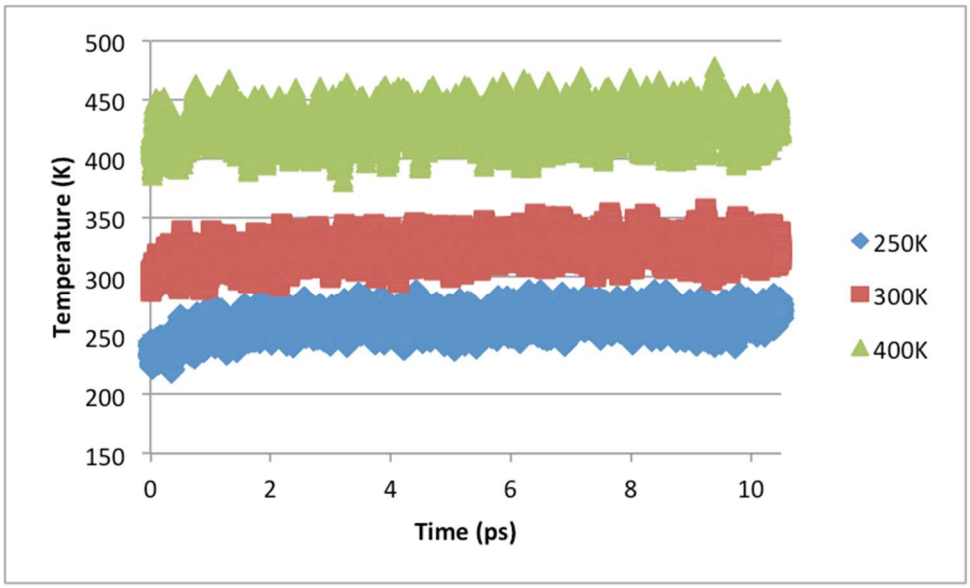

Figure 2: Temperature change as the EFMO NPH simulations evolve, starting from initial conditions generated from a 250K, 300K, and 400K NPT ensembles.

As mentioned above, it is possible that the melting temperature was not found due to the small basis set used. Thus, the next step is to try the calculations with a bigger basis set.

References

1. Yoo, S.; Zeng, X. C.; Xantheas, S. S., On the phase diagram of water with density functional theory potentials: The melting temperature of ice Ih with the Perdew–Burke–Ernzerhof and Becke–Lee–Yang–Parr functionals. *The Journal of Chemical Physics* **2009,** *130* (22), 221102.

2. Yoo, S.; Xantheas, S. S., Communication: The effect of dispersion corrections on the melting temperature of liquid water. *The Journal of Chemical Physics* **2011,** *134* (12), 121105.

3. Jorgensen, W. L.; Chandrasekhar, J.; Madura, J. D.; Impey, R. W.; Klein, M. L., Comparison of simple potential functions for simulating liquid water. *The Journal of Chemical Physics* **1983,** *79* (2), 926-935.

4. Berendsen, H. J. C.; Grigera, J. R.; Straatsma, T. P., The missing term in effective pair potentials. *The Journal of Physical Chemistry* **1987,** *91* (24), 6269-6271.

5. Horn, H. W.; Swope, W. C.; Pitera, J. W.; Madura, J. D.; Dick, T. J.; Hura, G. L.; Head-Gordon, T., Development of an improved four-site water model for biomolecular simulations: TIP4P-Ew. *The Journal of Chemical Physics* **2004,** *120* (20), 9665-9678.

6. Abascal, J. L. F.; Vega, C., The melting point of hexagonal ice (Ih) is strongly dependent on the quadrupole of the water models. *Physical Chemistry Chemical Physics* **2007,** *9* (22), 2775-2778.

7. Abascal, J. L. F.; Sanz, E.; García Fernández, R.; Vega, C., A potential model for the study of ices and amorphous water: TIP4P/Ice. *The Journal of Chemical Physics* **2005,** *122* (23), 234511.

8. Fanourgakis, G. S.; Xantheas, S. S., Development of transferable interaction potentials for water. V. Extension of the flexible, polarizable, Thole-type model potential (TTM3-F, v. 3.0) to describe the vibrational spectra of water clusters and liquid water. *Journal of Chemical Physics* **2008,** *128* (7), 074506.

9. Wang, L.-P.; Head-Gordon, T.; Ponder, J. W.; Ren, P.; Chodera, J. D.; Eastman, P. K.; Martinez, T. J.; Pande, V. S., Systematic Improvement of a Classical Molecular Model of Water. *The Journal of Physical Chemistry B* **2013,** *117* (34), 9956-9972.

10. Nohad, G., Development, Validation, and Applications of Anisotropic Polarizable Molecular Mechanics to Study Ligand and Drug-Receptor Interactions. *Current Pharmaceutical Design* **2006,** *12* (17), 2121-2158.

11. Gordon, M. S.; Freitag, M. A.; Bandyopadhyay, P.; Jensen, J. H.; Kairys, V.; Stevens, W. J., The Effective Fragment Potential Method: A QM-Based MM Approach to Modeling Environmental Effects in Chemistry. *The Journal of Physical Chemistry A* **2001,** *105* (2), 293-307.

12. Day, P. N.; Jensen, J. H.; Gordon, M. S.; Webb, S. P.; Stevens, W. J.; Krauss, M.; Garmer, D.; Basch, H.; Cohen, D., An effective fragment method for modeling solvent effects in quantum mechanical calculations. *The Journal of Chemical Physics* **1996,** *105* (5), 1968-1986.

13. Brorsen, K. R.; Willow, S. Y.; Xantheas, S. S.; Gordon, M. S., The Melting Temperature of Liquid Water with the Effective Fragment Potential. *The Journal of Physical Chemistry Letters* **2015,** *6* (18), 3555-3559.

14. Webb, S. P.; Iordanov, T.; Hammes-Schiffer, S., Multiconfigurational nuclear-electronic orbital approach: Incorporation of nuclear quantum effects in electronic structure calculations. *The Journal of Chemical Physics* **2002,** *117* (9), 4106-4118.

15. Kitaura, K.; Ikeo, E.; Asada, T.; Nakano, T.; Uebayasi, M., Fragment molecular orbital method: an approximate computational method for large molecules. *Chemical Physics Letters* **1999,** *313* (3–4), 701-706.

16. Pruitt, S. R.; Steinmann, C.; Jensen, J. H.; Gordon, M. S., Fully Integrated Effective Fragment Molecular Orbital Method. *Journal of Chemical Theory and Computation* **2013,** *9* (5), 2235-2249.

17. Steinmann, C.; Fedorov, D. G.; Jensen, J. H., Effective Fragment Molecular Orbital Method: A Merger of the Effective Fragment Potential and Fragment Molecular Orbital Methods. *The Journal of Physical Chemistry A* **2010,** *114* (33), 8705-8712.

18. Bertoni, C.; Gordon, M. S., Analytic Gradients for the Effective Fragment Molecular Orbital Method. *Journal of Chemical Theory and Computation* **2016,** *12* (10), 4743-4767.

19. Noya, C. V. a. E. S. a. J. L. F. A. a. E. G., Determination of phase diagrams via computer simulation: methodology and applications to water, electrolytes and proteins. *Journal of Physics: Condensed Matter* **2008,** *20* (15), 153101.

20. Schmidt, M. W.; Baldridge, K. K.; Boatz, J. A.; Elbert, S. T.; Gordon, M. S.; Jensen, J. H.; Koseki, S.; Matsunaga, N.; Nguyen, K. A.; Su, S.; Windus, T. L.; Dupuis, M.; Montgomery, J. A., General atomic and molecular electronic structure system. *Journal of Computational Chemistry* **1993,** *14* (11), 1347-1363.

21. Gordon , M. S.; Schmidt , M. W., Advances in Electronic Structure Theory: GAMESS a Decade Later . In *Theory and Applications of Computational Chemistry: The First Forty Years*, Elsevier B.V.: Amsterdam, The Netherlands, 2005; pp 1167 – 1189.

22. Hayward, J. A.; Reimers, J. R., Unit cells for the simulation of hexagonal ice. *The Journal of Chemical Physics* **1997,** *106* (4), 1518-1529.

CHAPTER 5. SUMMARY AND CONCLUSIONS

Much of chemistry happens in solvated systems, or with large molecules. Overall, the goal of this dissertation has been to work towards accurate but computationally inexpensive calculations on large systems. The two main ways discussed here of decreasing computational expense without losing too much accuracy have been fragmentation methods and intermolecular interaction methods.

Central to every chapter is the Effective Fragment Potential (EFP) method, a sophisticated *ab initio*-based interaction energy method.

Chapter 2 discussed the derivation and implementation of the gradient for the Effective Fragment Molecular Orbital (EFMO) method. The fully analytic gradient for the EFMO method differs from the gradient for the (EFP) method in that the geometry of each EFMO fragment is flexible. The EFMO gradient requires multiple response terms, arising from the derivative of the *ab-initio*-calculated parameters in the EFP terms. The accuracy of the EFMO gradient was tested by comparing the analytic gradient to the numeric gradient and by confirming that energy was conserved during an NVE ensemble molecular dynamics simulation. The gradient was parallelized using multi-level parallelization. Discontinuities in the potential energy surface due to cutoffs were discussed.

In Chapter 3, the accuracy of the EFP interaction energies was benchmarked using several sets of multipole moments. The multipole moments considered were the basis space-based and numeric grid-based Stone Distributed Multipole Analysis (DMA), with varied basis sets, and the basis space-iterated stockholder atom (BS-ISA+DF) by

Misquitta and Stone. Both sets of multipole moments led to reasonable results. The mean unsigned errors with respect to the CCSD(T)/CBS interaction energies are 0.78 and 0.72 kcal/mol for the BS-ISA+DF and DMA-generated (using a smaller basis set and the analytic DMA procedure) multipole moments, respectively. The MUEs are on the same order of accuracy as the MUEs for the MP2 and SCS-MP2 methods.

Chapter 4 discussed computing the melting temperature of ice I_h using the EFMO method. The direct coexistence method using the NPH ensemble was used to calculate the melting temperature. A previous study determined that the melting temperature of ice I_h using the EFP method is ~ 380K, which is about 100 K different from the experimental melting temperature. However, the direct coexistence method did not find a melting temperature for the range of temperatures (250 to 400 K) considered in the current study. One potential issue is that the current study performed EFMO and EFP calculations using parameters generated from a smaller basis set than in the previous study. A next step is to try the EFMO calculations with a larger basis set.